PACIFIC GAS AND ELECTRIC COMPANY
GEOSCIENCES DEPARTMENT
CALCULATION DOCUMENT

Calc Pages: 75

Verification Method: A
Verification Pages: 1
Supplemental Verification Pages: NA*

1. CALCULATION COVER SHEET

TITLE: Development of ISFISI Spectra

PREPARED BY: _____ DATE 9/6/01

Norman Abrahamson — Geosciences
Printed Name — Organization

VERIFIED BY: _____ DATE 9/6/01

MARCIA MCLAREN — GEOSCIENCES
Printed Name — Organization

VERIFIED BY: NA* DATE _____
(Supplemental ITR)

_____ — _____
Printed Name — Organization

APPROVED BY: _____ DATE 9/7/01

Lloyd Cluff — Geosciences
Printed Name — Organization

LLOYD S. CLUFF No. EG567 CERTIFIED ENGINEERING GEOLOGIST REGISTERED GEOLOGIST STATE OF CALIFORNIA

Expires 12/ /02

*No Supplemental ITR is required, as was done for GEO.DCPP.01.11 Rev. 0, due to no changes to the Supplemental ITR areas of review except for verification of the Somerville (2001) reference in assumption 3.7, which ITR Marcia McLaren verified.

Rev. No.	Reason for Revisions	Revision Date
00	Initial Issue	07/27/01
01	- Editorial changes per A. Tafoya's comments dated 08/6/01. - Somerville (2001) reference added to Assumption 3.7. - Second-to-last sentence of first paragraph of Assumption 3.7 changed to be consistent with the Somerville (2001) reference.	09/07/01

2. PURPOSE

The NRC-approved DDE, Hosgri, and LTSP spectra are defined for spectral periods up to 1.0 sec, 0.8 sec, and 2 sec, respectively. For the DCPP ISFSI, some components may be affected by longer period ground motions than have been defined in the DDE, Hosgri, and LTSP spectra. The purpose of this calculation is to develop 84th percentile spectra at damping values of 2%, 4%, 5%, and 7% for the horizontal and vertical components that extend out to a period of 10 seconds and which include near fault effects of directivity. The work plan requires that the spectrum envelope the DDE spectra at 2% and 5% damping, the Hosgri spectra at 4%, 5% and 7% damping, and the LTSP spectra at 5% damping. Near-fault effects of fling are developed in a separate calculation (GEO.DCPP.01.012). The spectra are to be used for the seismic design of the ISFSI (part 72 only) including the development of spectrum compatible time histories (see Calculation GEO.DCPP.01.013).

3. ASSUMPTIONS

3.1 Horizontal Component Attenuation Relations for Long Periods

The Abrahamson and Silva (1997), Sadigh et al (1997), Idriss (1991; 1994; 1995), and Campbell (1997) attenuation relations for horizontal response spectral values are assumed to be representative attenuation relations for rock sites close to large earthquakes for long periods (T>2 sec) for evaluating the long period extension of the DCPP spectra. The parameters of the Idriss (1991) model are given in the summary report by Idriss (1992). The basis for this assumption is that these attenuation relations represent the state-of-the practice. One other commonly used attenuation model is the Boore et al, 1997 model. This model is not considered applicable for this case. The Boore et al (1997) model produces very low ground motions on rock for sites close to the rupture. This is a result of the very sparse near-fault data used to derive the model and the assumption of linear site response. Therefore, this model is not included. If this model were included, the ground motions would be lower than estimated using the other four models.

3.2 Vertical Component Attenuation Relations for Long Periods

The Abrahamson and Silva (1997), Sadigh et al. (1993), and Campbell (1997) attenuation relations for vertical response spectral values are assumed to be representative attenuation relations for rock site close to large earthquakes for long periods (T> 2 sec) for evaluating the Vertical/Horizontal ratio. (Idriss, 1991 does not include a vertical component attenuation relation). The basis for this assumption is that there are only three recent attenuation relations for vertical spectral accelerations: Sadigh et al (1993), Abrahamson and Silva (1997) and Campbell (1997).

3.3 Style-of Faulting

During the LTSP, there was uncertainty in the style-of-faulting of the Hosgri fault. As a result, three alternative style-of-faulting models were considered: Strike-slip, oblique, and thrust with weights of 0.65, 0.30, and 0.05, respectively. Subsequent to the completion of the LTSP, additional earthquakes have been recorded along the Hosgri. These new

earthquakes indicate that the Hosgri is strike-slip (Hanson et al, 1992; McLaren, and Savage, in press). The Hosgri fault is assumed to be strike-slip. The basis for this assumption is the McLaren and Savage (in press) paper and the Hanson et al (1992) paper.

3.4 Directivity Effects Models

The Abrahamson (2000) model is assumed to quantify the effect of rupture directivity on the response spectral values for the average horizontal component. This model is also known as the "Bay Bridge" model. The basis for this assumption are that this directivity model was carefully reviewed and adopted by an ad hoc Caltrans ground motion committee for the new San Francisco Oakland Bay Bridge.

The Somerville et al (1997) model is assumed to quantify the effects of rupture directivity on the fault normal and fault parallel components. The basis for this assumption is that it is the only model currently available.

3.5 Epicenter Location

For the purpose of estimating rupture directivity effects, the hypocenter is assumed to be at the most unfavorable position (located at the southern end of the Hosgri fault). The basis for this assumption is that it is the largest directivity effect.

3.6 Damping Scale Factors

The response spectral attenuation relations are for 5% damping. To compute the spectra for damping values other than 5%, the damping scale factors developed by Abrahamson and Silva (1996) are assumed to be applicable. The basis for this assumption is that these scale factors were derived from a much larger data set than previous models.

3.7 Extrapolation of Directivity Effects to Periods Greater than 5 seconds

The assumed directivity effects models are defined for period up to 5 seconds. The directivity effects scale factors for the average horizontal component are assumed to be unity at periods greater than or equal to 10 seconds for a magnitude 7.2 earthquake. The basis for this assumption is that the period of directivity effects is related to the rise-time of the earthquake. The directivity effect on the average horizontal component should not occur at periods greater than twice the directivity period (T_{DIR}). For a magnitude 7.2 earthquake, the directivity period is expected to be 3.2 seconds using the Somerville (2001) model. Therefore, at a period of 10 seconds or more, there should be no directivity effect on the average horizontal component.

The FN/Ave and FP/Ave ratios at T=5 seconds are assumed to apply to periods greater than 5 seconds (up to a period of 10 seconds). The basis for this assumption is that the directivity effect on the FN/Ave and FP/Ave ratio could extend to longer periods than the effect on the average horizontal component because it is related to the radiation pattern of the focal mechanism.

4. DESIGN INPUTS

4.1 DDE spectra

Digital values for the DDE horizontal spectrum at 2% and 5% damping are taken from Calculation 64-T-254, rev 0 and computer output T1156 (RLOC 00803-00051). These digital values are consistent with the plot of the DDE horizontal spectrum given in DCM C-30, rev 7A (Figure 1 in DCM C-30). The digital values are listed in Table 4-1.

For the DDE, the vertical component ground motion is defined as 2/3 of the horizontal component (DCM C-30).

4.2 Hosgri Spectra

Digital values for the Blume Hosgri horizontal spectra at 4%, 5%, and 7% damping and for the Newmark Hosgri at 3%, 5%, and 7% damping are taken from URS Blume transmittal (Job No. 0902-00 Miscellaneous Computer Outputs, "Digitized Values of Some Spectra"). This transmittal includes the "Diablo Canyon Specification for Seismic review of Major Structures for M7.5 Hosgri earthquake" dated February 8, 1977. The spectral values are on microfilm starting at RLOC 02804-0332. These digital values are consistent with plots of the Newmark Hosgri and Blume Hosgri spectra given in DCM C-17 (Figures 3-2 and 3-3 in DCM C-17). The digital values for the Newmark and Blume spectra are listed in Tables 4-2 and 4-3, respectively.

For the Newmark and Blume spectra, the vertical component is defined as 2/3 of the horizontal (DCM C-17).

4.3 LTSP Spectra

Digital values for the LTSP horizontal and vertical spectra at 5% damping are taken from Calculation 72.2.7 (page 21) for periods less than 1 sec. These values include the 15% increase in the vertical component over the period range of 0.1 to 1 second required in SSER 34. The value at T=1 second for the horizontal component given in Calculation 72.2.7 is incorrect. It does not include the SSER 34 adjustment. The digital values are listed in Table 4-4.

4.4 SSER 34 adjustments to the LTSP

Adjustments to the long period horizontal spectrum required by SSER 34 were not included in calculation 72.2.7. The increased spectral values for periods of 1.0 to 2.0 seconds determined in calculation GEO.DCPP.01.010 are used. The digital values are included in Table 4-4.

4.5 Earthquake Magnitude

The magnitude of the earthquake used in the attenuation relations is 7.2 (SSER 34, page 2-43)

4.6 Distance from the Hosgri Fault

The Abrahamson and Silva (1997), Sadigh et al. (1997), and Idriss (1991, 1994, 1995) attenuation relations use the closest distance from the fault rupture to the site as the

distance measure. This distance is called the "rupture distance". The shortest rupture distance from the DCPP site to the Hosgri fault given in SSER 34 (page 2-43) is 4.5 km. Although the ISFSI is located east of DCPP (e.g. slightly further from the Hosgri fault), a rupture distance of 4.5 km is used.

Campbell (1997) use seismogenic distance as the distance measure in his attenuation relations. The seismogenic distances from DCPP to the Hosgri fault are also given in SSER 34 (page 2-43). For a strike-slip earthquake the seismogenic distance is 4.9 km.

4.7 Style-of-Faulting

As described in the assumption 3.3, the style-of-faulting for the Hosgri fault is strike-slip.

4.8 ISFSI site classification

The shear wave velocity at the ISFSI site is given in Agbabian (1998). The average shear-wave velocity in the top 30 m exceeds 750 m/s (Agbabian, 1998).

Campbell (1997, page 157, Table 2) define hard-rock sites as having the site class A for Boore et al 1993, which is defined as an average shear-wave velocity of greater than 750m/s in the top 30 m. Based on the measured shear-wave velocity, the ISFSI site is classified as a "hard rock" site for the Campbell (1997) attenuation relation. For a hard rock site, the depth to basement rock is 0 km so D=0 in the Campbell equations.

The Sadigh et al (1997) model defines rock sites as sites with bedrock within 1 meter of the surface with a shear-wave velocity of greater than 750 m/s (Sadigh et al,1997, page 180). Using this definition, the ISFSI site is "rock". Sadigh et al (1997) note that their "rock" category includes both rock and soft-rock sites.

The Abrahamson and Silva (1997) model uses a site classification consistent with Sadigh et al (1997). Therefore, the ISFSI site is a "rock" site.

The Idriss (1991,1995) model uses a subjective definition of rock. Based on the shear-wave velocity, the ISFSI site is classified as "rock".

4.9 Length of the Hosgri Fault

The total length of the Hosgri fault is 110 km (PG&E, 1988 LTSP final report).

4.10 Location of DCPP along the Hosgri Fault

The DCPP site is 70 km from the southern end of the Hosgri fault (PG&E, 1988 LTSP final report)

4.11 Epicenter Location

As discussed in the assumptions, the epicenter is assumed to be located at the southern end of the Hosgri fault.

Table 4-1. Digital values for the DDE horizontal spectra at 2% and 5% damping

Period (sec)	Frequency (Hz)	2% damping	5% damping
0.001	1000.000	0.400	0.402
0.05	20.000	0.400	0.402
0.06	16.667	0.432	0.432
0.07	14.286	0.664	0.498
0.08	12.500	1.104	0.666
0.09	11.111	1.520	0.930
0.10	10.000	1.920	1.266
0.11	9.091	2.080	1.386
0.12	8.333	2.164	1.434
0.13	7.692	2.176	1.464
0.14	7.143	2.160	1.476
0.15	6.667	2.084	1.473
0.16	6.250	2.004	1.467
0.17	5.882	1.888	1.443
0.18	5.556	1.800	1.413
0.19	5.263	1.744	1.374
0.20	5.000	1.680	1.338
0.21	4.762	1.616	1.302
0.22	4.545	1.560	1.281
0.23	4.348	1.520	1.245
0.24	4.167	1.476	1.215
0.25	4.000	1.468	1.182
0.26	3.846	1.472	1.146
0.27	3.704	1.484	1.119
0.28	3.571	1.492	1.080
0.29	3.448	1.500	1.047
0.30	3.333	1.504	1.005
0.31	3.226	1.504	1.011
0.32	3.125	1.496	1.003
0.33	3.030	1.484	1.005
0.34	2.941	1.464	0.999
0.35	2.857	1.444	0.993
0.36	2.778	1.424	0.981
0.37	2.703	1.404	0.972
0.38	2.632	1.384	0.963
0.39	2.564	1.364	0.948
0.40	2.500	1.344	0.936
0.42	2.381	1.296	0.909
0.44	2.273	1.240	0.882
0.46	2.174	1.184	0.852
0.48	2.083	1.132	0.819
0.50	2.000	1.080	0.786

Table 4-1 (cont)

Period (sec)	Frequency (Hz)	2% damping	5% damping
0.52	1.923	1.024	0.759
0.54	1.852	0.980	0.741
0.56	1.786	0.944	0.723
0.58	1.724	0.904	0.705
0.60	1.667	0.864	0.687
0.62	1.613	0.824	0.672
0.64	1.563	0.788	0.657
0.66	1.515	0.764	0.639
0.68	1.471	0.752	0.630
0.70	1.429	0.740	0.621
0.72	1.389	0.724	0.615
0.74	1.351	0.704	0.609
0.76	1.316	0.692	0.606
0.78	1.282	0.680	0.603
0.80	1.250	0.672	0.600
0.82	1.220	0.664	0.600
0.84	1.190	0.656	0.597
0.86	1.163	0.644	0.596
0.88	1.136	0.632	0.595
0.90	1.111	0.624	0.594
0.92	1.087	0.620	0.594
0.94	1.064	0.616	0.594
0.96	1.042	0.612	0.594
0.98	1.020	0.608	0.594
1.00	1.000	0.604	0.594

Table 4-2. Digital values for the Newmark Hosgri horizontal spectra at 3%, 5% and 7% damping

Period (sec)	Frequency (Hz)	3% damping	5% damping	7% damping
0.010	100.000	0.750	0.750	0.750
0.029	34.483	0.750	0.750	0.750
0.032	31.250	0.790	0.784	0.779
0.036	27.778	0.860	0.842	0.830
0.040	25.000	0.944	0.912	0.890
0.045	22.222	1.050	0.997	0.963
0.050	20.000	1.136	1.067	1.022
0.056	17.857	1.240	1.149	1.091
0.059	16.949	1.300	1.195	1.130
0.063	15.873	1.367	1.268	1.173
0.067	14.925	1.443	1.306	1.221
0.069	14.493	1.484	1.334	1.246
0.071	14.085	1.528	1.371	1.274
0.074	13.514	1.574	1.408	1.303
0.075	13.333	1.588	1.425	1.318
0.077	12.987	1.624	1.444	1.334
0.078	12.821	1.651	1.464	1.350
0.080	12.500	1.678	1.489	1.366
0.082	12.195	1.706	1.506	1.383
0.083	12.048	1.736	1.528	1.401
0.085	11.765	1.767	1.551	1.419
0.087	11.494	1.795	1.574	1.438
0.089	11.236	1.831	1.599	1.458
0.091	10.989	1.866	1.624	1.478
0.093	10.753	1.902	1.651	1.500
0.095	10.526	1.939	1.678	1.522
0.098	10.204	1.978	1.707	1.544
0.100	10.000	2.019	1.737	1.568
0.103	9.709	2.062	1.768	1.593
0.105	9.524	2.107	1.801	1.619
0.108	9.259	2.154	1.835	1.646
0.111	9.009	2.204	1.870	1.674
0.114	8.772	2.256	1.908	1.703
0.118	8.475	2.311	1.947	1.734
0.121	8.264	2.369	1.989	1.766
0.125	8.000	2.430	2.032	1.800
0.127	7.874	2.430	2.032	1.800
0.129	7.752	2.430	2.032	1.800

Table 4-2. (cont)

Period (sec)	Frequency (Hz)	3% damping	5% damping	7% damping
0.131	7.634	2.430	2.032	1.800
0.133	7.519	2.430	2.032	1.800
0.136	7.353	2.430	2.032	1.800
0.138	7.246	2.430	2.032	1.800
0.140	7.143	2.430	2.032	1.800
0.143	6.993	2.430	2.032	1.800
0.146	6.849	2.430	2.032	1.800
0.148	6.757	2.430	2.032	1.800
0.151	6.623	2.430	2.032	1.800
0.154	6.494	2.430	2.032	1.800
0.157	6.369	2.430	2.032	1.800
0.160	6.250	2.430	2.032	1.800
0.163	6.135	2.430	2.032	1.800
0.167	5.988	2.430	2.032	1.800
0.170	5.882	2.430	2.032	1.800
0.174	5.747	2.430	2.032	1.800
0.178	5.618	2.430	2.032	1.800
0.182	5.495	2.430	2.032	1.800
0.186	5.376	2.430	2.032	1.800
0.190	5.263	2.430	2.032	1.800
0.195	5.128	2.430	2.032	1.800
0.200	5.000	2.430	2.032	1.800
0.204	4.902	2.430	2.032	1.800
0.208	4.808	2.430	2.032	1.800
0.213	4.695	2.430	2.032	1.800
0.217	4.608	2.430	2.032	1.800
0.222	4.505	2.430	2.032	1.800
0.227	4.405	2.430	2.032	1.800
0.233	4.292	2.430	2.032	1.800
0.238	4.202	2.430	2.032	1.800
0.244	4.098	2.430	2.032	1.800
0.250	4.000	2.430	2.032	1.800
0.256	3.906	2.430	2.032	1.800
0.263	3.802	2.430	2.032	1.800
0.270	3.704	2.430	2.032	1.800
0.278	3.597	2.430	2.032	1.800
0.290	3.448	2.430	2.032	1.800
0.303	3.300	2.430	2.032	1.800
0.317	3.155	2.430	2.032	1.800
0.333	3.003	2.430	2.032	1.800
0.345	2.899	2.430	2.032	1.800
0.357	2.801	2.430	2.032	1.800

Table 4-2. (cont)

Period (sec)	Frequency (Hz)	3% damping	5% damping	7% damping
0.370	2.703	2.430	2.032	1.800
0.385	2.597	2.430	2.032	1.800
0.400	2.500	2.430	2.032	1.800
0.417	2.398	2.430	2.032	1.800
0.427	2.342	2.430	2.032	1.800
0.435	2.299	2.378	2.032	1.800
0.445	2.247	2.315	2.032	1.800
0.455	2.198	2.265	1.975	1.800
0.476	2.101	2.165	1.885	1.707
0.500	2.000	2.062	1.795	1.626
0.526	1.901	1.959	1.705	1.545
0.556	1.799	1.856	1.616	1.464
0.588	1.701	1.753	1.526	1.382
0.625	1.600	1.650	1.436	1.301
0.667	1.499	1.546	1.346	1.220
0.714	1.401	1.443	1.257	1.138
0.769	1.300	1.340	1.167	1.057
0.833	1.200	1.237	1.077	0.976
0.909	1.100	1.134	0.987	0.894
1.000	1.000	1.031	0.898	0.813
1.111	0.900	0.928	0.808	0.732
1.250	0.800	0.825	0.718	0.650
1.429	0.700	0.722	0.628	0.569
1.538	0.650	0.670	0.583	0.529
1.667	0.600	0.619	0.539	0.488
2.000	0.500	0.457	0.411	0.383
2.500	0.400	0.283	0.263	0.245
3.333	0.300	0.165	0.148	0.138
4.000	0.250	0.114	0.103	0.096
5.000	0.200	0.073	0.066	0.061
10.000	0.100	0.018	0.016	0.015

Table 4-3. Digital values for the Blume Hosgri horizontal spectra at 4%, 5%, and 7% damping

Period (sec)	Frequency (Hz)	4% damping	5% damping	7% damping
0.010	100.000	0.750	0.750	0.750
0.029	34.483	0.750	0.750	0.750
0.032	31.250	0.777	0.773	0.766
0.036	27.778	0.810	0.801	0.786
0.040	25.000	0.850	0.835	0.810
0.045	22.222	0.921	0.899	0.860
0.050	20.000	0.979	0.952	0.902
0.056	17.857	1.051	1.016	0.953
0.059	16.949	1.093	1.055	0.983
0.063	15.873	1.141	1.097	1.017
0.067	14.925	1.195	1.146	1.055
0.069	14.493	1.225	1.173	1.076
0.071	14.085	1.256	1.202	1.099
0.074	13.514	1.291	1.233	1.123
0.075	13.333	1.309	1.249	1.136
0.077	12.987	1.328	1.266	1.150
0.078	12.821	1.347	1.283	1.164
0.080	12.500	1.367	1.302	1.178
0.082	12.195	1.388	1.321	1.193
0.083	12.048	1.410	1.341	1.209
0.085	11.765	1.433	1.361	1.225
0.087	11.494	1.457	1.383	1.242
0.089	11.236	1.482	1.405	1.260
0.091	10.989	1.508	1.429	1.278
0.093	10.753	1.536	1.454	1.298
0.095	10.526	1.564	1.479	1.318
0.098	10.204	1.594	1.507	1.340
0.100	10.000	1.626	1.535	1.362
0.103	9.709	1.659	1.565	1.386
0.105	9.524	1.694	1.596	1.410
0.108	9.259	1.731	1.630	1.437
0.111	9.009	1.770	1.665	1.464
0.114	8.772	1.811	1.702	1.493
0.118	8.475	1.841	1.736	1.521
0.121	8.264	1.867	1.767	1.548
0.125	8.000	1.890	1.790	1.572
0.127	7.874	1.902	1.802	1.585
0.129	7.752	1.914	1.814	1.599
0.131	7.634	1.927	1.827	1.612

Table 4-3 (cont.)

Period (sec)	Frequency (Hz)	4% damping	5% damping	7% damping
0.133	7.519	1.940	1.840	1.627
0.136	7.353	1.954	1.854	1.641
0.138	7.246	1.968	1.868	1.657
0.140	7.143	1.982	1.882	1.671
0.143	6.993	1.996	1.894	1.680
0.145	6.897	2.010	1.907	1.689
0.148	6.757	2.025	1.921	1.699
0.151	6.623	2.040	1.935	1.708
0.154	6.494	2.056	1.949	1.718
0.157	6.369	2.073	1.964	1.729
0.160	6.250	2.090	1.980	1.740
0.163	6.135	2.101	1.990	1.747
0.167	5.988	2.113	2.000	1.753
0.170	5.882	2.126	2.011	1.760
0.174	5.747	2.139	2.022	1.768
0.178	5.618	2.152	2.033	1.776
0.182	5.495	2.165	2.044	1.782
0.186	5.376	2.178	2.052	1.786
0.190	5.263	2.191	2.061	1.790
0.195	5.128	2.205	2.070	1.795
0.200	5.000	2.220	2.080	1.800
0.204	4.902	2.228	2.086	1.802
0.208	4.808	2.237	2.092	1.804
0.213	4.695	2.246	2.099	1.806
0.217	4.608	2.255	2.106	1.809
0.222	4.505	2.263	2.112	1.811
0.227	4.405	2.271	2.117	1.814
0.233	4.292	2.279	2.123	1.816
0.238	4.202	2.287	2.128	1.818
0.244	4.098	2.290	2.126	1.818
0.250	4.000	2.290	2.125	1.815
0.256	3.906	2.290	2.122	1.812
0.263	3.802	2.288	2.118	1.808
0.270	3.704	2.285	2.115	1.805
0.278	3.597	2.281	2.111	1.801
0.290	3.448	2.265	2.095	1.790
0.303	3.300	2.245	2.075	1.775
0.317	3.155	2.224	2.054	1.754
0.333	3.003	2.187	2.030	1.723
0.345	2.899	2.158	2.008	1.703

Table 4.3 (cont.)

Period (sec)	Frequency (Hz)	4% damping	5% damping	7% damping
0.357	2.801	2.127	1.977	1.684
0.370	2.703	2.089	1.944	1.654
0.385	2.597	2.048	1.904	1.618
0.400	2.500	2.010	1.850	1.580
0.417	2.398	1.960	1.808	1.538
0.435	2.299	1.906	1.763	1.493
0.455	2.198	1.846	1.714	1.451
0.476	2.101	1.781	1.660	1.408
0.500	2.000	1.720	1.605	1.360
0.526	1.901	1.654	1.546	1.307
0.556	1.799	1.581	1.480	1.249
0.588	1.701	1.510	1.417	1.198
0.625	1.600	1.432	1.348	1.142
0.667	1.499	1.357	1.273	1.090
0.714	1.401	1.279	1.190	1.036
0.769	1.300	1.202	1.118	0.975
0.833	1.200	1.126	1.049	0.916
0.909	1.100	1.050	0.978	0.862
1.000	1.000	0.958	0.894	0.796
1.111	0.900	0.881	0.822	0.732
1.250	0.800	0.784	0.732	0.653
1.429	0.700	0.685	0.640	0.572
1.538	0.650	0.628	0.586	0.540
1.667	0.600	0.563	0.526	0.491
2.000	0.500	0.426	0.407	0.380
2.500	0.400	0.273	0.261	0.244
3.333	0.300	0.157	0.150	0.137
4.000	0.250	0.106	0.101	0.093
5.000	0.200	0.067	0.064	0.059
10.000	0.100	0.017	0.016	0.014

Table 4-4. Digital Values for the LTSP / SSER 34 Spectra at 5% damping

Period (sec)	Frequency (Hz)	Horizontal Sa (g) with SSER 34 Adjustment	Vertical Sa(g) with SSER 34 adjustment
0.025	40.00	0.830	0.70
0.030	33.00	0.830	0.83
0.040	25.00	0.964	1.11
0.050	20.00	1.110	1.41
0.070	14.29	1.344	1.71
0.085	11.76	1.508	1.76
0.100	10.00	1.654	1.99
0.120	8.33	1.819	1.89
0.140	7.14	1.918	1.76
0.150	6.67	1.947	1.72
0.170	5.88	1.976	1.61
0.200	5.00	2.006	1.47
0.250	4.00	2.015	1.29
0.300	3.33	1.962	1.16
0.400	2.50	1.763	0.96
0.500	2.00	1.554	0.82
0.750	1.33	1.109	0.61
1.000	1.00	0.89	0.47
1.500	0.67	0.58	
2.000	0.50	0.40	

5. METHOD AND EQUATION SUMMARY

5.1 Methods

The method used to develop the ISFSI horizontal spectra uses the following steps. These steps are identified in section 6.

1. The short-moderate period part (T< 2 sec) of the horizontal spectrum at 5% damping is defined by the envelop of the DDE, Newmark Hosgri, Blume Hosgri, and LTSP/SSER 34 spectra.

2. Current empirical attenuation relations are used to develop and estimate the 84th percentile spectrum for periods between 2 and 5 seconds for the average horizontal component. This is used along with the DCPP spectra to define the long period spectrum in step 3 below.

3. The envelope of the 5% damped spectra from the DDE, Newmark Hosgri, Blume Hosgri, and empirical attenuation relations is used to define the average horizontal component (w/o explicit directivity) for periods between 2 and 5 seconds.

4. The horizontal spectrum is extrapolated to a period of 10 seconds.

5. Rupture directivity effects based on the Abrahamson (2000) model are used to determine scale factors to compute the 84th percentile average horizontal component for forward directivity conditions.

6. Rupture directivity effects based on the Somerville et al. (1997) model are used to determine scale factors to compute the fault normal and fault parallel (w/o fling) components.

7 Combination of directivity effects.

8 Estimating of spectra including directivity effects.

9. Additional conservatism for the fault normal component at periods near 1 second is incorporated to accommodate potential results of ongoing research.

10 Interpolate the Newmark Hosgri spectrum for 4% damping.

11. Spectra at damping values of 2%, 4%, and 7% are developed using the Silva and Abrahamson (1996) model for damping scale factors.

12. Check that the horizontal spectra (FN and FP) envelope the DDE at 2%, HE at 4% and 7% damping. If needed, adjust the 5% damped spectra such that scaled spectra at other damping values meet the envelope requirement.

The method used to develop the ISFSI vertical spectrum uses the following steps. These steps are identified in section 6.

1. The short to moderate part (T<2 sec) of the vertical spectrum at 5% damping is defined by the envelop of the DDE, Newmark Hosgri, Blume Hosgri, and LTSP/SSER 34 spectra.

2. Current empirical attenuation relations are used to develop an estimate of the vertical/horizontal ratio for frequencies less than 0.5 Hz. These ratios are then used to provide an estimate of the long period vertical spectrum in step 3 below.

3. The envelope of the 5% damped spectra from the DDE, Newmark Hosgri, Blume Hosgri, and scaled empirical attenuation relations is used to define the vertical component for periods between 2 and 10 seconds

4. Spectra at damping values of 2%, 4%, and 7% are developed using the Silva and Abrahamson (1996) model for damping scale factors.

5. Check that the vertical spectra envelope the DDE at 2%, HE at 4% and 7% damping. If needed, adjust the 5% damped spectra such that scaled spectra at other dampings meet the envelope requirement.

5.2 Equations

5.2.1 Sadigh et al. (1997) Attenuation Equation

The Sadigh et al (1997) median horizontal spectral acceleration attenuation relation for a strike-slip earthquake at a rock site is:

$$\ln (Sa_{med}(g)) = C_1 + 1.1\,M + C_3(8.5-M)^{2.5} + C_4 \ln(R+\exp(C_5+C_6M)) + C_7 \ln(R+2) \quad (1)$$

where R is the rupture distance, and M is the magnitude. The coefficients for this model are listed in Table 5-1.

Table 5-1. Coefficients for the Sadigh et al (1997) attenuation relation for horizontal spectral acceleration for M > 6.5 earthquakes on strike slip faults (page 185-186 in Sadigh et al)

Period(s)	C_1	C_3	C_4	C_5	C_6	C_7	σ (M<7.21)
1.00	-2.355	-0.055	-1.800	-0.48451	0.524	0.0	1.53 - 0.14M
1.50	-3.057	-0.065	-1.725	-0.48451	0.524	0.0	1.53 - 0.14M
2.00	-3.595	-0.070	-1.670	-0.48451	0.524	0.0	1.53 - 0.14M
3.00	-4.350	-0.080	-1.610	-0.48451	0.524	0.0	1.53 - 0.14M
4.00	-4.880	-0.100	-1.570	-0.48451	0.524	0.0	1.53 - 0.14M

5.2.2 Idriss (1991,1994,1995) Attenuation Equation

The Idriss (1991,1995) median horizontal spectral acceleration attenuation relations for strike-slip earthquakes recorded at rock sites use the form:

$$\ln(Sa_{med}(g)) = \alpha_0 + \exp(\alpha_1 + \alpha_2 M) + (\beta_0 - \exp(\beta_1 + \beta_2 M))*\ln(R+C) \quad (2)$$

where R is the rupture distance. Idriss (1991), which is summarized in the Idriss (1992) review paper, developed coefficients for peak acceleration and response spectral acceleration. Subsequently, the peak acceleration model was updated in Idriss (1995). To estimate the corresponding update for the response spectral values, the 1991 spectral values are scaled by the ratio of the 1995 pga over the 1991 pga. That is the spectral shape (Sa/pga) is assumed to remain the same. The spectral shape is given by the ratio of the spectral acceleration to the peak acceleration: Sa(T)/ pga. If the spectral is not changed, then

$$Sa_{95}(T) / pga_{95} = Sa_{91}(T) / pga_{91}$$

Therefore,

$$\ln(Sa_{95}(g)) = \ln(Sa_{91}(g)) + \ln(PGA_{95} / PGA_{91}) \quad (3)$$

The coefficients for this model are listed in Table 5-2. The standard deviation for the response spectral values was updated by Idriss (1994). These updated standard deviations are also listed in Table 5-2.

Table 5-2. Coefficients for the Idriss (1991) attenuation relation for horizontal spectral acceleration for M > 6.0

Period(s)	α_0	α_1	α_2	β_0	β_1	β_2	C	σ (1994)
PGA (95)	0	2.763	-0.262	0.0	2.215	-0.288	10	
PGA (91)	-0.050	3.477	-0.284	0	2.475	-0.286	20	
1.00 (91)	-0.867	2.662	-0.162	0.123	2.475	-0.286	20	1.47-0.12M
1.50 (91)	-0.970	2.536	-0.160	0.136	2.475	-0.286	20	1.47-0.12M
2.00 (91)	-1.046	2.447	-0.160	0.146	2.475	-0.286	20	1.47-0.12M
3.00 (91)	-1.143	2.295	-0.159	0.160	2.475	-0.286	20	1.47-0.12M
4.00 (91)	-1.177	2.169	-0.159	0.169	2.475	-0.286	20	1.47-0.12M
5.00 (91)	-1.214	2.042	-0.157	0.177	2.475	-0.286	20	1.47-0.12M

5.2.3 Abrahamson and Silva (1997) Attenuation Equation

The Abrahmson and Silva (1997) median horizontal and median vertical spectral acceleration attenuation relation for strike-slip earthquakes on rock site conditions for M>6.4 is :

$$\ln(Sa_{med}(g)) = a_1 + a_4(M - c_1) + a_{12}(8.5 - M)^n + [a_3 + a_{13}(M - c_1)]\ln R_1 \qquad (4)$$

where $R_1 = \sqrt{R^2 + c_4^2}$ and n=2 for the horizontal component and n=3 for the vertical component.

The coefficients for horizontal component are listed in Table 5-3 and the coefficients for the vertical component are listed in Table 5-4 . The standard deviations, for M ≥7.0 are given by

$$\sigma = b_5 - 2b_6 \qquad (5)$$

The coefficients for the standard deviation for the horizontal component are also listed in Table 5-3.

Table 5-3. Coefficients for the Abrahamson and Silva (1997) attenuation relation for horizontal spectral acceleration for M > 6.4 (from Abrahamson and Silva, page 108-109)

Period (s)	c_4	a_1	a_3	a_4	a_{12}	a_{13}	c_1	b_5	b_6
1.00	3.70	0.828	-0.8383	-0.144	-0.1020	0.17	6.4	0.83	0.118
1.50	3.55	0.260	-0.7721	-0.144	-0.1200	0.17	6.4	0.84	0.110
2.00	3.50	-0.150	-0.7250	-0.144	-0.1400	0.17	6.4	0.85	0.105
3.00	3.50	-0.690	-0.7250	-0.144	-0.1726	0.17	6.4	0.87	0.097
4.00	3.50	-1.130	-0.7250	-0.144	-0.1956	0.17	6.4	0.88	0.092
5.00	3.50	-1.460	-0.7250	-0.144	-0.2150	0.17	6.4	0.89	0.087

Table 5-4. Coefficients for the Abrahamson and Silva (1997) attenuation relation for vertical spectral acceleration for M > 6.4 (from Abrahamson and Silva, page 116)

Period (s)	c_4	a_1	a_3	a_4	a_{12}	a_{13}	c_1
1.00	2.50	-0.602	-0.7404	0.275	-0.0115	0.06	6.4
1.50	2.50	-0.966	-0.7285	0.275	-0.0180	0.06	6.4
2.00	2.50	-1.224	-0.7200	0.275	-0.0240	0.06	6.4
3.00	2.50	-1.581	-0.7200	0.275	-0.0431	0.06	6.4
4.00	2.50	-1.857	-0.7200	0.275	-0.0565	0.06	6.4
5.00	2.50	-2.053	-0.7200	0.275	-0.0670	0.06	6.4

5.2.4 Sadigh et al. (1993) Attenuation Equations

The Sadigh et al. (1993) median vertical spectral acceleration attenuation relation for strike-slip earthquakes at rock sites is of the form:

$$\ln(Sa(g)) = c_1 + 1.1M + c_3(8.5 - M)^{2.5} + c_4 \ln(R + \exp(-0.3524 + 0.478M)) \quad (6)$$

where R is the rupture distance. The coefficients for this model are listed in Table 5-5.

Table 5-5. Coefficients for the Sadigh et al. (1993) attenuation relation for vertical spectral acceleration for M > 6.5 (From Sadigh et al. 1993, page 68)

Period (s)	c_1	c_3	c_4
1.00	-4.5318	-0.08000	-1.400
1.50	-4.9118	-0.08554	-1.400
2.00	-5.2219	-0.08946	-1.400
3.00	-5.6864	-0.09500	-1.400

5.2.5 Computation of 84th Percentile Spectral Values

For a log-normal distribution, the 84th percentile corresponds to 1.0 standard deviations above the median. The 84th percentile response spectral values are given by:

$$\ln(Sa_{84th}) = \ln(Sa_{med}) + \sigma \quad (7)$$

5.2.6 Abrahamson (2000) Rupture Directivity Model

For magnitudes greater than 6.5 and rupture distances less than 30 km, the Abrahamson (2000) model for the natural log of the directivity scale factor for the average horizontal component is given by

$$\ln(Dir(x, \theta, T)) = C_1(T) + 1.88\, C_2(T)\, X \cos(\theta) \quad \text{for } X\cos(\theta) = 0.4 \quad (8)$$
$$\ln(Dir(x, \theta, T)) = C_1(T) + 0.75\, C_2(T) \quad \text{for } X\cos(\theta) > 0.4$$

where $C_1(T) + C_2(T)$ are listed in Table 5-6, and X and θ are directivity parameters defined by Somerville et al. (1997). X is the ratio of the fault length between the site and the epicenter and the fault length, and θ is then angle between the strike of the fault and the site-epicenter direction (See Somerville et al 1997 figure 5).

Table 5-6. Coefficients for the Abrahamson (2000) directivity model for the average horizontal component (from Abrahamson 2000, page 3).

Period (sec)	C_1	C_2
0.60	0.000	0.000
0.75	-0.084	0.185
1.00	-0.192	0.423
1.50	-0.344	0.759
2.00	-0.452	0.998
3.00	-0.605	1.333
4.00	-0.713	1.571
5.00	-0.797	1.757

5.2.7 Somerville et al (1997) Rupture Directivity Model

For magnitudes greater than 6, the Somerville et al (1997) model for the difference between the fault normal and fault parallel components of the horizontal ground motion is given by

$$\ln(FN/Ave\ H) = \cos(2\theta)\,[C_1 + C_2 \ln(R+1) + C_3(M-6)] \quad \text{for } \theta<45 \qquad (9a)$$

$$\ln(FN/Ave\ H) = 0 \quad \text{for } \theta>=45$$

The coefficients for this model are listed in Table 5-7. The average horizontal component is based on the geometric mean of the two horizontals (Abrahamson and Silva, 1997, page 105). That is AveH = FP*FN. Therefore the ratio of the FP/Ave H is given by

$$\ln(FP/Ave\ H) = -\ln(FN/ave\ H) \qquad (9b)$$

where ln(FN/Ave H) is given in equation 9a.

Table 5-7. Model Coefficients for the Somerville et al. (1997) Directivity Effects Including the dependence on the angle θ (from Somerville et al, 1997 Page 209)

Period (sec)	C_1	C_2	C_3
0.50	0.000	0.000	0.000
0.60	0.027	-0.007	0.000
0.75	0.061	-0.016	0.000
1.00	0.104	-0.026	0.000
1.50	0.164	-0.049	0.034
2.00	0.207	-0.061	0.059
3.00	0.353	-0.101	0.093
4.00	0.456	-0.128	0.118
5.00	0.450	-0.127	0.137

5.2.8 Combination of directivity factors

The two directivity scale factors are combined to give the total effect. The scale factors for the FN and FP components are:

$$Scale_{FN}(T) = Dir(T) * FN/AveH(T) \quad (10a)$$

$$Scale_{FP}(T) = Dir(T) * FP/AveH(T) \quad (10b)$$

Where Dir is from equation 8 and FN/AveH is from equation 9a, and FP/AveH is from Equation 9b.

5.2.9 Computation of fault normal and fault parallel ground motion

The directivity factors are scale factors that are used to scale ground motions from standard attenuation relations for the average horizontal component. The response spectrum for the fault normal component, including directivity effects, is computed using the following equation:

$$Sa_{FN}(T) = Sa_{AveH}(T) * Scale_{FN}(T) \quad (11a)$$

The response spectrum for the fault parallel component, including directivity effects, is computed using the following equation:

$$Sa_{FP}(T) = Sa_{AveH}(T) * Scale_{FP}(T) \quad (11b)$$

5.2.10 Equations for Scale Factors for Damping values other than 5%

The Abrahamson and Silva (1996) model for natural log of the scale factors for response spectral values at dampings other than 5% is given by

$$\ln\left(\frac{Sa_{x\%}}{Sa_{5\%}}\right) = C_1 + G_2(M - 6.0) + G_3(8.5 - M)^2 \quad (12a)$$

where x% is the desired damping percentage (e.g. 2% or 5% or 7%). The coefficients for the horizontal component are given in Tables 5-8a, 5-8b, and 5-8c. The coefficients for the vertical component are given in Tables 5-9a, 5-9b, and 5-9c.

The scale factor for the different damping ratio is given by

$$Scale_{damp}(T,x\%) = \exp(\ \ln(Sa_{x\%}(T)/Sa_{5\%}(T))\ ), \quad (12b)$$

where ($\ln(Sa_{x\%}(T)/Sa_{5\%}(T))$ is given in equation (12a). The damping scale factors are applied to the 5% damped spectrum. That is, the spectral values at x% damping are computed using the following equation:

$$Sa_{x\%}(T) = Sa_{5\%}(T) * Scale_{damp}(T,x\%) \quad (13)$$

Table 5-8a. Abrahamson and Silva (1996) coefficient C_1 for damping scale factors for the horizontal component (from Abrahamson and Silva 1996, Table 4-4a)

Period (sec)	2% damping	3% damping	7% damping
0.010	0	0	0
0.020	0	0	0
0.030	0.0462	0.0273	-0.0205
0.040	0.0828	0.0490	-0.0367
0.050	0.1094	0.0648	-0.0486
0.075	0.1580	0.0936	-0.0701
0.100	0.1922	0.1138	-0.0853
0.120	0.2141	0.1268	-0.0950
0.125*	0.2167	0.1284	-0.0962
0.150	0.2284	0.1353	-0.1014
0.170-0.750	0.2379	0.1409	-0.1056
1.000	0.2365	0.1401	-0.1050
1.500	0.2309	0.1368	-0.1025
2.000	0.2239	0.1326	-0.0994
3.000	0.2095	0.1241	-0.0930
4.000	0.1957	0.1159	-0.0869
5.000	0.1830	0.1084	-0.0812

* interpolated using equation 14.

Table 5-8b. Abrahamson and Silva (1996) coefficient G_2 for damping scale factors for the horizontal component (from Abrahamson and Silva 1996, Table 4-5a)

Period (sec)	2% damping	3% damping	7% damping
0.010	0	0	0
0.020	0	0	0
0.030	0	0	0
0.040	0	0	0
0.050	0	0	0
0.075	0	0	0
0.100	0	0	0
0.120	0	0	0
0125	0	0	0
0.150	0	0	0
0.170 – 0.750	0	0	0
1.000	0.0016	0.001	-0.0007
1.500	0.0039	0.0023	-0.0017
2.000	0.0055	0.0032	-0.0024
3.000	0.0078	0.0046	-0.0034
4.000	0.0094	0.0055	-0.0042
5.000	0.0106	0.0063	-0.0047

Table 5-8c. Abrahamson and Silva (1996) coefficient G_3 for damping scale factors for the horizontal component (from Abrahamson and Silva 1996, Table 4-6a)

Period (sec)	2% damping	3% damping	7% damping
0.010	0	0	0
0.020	0	0	0
0.030	0	0	0
0.040	0	0	0
0.050	0	0	0
0.075	0	0	0
0.100	0	0	0
0.120	0	0	0
0.125	0	0	0
0.150	0	0	0
0.170-0.750	0	0	0
1.000	-0.0012	-0.0007	0.0006
1.500	-0.0030	-0.0018	0.0013
2.000	-0.0042	-0.0025	0.0019
3.000	-0.0060	-0.0036	0.0027
4.000	-0.0072	-0.0043	0.0032
5.000	-0.0082	-0.0049	0.0036

Table 5-9a. Abrahamson and Silva (1996) coefficient C_1 for damping scale factors for the vertical component (from Abrahamson and Silva 1996, Table 4-4b)

Period (sec)	2% damping	3% damping	7% damping
0.010	0	0	0
0.020	0	0	0
0.030	0.1232	0.0725	-0.0528
0.040	0.1844	0.1085	-0.0790
0.050	0.2072	0.1220	-0.0888
0.075	0.2488	0.1464	-0.1067
0.100	0.2818	0.1658	-0.1208
0.120	0.2890	0.1701	-0.1239
0.125*	0.2898	0.1706	-0.1242
0.150	0.2932	0.1726	-0.1257
0.170	0.2910	0.1713	-0.1247
0.200	0.2839	0.1671	-0.1217
0.240	0.2776	0.1634	-0.1190
0.300 – 0.750	0.2727	0.1605	-0.1169
1.000	0.2709	0.1594	-0.1161
1.500	0.2637	0.1552	-0.1131
2.000	0.2549	0.1500	-0.1093
3.000	0.2366	0.1393	-0.1014
4.000	0.2193	0.1291	-0.0940
5.000	0.2033	0.1196	-0.0871

* interpolated using equation 14

Table 5-9b. Abrahamson and Silva (1996) coefficient G_2 for damping scale factors for the vertical component (from Abrahamson and Silva 1996, Table 4-5b)

Period (sec)	2% damping	3% damping	7% damping
0.010	0	0	0
0.020	0	0	0
0.030	0	0	0
0.040	0	0	0
0.050	0	0	0
0.075	0	0	0
0.100	0	0	0
0.120	0	0	0
0.125	0	0	0
0.150	0	0	0
0.170	0	0	0
0.200	0	0	0
0.240	0	0	0
0.300 - 0750	0	0	0
1.000	0.0018	0.0011	-0.0008
1.500	0.0044	0.0026	-0.0019
2.000	0.0063	0.0037	-0.0027
3.000	0.0089	0.0052	-0.0038
4.000	0.0107	0.0063	-0.0046
5.000	0.0122	0.0072	-0.0052

Table 5-9c. Abrahamson and Silva (1996) coefficient G_3 for damping scale factors for the vertical component (from Abrahamson and Silva 1996, Table 4-6b)

Period (sec)	2% damping	3% damping	7% damping
0.010	0	0	0
0.020	0	0	0
0.030	0	0	0
0.040	0	0	0
0.050	0	0	0
0.075	0	0	0
0.100	0	0	0
0.120	0	0	0
0.125	0	0	0
0.150	0	0	0
0.170	0	0	0
0.200	0	0	0
0.240	0	0	0
0.300 – 0.750	0	0	0
1.000	-0.0014	-0.0008	0.0006
1.500	-0.0034	-0.0020	0.0015
2.000	-0.0049	-0.0029	0.0021
3.000	-0.0069	-0.0040	0.0029
4.000	-0.0083	-0.0049	0.0036
5.000	-0.0094	-0.0055	0.0040

5.2.11 Equation for log-log interpolation/extrapolation of response spectra or damping ratios

The interpolation or extrapolation of the response spectral values and damping ratios is done using linear interpolation on the log spectral acceleration – log period. Given the spectral values (or damping values) Y_1 and Y_2 at periods T_1 and T_2, respectively, then using linear interpolation on the log-log values, the spectral acceleration at period T is given by

$$\ln(Y(T)) = \ln(Y(T_1)) + [\ln(T) - \ln(T_1)] * [\ln(Y(T_2)) - \ln(Y(T_1))] / [\ln(T_2)-\ln(T_1)] \quad (14)$$

5.2.12 Campbell (1997) Attenuation Equations

The Campbell (1997) median horizontal spectral acceleration attenuation relations for strike-slip earthquakes use the form (Campbell eq 8, page 170):

$$\ln(Sa_H(g)) = \ln(A_H) + c_1 + c_2\tanh[c_3(M-4.7)]+(c_4+c_5M)R_{SEIS}+0.5c_6S_{SR}+c_6S_{HR} + c_7 \tanh(c_8D)(1- S_{HR}) + f_{SA}(D) \quad (15)$$

where M is magnitude, R_{SEIS} is the seismogenic distance, D is the depth to basement rock, S_{SR} =1 for soft-rock and 0 otherwise, and S_{HR} =1 for hard-rock sites and 0 otherwise. For D< 1 km, the function $f_{sa}(D)$ is given by

$$f_{sa}(D) = c_6 (1-S_{HR})(1-D) + 0.5\, c_6 (1-D)S_{SR} \quad (15b)$$

For a hard-rock site, (S_{SR}=0, S_{SR}=1), equation (15) becomes

$$\ln(Sa_H(g)) = \ln(pga) + c_1 + c_2\tanh[c_3(M-4.7)]+(c_4+c_5M)R_{SEIS}+c_6 \quad (16)$$

The coefficients for this relation are given in Table 5-10. For a hard-rock site (S_{HR}=1, S_{SR}=0) and a strike-slip earthquake (F=0), the mean horizontal component of peak acceleration, A_H, is given by (Campbell, eq 3, page 164)

$$\ln(A_H) = -3.512 + 0.904M - 1.328\ln\left(\sqrt{R_{SEIS}^2 + [0.149\exp(0.647M)]^2}\right) + \left[0.405 - 0.222\ln(R_{SEIS})\right] \quad (17)$$

The standard deviation for the horizontal component, σ_H, is given by (Campbell eq 10, page 171 and eq 5, page 164)

$$\sigma_H = \sqrt{\sigma_{pga}^2 + 0.27^2} \quad (18)$$

where σ_{pga} = 0.889 – 0.0691 M for M< 7.4 (19)
0.38 for M >=7.4

Table 5-10. Coefficients for the Campbell (1997) attenuation relation for horizontal spectral acceleration (from Campbell, page 170)

Period (sec)	c_1	c_2	c_3	c_4	c_5	c_6
1.0	-1.79	1.59	0.66	0.0085	-0.00100	-0.38
1.5	-2.65	1.98	0.66	0.0094	-0.00100	-0.32
2.0	-3.28	2.23	0.66	0.0100	-0.00100	-0.36
3.0	-4.07	2.39	0.66	0.0108	-0.00100	-0.22
4.0	-4.26	2.03	0.66	0.0112	-0.00100	-0.30

The Campbell (1997) median vertical spectral acceleration attenuation relations for strike-slip earthquakes (F=0) use the form (Campbell eq 13, page 171):

$$\ln(Sa_{med}(g)) = \ln(SA_H) + c_1 - 0.10M + c_2\tanh[0.71(M-4.7)] + c_3\tanh[0.66(M-4.7)] \\ -1.50\ln(R_{seis}+0.071\exp(0.661M)) + 1.89\ln(R_{seis}+0.361\exp(0.576M)) \\ + c_4\tanh(0.51D) + c_5\tanh(0.57D) \qquad (20)$$

The coefficients for this model are listed in Table 5-11. The standard deviation for the vertical component is given by (Campbell eq 16, page 171)

$$\sigma_V = \sqrt{\sigma_H^2 + 0.39^2} \qquad (21)$$

Table 5-11. Coefficients for the Campbell (1997) attenuation relation for vertical spectral acceleration (from Campbell, page 171)

Period (sec)	C1	C2	C3	C4	C5
1.0	-1.82	1.13	-1.59	0.18	-0.18
1.5	-1.81	1.52	-1.98	0.57	-0.49
2.0	-1.65	1.65	-2.23	0.61	-0.63
3.0	-1.31	1.28	-2.39	1.07	-0.84
4.0	-1.35	1.15	-2.03	1.26	-1.17

6. BODY OF CALCULATIONS

6A. Horizontal Spectra

Step 1: Short and Moderate Period Envelope

The 5% damped horizontal spectra for the DDE, Newmark Hosgri, Blume Hosgri, and LTSP/SSER 34 given in Tables 4-1, 4-2, 4-3, and 4-4 are plotted in Figure 1. Based on this figure, the spectra controlling the envelope spectrum over different period ranges are listed in Table 6-1. The resulting 5% damped high and moderate frequency envelope horizontal spectrum is developed by selecting spectral values for the period ranges listed in Table 6-1 from Tables 4-2, 4-3 and 4-4. These spectral values are listed in Table 6-2. Not all of the periods are needed to adequately define the spectrum. A few periods were interpolated to more commonly used values (indicated by the asterisks in Table 6-2).

Table 6-1. Period ranges of controlling 5% damped horizontal spectra for the short-moderate period envelope

Period range (sec)	Controlling Horizontal Spectrum
0.00 - 0.06 sec	LTSP
0.06 - 0.18 sec	Newmark Hosgri
0.18 - 0.33 sec	Blume Hosgri
0.33 - 1.00 sec	Newmark Hosgri
1.00 - 1.54 sec	Blume Hosgri
1.54 - 2.00 sec	Newmark Hosgri

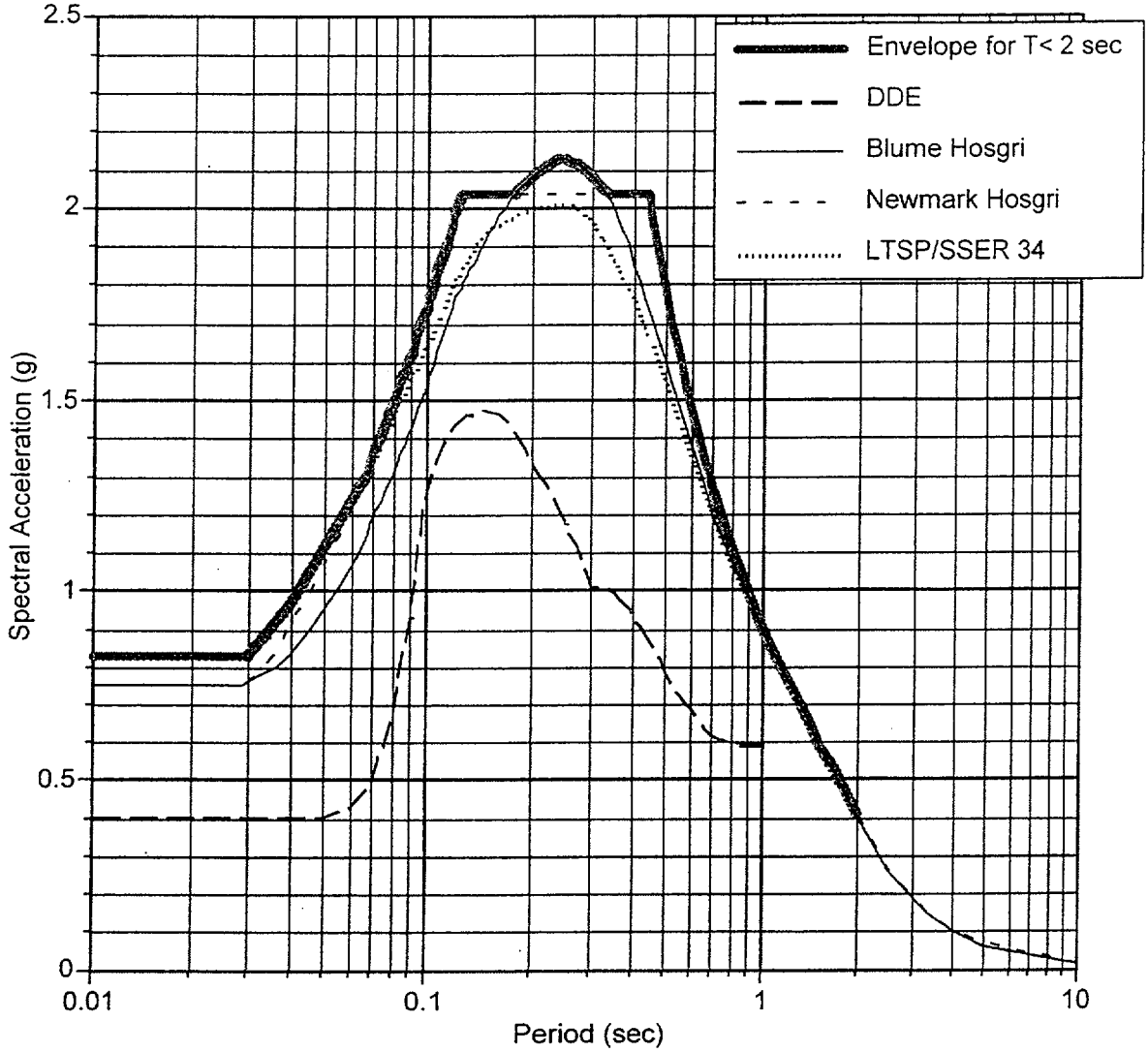

Figure 1. Comparison of the horizontal spectra for 5% damping.

Table 6-2. Short and Moderate Period (T<2 sec) Envelope for the 84th Percentile Horizontal Spectrum for 5% damping

Period (sec)	Frequency (Hz)	Sa(g)	Spectrum
0.010	100.000	0.830	LTSP
0.025	40.000	0.830	LTSP
0.030	33.333	0.830	LTSP
0.040	25.000	0.964	LTSP
0.050	20.000	1.110	LTSP
0.075	13.333	1.425	Newmark Hosgri
0.100	10.000	1.737	Newmark Hosgri
0.125	8.000	2.032	Newmark Hosgri
0.150*	6.667	2.032	Newmark Hosgri
0.170	5.882	2.032	Newmark Hosgri
0.174	5.747	2.032	Newmark Hosgri
0.178	5.618	2.033	Blume Hosgri
0.200	5.000	2.080	Blume Hosgri
0.230	4.202	2.120	Blume Hosgri
0.250	4.000	2.125	Blume Hosgri
0.270	3.704	2.115	Blume Hosgri
0.300*	3.300	2.073	Blume Hosgri
0.333	3.003	2.032	Newmark Hosgri
0.400	2.500	2.032	Newmark Hosgri
0.445	2.247	2.032	Newmark Hosgri
0.500	2.000	1.795	Newmark Hosgri
0.600*	1.667	1.496	Newmark Hosgri
0.750	1.333	1.197	Newmark Hosgri
1.000	1.000	0.898	Newmark Hosgri
1.500*	0.900	0.604	Blume Hosgri
2.000	0.500	0.411	Newmark Hosgri

* indicates an interpolated value computed using equation 14

Step 2: Estimation of Long Period Spectral Values Using Empirical Attenuation Relations

The long period horizontal 84th percentile spectral values are computed for the three empirical attenuation relations using

$M = 7.2$
$R_{rup} = 4.5$ km
$R_{seis} = 4.9$ km

For the Abrahamson and Silva (1997) relation, equation (4) with coefficients in Table 5-3 is used to compute the median ground motion. Equation (5) with coefficients in Table 5-3 and equation (7) are used to compute the 84th percentile.

For the Sadigh et al (1997) relation, equation 1 with coefficients from Table 5-1 are used to compute the median ground motion and equation 7 is used to compute the 84th percentile.

For the Idriss (1991,1994,1995) relation, equations (2) and (3) with coefficients from Table 5-2 are used to compute the median ground motion and equation 7 is used to compute the 84th percentile ground motion.

For the Campbell (1997) relation, equations (15, 16, 17) with coefficients from table 5-10 are used to compute the median ground motion and equations 18, 19 and 7 are used to compute the 84th percentile ground motion.

The computed 84th percentile spectral values are listed in Table 6-3.

Table 6-3. Long Period 5% Damped 84th Percentile Response Spectral Values From Empirical Attenuation Relations

		Spectral Acceleration (g)			
Period (sec)	Freq (Hz)	Sadigh et al. (1997)	Idriss (1991,1994, 1995)	Abrahamson and Silva (1997)	Campbell (1997)
1.0	1.00	0.805	0.802	0.902	0.414
1.5	0.67	0.506	0.471	0.578	0.268
2.0	0.50	0.354	0.321	0.412	0.174
3.0	0.33	0.201	0.186	0.235	0.106
4.0	0.25	0.130	0.127	0.149	0.058
5.0	0.20		0.094	0.106	

The long period spectra are plotted in Figure 2. The spectrum based on the Abrahamson and Silva (1997) attenuation relation is consistent with the high and moderate frequency envelope spectrum at T=2 seconds and has a long period slope that is similar to the slope of the spectra from the Sadigh et al (1997) and Idriss (1991,1994,1995) attenuation

relations. Therefore, the Abrahamson and Silva attenuation relation is used as the empirical estimate of the long period spectrum.

Step 3: Long Period Envelope Spectrum

The long period spectra from the Newmark Hosgri, Blume Hosgri, and empirical attenuation relations are shown in Figure 2. At periods greater than 2 seconds, the Abrahamson and Silva (1997) empirical attenuation relation gives the largest spectral values. These spectral values (from Table 6-3) are used to determine the long period spectrum for periods up to 5 seconds.

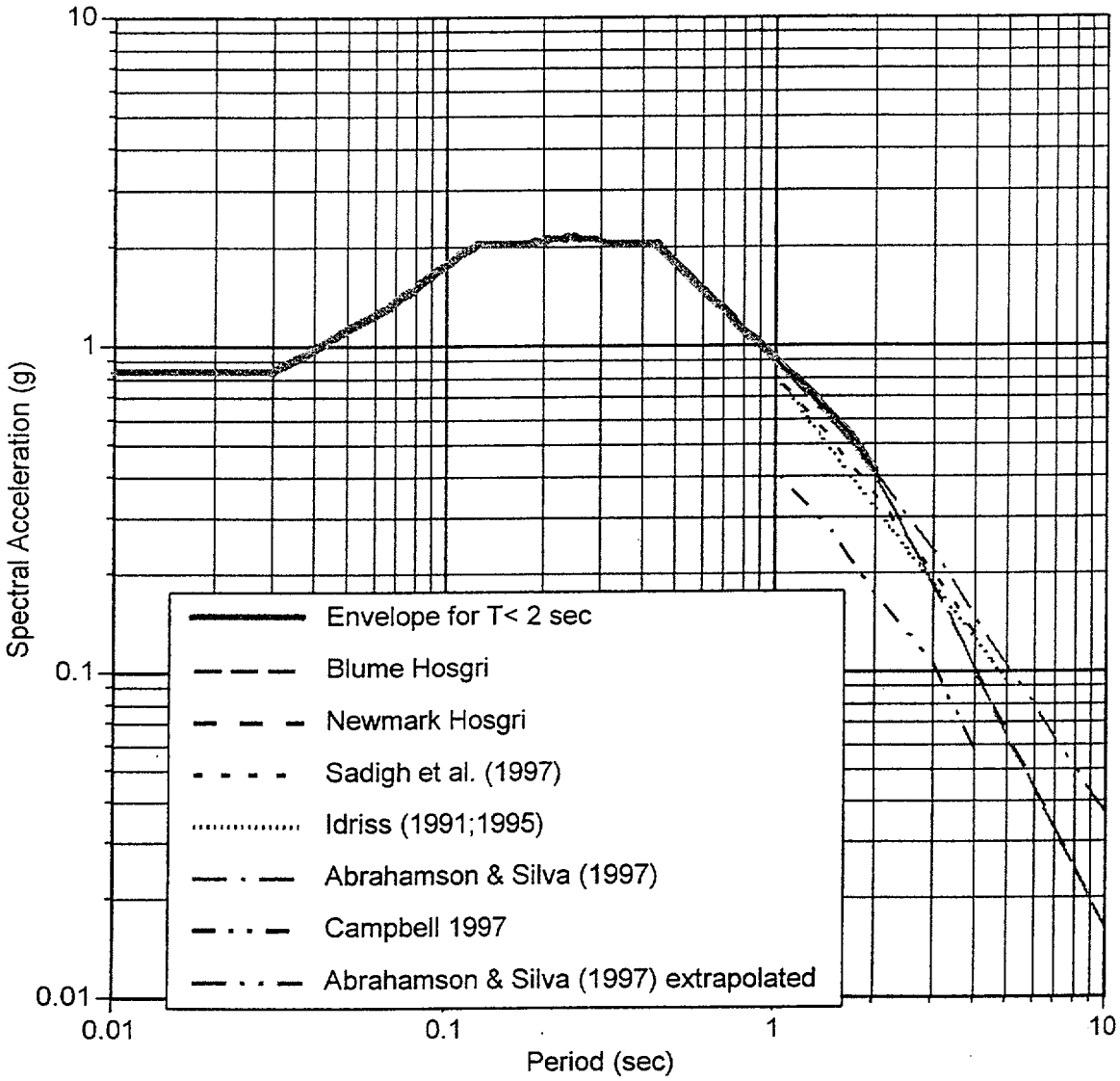

Figure 2. Comparison of long period horizontal spectra from the Blume Hosgri and Newmark Hosgri events with 84th percentile long period horizontal spectra from state-of-practice attenuation relations. (5% damping)

Step 4: Extrapolation from 5 seconds to 10 seconds

At periods greater than 5 seconds, the spectrum based on the Abrahamson & Silva attenuation relation is extrapolated using equation (14) with the following values:

$T_1 = 5.0$
$T_2 = 4.0$
$Y_1 = Sa_1 = 0.105g$
$Y_2 = Sa_2 = 0.148g$

The computed spectral values at periods greater than 5 seconds are listed in Table 6-4. These values give the average horizontal component without directivity effects.

Table 6-4. Extrapolated 84th percentile horizontal response spectrum at 5% damping.

Period (sec)	Sa (g)
5	0.105
6	0.079
7	0.063
8	0.051
9	0.042
10	0.036

Tables 6-2, 6-3 (Abrahamson and Silva, 1997 column), and 6-4 are combined to define the average horizontal component without explicit directivity effects. The resulting 84th percentile horizontal spectrum is given in Table 6-5.

Table 6-5. 84th Percentile Horizontal Spectrum for 5% damping without explicit directivity effects

Period (sec)	Frequency (Hz)	Sa(g)
0.010	100.000	0.830
0.025	40.000	0.830
0.030	33.333	0.830
0.040	25.000	0.964
0.050	20.000	1.110
0.075	13.333	1.425
0.100	10.000	1.737
0.125	8.000	2.032
0.150	6.667	2.032
0.170	5.882	2.032
0.174	5.747	2.032
0.178	5.618	2.033
0.200	5.000	2.080
0.230	4.202	2.120
0.250	4.000	2.125
0.270	3.704	2.115
0.300	3.300	2.080
0.333	3.003	2.032
0.400	2.500	2.032
0.445	2.247	2.032
0.500	2.000	1.795
0.600	1.667	1.497
0.750	1.333	1.197
1.000	1.000	0.898
1.500	0.900	0.605
2.000	0.500	0.411
3.000	0.333	0.235
4.000	0.250	0.149
5.000	0.200	0.106
6.000	0.167	0.079
7.000	0.143	0.063
8.000	0.125	0.051
9.000	0.111	0.042
10.000	0.100	0.036

Step 5: Directivity Effects for the Average Horizontal Component

The directivity scale factors for the average horizontal component computed using the Abrahamson (2000) model with the following variables:

Down-strike distance to Epicenter = 70 km
Fault Length = 110 km
Distance to fault = 4.5 km

Then

$X = 70 \text{ km} / 110 \text{ km} = 0.64$
$\theta = \text{atan}(4.5 \text{ km} / 70 \text{ km}) = 0.06 \text{ radian}$
$X \cos(\theta) = 0.64$

This value of $X\cos(\theta)$ is used along with

$M = 7.2$
$R = 4.5 \text{ km}$

in equation (8) to compute the effect of the directivity on the average horizontal component. Since $X \cos(\theta)$ is > 0.4, then the part of equation for $X \cos(\theta) > 0.4$ is used. The results are listed in the second column of Table 6-6.

Step 6: Directivity Effects for Fault Normal and Fault Parallel
The directivity scale factors for the FN/aveH and FP/aveH components are computed using the Somerville et al (1997) model (eq. 9a and 9b). The resulting scale factors are listed columns 3 and 4 in Table 6-6.

Table 6-6. Computed Median Scale Factors for Directivity Effects

Period (sec)	Scale factor for average horizontal	FN / AVE	FP / AVE	$scale_{FN}$	$scale_{FP}$
0.01 – 0.5	1.00	1.00	1.00	1.00	1.00
0.60	1.00	1.02	0.98	1.02	1.00**
0.75	1.06	1.04	0.96	1.10	1.02
1.0	1.13	1.06	0.94	1.20	1.07
1.5	1.25	1.13	0.88	1.41	1.11
2.0	1.35	1.19	0.84	1.61	1.13
3.0	1.48	1.34	0.75	1.98	1.10
4.0	1.59	1.46	0.68	2.32	1.09
5.0	1.68	1.49	0.67	2.50	1.13
6.0	1.47*	1.49	0.67	2.18	1.00**
7.0	1.31*	1.49	0.67	1.95	1.00**
8.0	1.18*	1.49	0.67	1.76	1.00**
9.0	1.08*	1.49	0.67	1.61	1.00**
10.0	1.00***	1.49	0.67	1.49	1.00**

* Scale factors based on interpolation using equation 14.
** The computed values is less than 1.0, but a value of 1.0 is used for conservatism
*** Assumed value (see assumption 3.7)

Step 7: Combination of Directivity Effects

The two directivity effects given in Table 6-6 (scale factor for the average horizontal and scale factor for the FN/ave or FP/ave) are multiplied to determine the total directivity effect (equation 10a and 10b). In Table 6-6, column 2 is multiplied by column 3 (FN/ave) to determine the directivity scale factor for the FN component. Similarly, column 2 is multiplied by column 4 (FP/ave) to determine the scale factor for the FP component. The combined scale factors for the FN and FP component are listed in columns 5 and 6, respectively, of Table 6-6.

The combined directivity scale factors are assumed to be unity at a period of 10 seconds (assumption 3.7, equations 8 through 10b). The directivity scale factors for periods between 5 and 10 seconds are computed using the linear interpolation on the log period-log Sa as defined in equation 14.

Step 8 Estimation of Response Spectra Including Directivity Effects

The directivity scale factors ($scale_{FN}$ and $scale_{FP}$) given in Table 6-6 are multiplied by the average horizontal component spectral values without directivity listed in Table 6-5. The resulting spectra are listed in Table 6-7 and are plotted in Figure 3.

Table 6-7. 84th Percentile Horizontal Spectrum for 5% damping including directivity effects

Period (sec)	Frequency (Hz)	Fault Normal Sa(g)	Fault Parallel Sa(g)
0.010	100.000	0.830	0.830
0.025	40.000	0.830	0.830
0.030	33.333	0.830	0.830
0.040	25.000	0.964	0.964
0.050	20.000	1.110	1.110
0.075	13.333	1.425	1.425
0.100	10.000	1.737	1.737
0.125	8.000	2.032	2.032
0.150	6.667	2.032	2.032
0.170	5.882	2.032	2.032
0.174	5.747	2.032	2.032
0.178	5.618	2.033	2.033
0.200	5.000	2.080	2.080
0.230	4.202	2.120	2.120
0.250	4.000	2.125	2.125
0.270	3.704	2.115	2.115
0.300	3.300	2.080	2.080
0.333	3.003	2.032	2.032
0.400	2.500	2.032	2.032
0.445	2.247	2.032	2.032
0.500	2.000	1.795	1.795
0.600	1.667	1.527	1.467
0.750	1.333	1.317	1.221
1.000	1.000	1.078	0.961
1.500	0.900	0.853	0.672
2.000	0.500	0.662	0.464
3.000	0.333	0.465	0.259
4.000	0.250	0.343	0.161
5.000	0.200	0.265	0.119
6.000	0.167	0.173	0.079
7.000	0.143	0.123	0.063
8.000	0.125	0.090	0.051
9.000	0.111	0.068	0.042
10.000	0.100	0.054	0.036

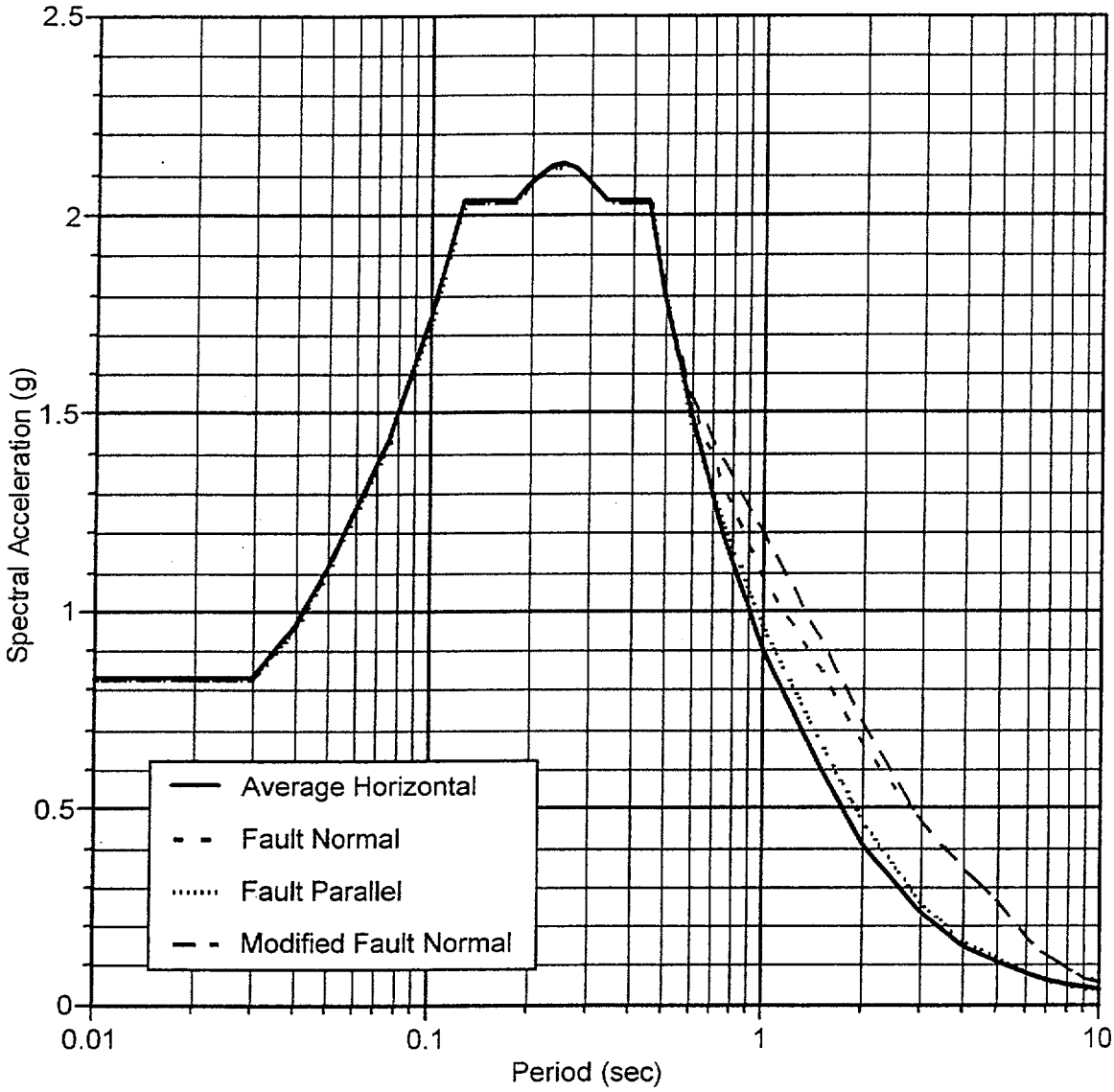

Figure 3. Incorporation of directivity effects into the horizontal spectra at 5% damping

Step 9: Added Conservatism for the Fault Normal Component

Conservatism was added to the computed fault normal spectrum by increasing the spectral acceleration at a period of 1 second from 1.078g to 1.2g. This increase was then smoothed over the period range of 0.5 sec to 3.0 sec such that there is no change at T=0.5 or at T=3. For the periods between 0.5 and 3.0 seconds, (0.6 0.75, 1.5, and 2.0 seconds), the modified values were selected such that the resulting spectrum is smooth (e.g. there is no formal calculation).

The reason for this added conservatism is to account for possible changes in the directivity effect that could impact directivity for earthquake with magnitudes less than 7.2. These smaller magnitude earthquakes may have strong directivity effects at periods near 1 second. The resulting fault normal spectrum is shown in Figure 3 as the "Modified Fault Normal". These increased spectral values for the fault normal component at 5% damping are listed in Table 6-8

Step 10: Interpolation of the Newmark Hosgri spectra for 4% damping
The Newmark Hosgri spectra (table 4-2) are given for damping values of 3% and 5%, but not for 4%. The values at 4% damping are computed using the geometric mean of the 3% and 5% damped spectra. The computed values are listed in Table 6-9.

Table 6-8. Modified 84th percentile fault normal spectral values at 5% damping including the added conservatism

Period (sec)	Frequency (Hz)	Fault Normal Sa(g)	Fault Parallel Sa(g)	
0.010	100.000	0.830	0.830	
0.025	40.000	0.830	0.830	
0.030	33.333	0.830	0.830	
0.040	25.000	0.964	0.964	
0.050	20.000	1.110	1.110	
0.075	13.333	1.425	1.425	
0.100	10.000	1.737	1.737	
0.125	8.000	2.032	2.032	
0.150	6.667	2.032	2.032	
0.170	5.882	2.032	2.032	
0.174	5.747	2.032	2.032	
0.178	5.618	2.033	2.033	
0.200	5.000	2.080	2.080	
0.230	4.202	2.120	2.120	
0.250	4.000	2.125	2.125	
0.270	3.704	2.115	2.115	
0.300	3.300	2.080	2.080	
0.333	3.003	2.032	2.032	
0.400	2.500	2.032	2.032	
0.445	2.247	2.032	2.032	
0.500	2.000	1.795	1.795	
0.600	1.667	1.541	1.467	Modified FN
0.750	1.333	1.383	1.221	Modified FN
1.000	1.000	1.200	0.961	Modified FN
1.500	0.900	0.931	0.672	Modified FN
2.000	0.500	0.713	0.464	Modified FN
3.000	0.333	0.465	0.259	
4.000	0.250	0.343	0.161	
5.000	0.200	0.265	0.119	
6.000	0.167	0.173	0.079	
7.000	0.143	0.123	0.063	
8.000	0.125	0.090	0.051	
9.000	0.111	0.068	0.042	
10.000	0.100	0.054	0.036	

Table 6-9. Interpolated Digital values for the Newmark Hosgri horizontal spectra at 4% damping.

Period (sec)	Frequency (Hz)	3% damping	5% damping	4% damping
0.029	34.483	0.750	0.750	0.750
0.032	31.250	0.790	0.784	0.787
0.036	27.778	0.860	0.842	0.851
0.040	25.000	0.944	0.912	0.928
0.045	22.222	1.050	0.997	1.023
0.050	20.000	1.136	1.067	1.101
0.056	17.857	1.240	1.149	1.194
0.059	16.949	1.300	1.195	1.246
0.063	15.873	1.367	1.268	1.317
0.067	14.925	1.443	1.306	1.373
0.069	14.493	1.484	1.334	1.407
0.071	14.085	1.528	1.371	1.447
0.074	13.514	1.574	1.408	1.489
0.075	13.333	1.588	1.425	1.504
0.077	12.987	1.624	1.444	1.531
0.078	12.821	1.651	1.464	1.555
0.080	12.500	1.678	1.489	1.581
0.082	12.195	1.706	1.506	1.603
0.083	12.048	1.736	1.528	1.629
0.085	11.765	1.767	1.551	1.655
0.087	11.494	1.795	1.574	1.681
0.089	11.236	1.831	1.599	1.711
0.091	10.989	1.866	1.624	1.741
0.093	10.753	1.902	1.651	1.772
0.095	10.526	1.939	1.678	1.804
0.098	10.204	1.978	1.707	1.838
0.100	10.000	2.019	1.737	1.873
0.103	9.709	2.062	1.768	1.909
0.105	9.524	2.107	1.801	1.948
0.108	9.259	2.154	1.835	1.988
0.111	9.009	2.204	1.870	2.030
0.114	8.772	2.256	1.908	2.075
0.118	8.475	2.311	1.947	2.121
0.121	8.264	2.369	1.989	2.171
0.125	8.000	2.430	2.032	2.222
0.127	7.874	2.430	2.032	2.222
0.129	7.752	2.430	2.032	2.222

Table 6-9. (cont)

Period (sec)	Frequency (Hz)	3% damping	5% damping	4% damping
0.131	7.634	2.430	2.032	2.222
0.133	7.519	2.430	2.032	2.222
0.136	7.353	2.430	2.032	2.222
0.138	7.246	2.430	2.032	2.222
0.140	7.143	2.430	2.032	2.222
0.143	6.993	2.430	2.032	2.222
0.146	6.849	2.430	2.032	2.222
0.148	6.757	2.430	2.032	2.222
0.151	6.623	2.430	2.032	2.222
0.154	6.494	2.430	2.032	2.222
0.157	6.369	2.430	2.032	2.222
0.160	6.250	2.430	2.032	2.222
0.163	6.135	2.430	2.032	2.222
0.167	5.988	2.430	2.032	2.222
0.170	5.882	2.430	2.032	2.222
0.174	5.747	2.430	2.032	2.222
0.178	5.618	2.430	2.032	2.222
0.182	5.495	2.430	2.032	2.222
0.186	5.376	2.430	2.032	2.222
0.190	5.263	2.430	2.032	2.222
0.195	5.128	2.430	2.032	2.222
0.200	5.000	2.430	2.032	2.222
0.204	4.902	2.430	2.032	2.222
0.208	4.808	2.430	2.032	2.222
0.213	4.695	2.430	2.032	2.222
0.217	4.608	2.430	2.032	2.222
0.222	4.505	2.430	2.032	2.222
0.227	4.405	2.430	2.032	2.222
0.233	4.292	2.430	2.032	2.222
0.238	4.202	2.430	2.032	2.222
0.244	4.098	2.430	2.032	2.222
0.250	4.000	2.430	2.032	2.222
0.256	3.906	2.430	2.032	2.222
0.263	3.802	2.430	2.032	2.222
0.270	3.704	2.430	2.032	2.222
0.278	3.597	2.430	2.032	2.222
0.290	3.448	2.430	2.032	2.222
0.303	3.300	2.430	2.032	2.222
0.317	3.155	2.430	2.032	2.222
0.333	3.003	2.430	2.032	2.222
0.345	2.899	2.430	2.032	2.222
0.357	2.801	2.430	2.032	2.222

Table 6-9. (cont)

Period (sec)	Frequency (Hz)	3% damping	5% damping	4% damping
0.370	2.703	2.430	2.032	2.222
0.385	2.597	2.430	2.032	2.222
0.400	2.500	2.430	2.032	2.222
0.417	2.398	2.430	2.032	2.222
0.427	2.342	2.430	2.032	2.222
0.435	2.299	2.378	2.032	2.198
0.445	2.247	2.315	2.032	2.169
0.455	2.198	2.265	1.975	2.115
0.476	2.101	2.165	1.885	2.020
0.500	2.000	2.062	1.795	1.924
0.526	1.901	1.959	1.705	1.828
0.556	1.799	1.856	1.616	1.732
0.588	1.701	1.753	1.526	1.636
0.625	1.600	1.650	1.436	1.539
0.667	1.499	1.546	1.346	1.443
0.714	1.401	1.443	1.257	1.347
0.769	1.300	1.340	1.167	1.251
0.833	1.200	1.237	1.077	1.154
0.909	1.100	1.134	0.987	1.058
1.000	1.000	1.031	0.898	0.962
1.111	0.900	0.928	0.808	0.866
1.250	0.800	0.825	0.718	0.770
1.429	0.700	0.722	0.628	0.673
1.538	0.650	0.670	0.583	0.625
1.667	0.600	0.619	0.539	0.578
2.000	0.500	0.457	0.411	0.433
2.500	0.400	0.283	0.263	0.273
3.333	0.300	0.165	0.148	0.156
4.000	0.250	0.114	0.103	0.108
5.000	0.200	0.073	0.066	0.069
10.000	0.100	0.018	0.016	0.017

Step 11: Horizontal Spectra at Damping Values of 2%, 4%, and 7%

The Abrahamson and Silva (1996) damping scale factors for the horizontal component are computed using equation 12b with coefficients given in Tables 5-8a, 5-8b, and 5-8c with a magnitude of 7.2. The resulting scale factors for 2%, 3%, and 7% damping are listed in Table 6-10. The Abrahamson and Silva (1996) scale factors are only defined for period up to 5 seconds. For periods greater than 5 seconds, the scale factor is assumed to be equal to the value at 5 seconds.

The scale factors were developed for 3% damping, but not 4% damping. To estimate the 4% damping scale factors, the square root of the 3% damping scale factor is used. This corresponds to assuming that the spectrum at 4% damping is given by the geometric mean of the 3% damping and 5% damping spectral values.

The spectral values for dampings of 2%, 4% and 7% are computed by multiplying the 5% damped spectra (Table 6-7) by the scale factors (see equation 13). The computed horizontal spectra are listed in Table 6-11 and 6-12 for the fault normal and fault parallel components, respectively.

Table 6-10. Median damping scale factors for the horizontal component based on the Abrahamson and Silva (1996) model.

Period (sec)	2%/5%	3%/5%	4%/5%	7%/5%
0.010	1.000	1.000	1.000	1.000
0.025	1.000	1.000	1.000	1.000
0.030	1.047	1.028	1.014	0.980
0.040	1.086	1.051	1.025	0.964
0.050	1.115	1.067	1.033	0.953
0.075	1.171	1.098	1.048	0.932
0.100	1.212	1.121	1.059	0.918
0.125	1.242	1.151	1.073	0.900
0.150	1.257	1.151	1.073	0.900
0.170	1.269	1.151	1.073	0.900
0.174	1.269	1.151	1.073	0.900
0.178	1.269	1.151	1.073	0.900
0.200	1.269	1.151	1.073	0.900
0.230	1.269	1.151	1.073	0.900
0.250	1.269	1.151	1.073	0.900
0.270	1.269	1.151	1.073	0.900
0.300	1.269	1.151	1.073	0.900
0.333	1.269	1.151	1.073	0.900
0.400	1.269	1.151	1.073	0.900
0.445	1.269	1.151	1.073	0.900
0.500	1.269	1.151	1.073	0.900
0.600	1.269	1.151	1.073	0.900
0.75	1.269	1.151	1.073	0.900
1	1.266	1.150	1.072	0.901
1.5	1.258	1.146	1.070	0.903
2	1.249	1.141	1.068	0.906
3	1.230	1.131	1.063	0.912
4	1.213	1.121	1.059	0.918
5	1.197	1.112	1.055	0.923
6	1.197	1.112	1.055	0.923
7	1.197	1.112	1.055	0.923
8	1.197	1.112	1.055	0.923
9	1.197	1.112	1.055	0.923
10	1.197	1.112	1.055	0.923

Table 6-11. 84th Percentile Fault Normal Spectra at Multiple Dampings (before adjustments)

Period (sec)	Frequency (Hz)	5% (from table 6-7)	2%	4%	7%
0.010	100.000	0.830	0.830	0.830	0.830
0.025	40.000	0.830	0.830	0.830	0.830
0.030	33.333	0.830	0.869	0.842	0.830
0.040	25.000	0.964	1.047	0.988	0.929
0.050	20.000	1.110	1.238	1.147	1.058
0.075	13.333	1.425	1.669	1.493	1.328
0.100	10.000	1.737	2.105	1.839	1.595
0.125	8.000	2.032	2.524	2.180	1.829
0.150	6.667	2.032	2.579	2.180	1.829
0.170	5.882	2.032	2.579	2.180	1.829
0.174	5.747	2.032	2.579	2.180	1.829
0.178	5.618	2.033	2.580	2.181	1.830
0.200	5.000	2.080	2.640	2.232	1.872
0.230	4.202	2.120	2.690	2.275	1.908
0.250	4.000	2.125	2.697	2.280	1.913
0.270	3.704	2.115	2.684	2.269	1.904
0.300	3.333	2.080	2.640	2.232	1.872
0.333	3.003	2.032	2.579	2.180	1.829
0.400	2.500	2.032	2.579	2.180	1.829
0.445	2.247	2.032	2.579	2.180	1.829
0.500	2.000	1.795	2.278	1.926	1.616
0.600	1.667	1.541	1.956	1.653	1.387
0.750	1.333	1.383	1.755	1.484	1.245
1.000	1.000	1.199	1.518	1.285	1.080
1.500	0.667	0.931	1.171	0.996	0.841
2.000	0.500	0.713	0.891	0.761	0.646
3.000	0.333	0.465	0.572	0.494	0.424
4.000	0.250	0.343	0.416	0.364	0.315
5.000	0.200	0.265	0.317	0.280	0.245
6.000	0.167	0.173	0.207	0.183	0.160
7.000	0.143	0.123	0.147	0.130	0.113
8.000	0.125	0.090	0.107	0.095	0.083
9.000	0.111	0.068	0.081	0.071	0.062
10.000	0.100	0.054	0.064	0.057	0.050

* Fixed at the PGA level.

Table 6-12. 84th Percentile Fault Parallel Spectra at Multiple Dampings (before adjustment)

Period (sec)	Frequency (Hz)	5% (from table 6-7)	2%	4%	7%
0.010	100.000	0.830	0.830	0.830	0.830
0.025	40.000	0.830	0.830	0.830	0.830
0.030	33.333	0.830	0.869	0.842	0.830*
0.040	25.000	0.964	1.047	0.988	0.929
0.050	20.000	1.110	1.238	1.147	1.058
0.075	13.333	1.425	1.669	1.493	1.328
0.100	10.000	1.737	2.105	1.839	1.595
0.125	8.000	2.032	2.524	2.180	1.829
0.150	6.667	2.032	2.579	2.180	1.829
0.170	5.882	2.032	2.579	2.180	1.829
0.174	5.747	2.032	2.579	2.180	1.829
0.178	5.618	2.033	2.580	2.181	1.830
0.200	5.000	2.080	2.640	2.232	1.872
0.230	4.202	2.120	2.690	2.275	1.908
0.250	4.000	2.125	2.697	2.280	1.913
0.270	3.704	2.115	2.684	2.269	1.904
0.300	3.333	2.080	2.640	2.232	1.872
0.333	3.003	2.032	2.579	2.180	1.829
0.400	2.500	2.032	2.579	2.180	1.829
0.445	2.247	2.032	2.579	2.180	1.829
0.500	2.000	1.795	2.278	1.926	1.616
0.600	1.667	1.467	1.862	1.574	1.320
0.750	1.333	1.007	1.278	1.080	0.906
1.000	1.000	0.961	1.216	1.030	0.866
1.500	0.667	0.672	0.845	0.719	0.606
2.000	0.500	0.464	0.580	0.496	0.421
3.000	0.333	0.259	0.318	0.275	0.236
4.000	0.250	0.161	0.196	0.171	0.148
5.000	0.200	0.119	0.143	0.126	0.110
6.000	0.167	0.079	0.095	0.083	0.073
7.000	0.143	0.063	0.075	0.066	0.058
8.000	0.125	0.051	0.061	0.054	0.047
9.000	0.111	0.042	0.050	0.044	0.039
10.000	0.100	0.036	0.043	0.038	0.033

* Fixed at the PGA level.

Step 12: Increase Spectra if needed to envelope DCPP spectra

The horizontal spectra at dampings of 2%, 4%, and 7% listed in Tables 6-11 and 6-12 are plotted in Figures 4, 5, and 6, respectively. In these figures, the horizontal spectra are compared to the DCPP spectra (DDE, HE) to check that the spectra envelop the DCPP spectra. Differences less than 1% are not considered to be significant.

At 2% damping (Figure 4), the horizontal spectra envelop the DDE spectra at all periods.

At 4% damping (Figure 5), the Newmark Hosgri spectrum slightly exceeds (by about 2%) the computed spectrum over the period range of 0.12 to 0.42 seconds. The Blume Hosgri spectrum slightly exceeds the computed spectrum over the period range of 0.24 to 0.32 seconds.

At 7% damping (Figure 6), the horizontal spectra envelop the Newmark Hosgri and Blume Hosgri spectra at all periods.

The 5% damped horizontal spectra are increased over the period range 0.10 to 0.42 seconds so that the scaled spectrum at 4%and 7% damping will envelop the Newmark and Blume Hosgri spectra. The adjusted horizontal spectra are listed in Tables 6-13 and 6-14 and the adjusted spectra at 4% damping are plotted in Figure 7. The adjusted 4% spectra envelop the Hosgri spectra at 4% damping at all periods (within 1% accuracy).

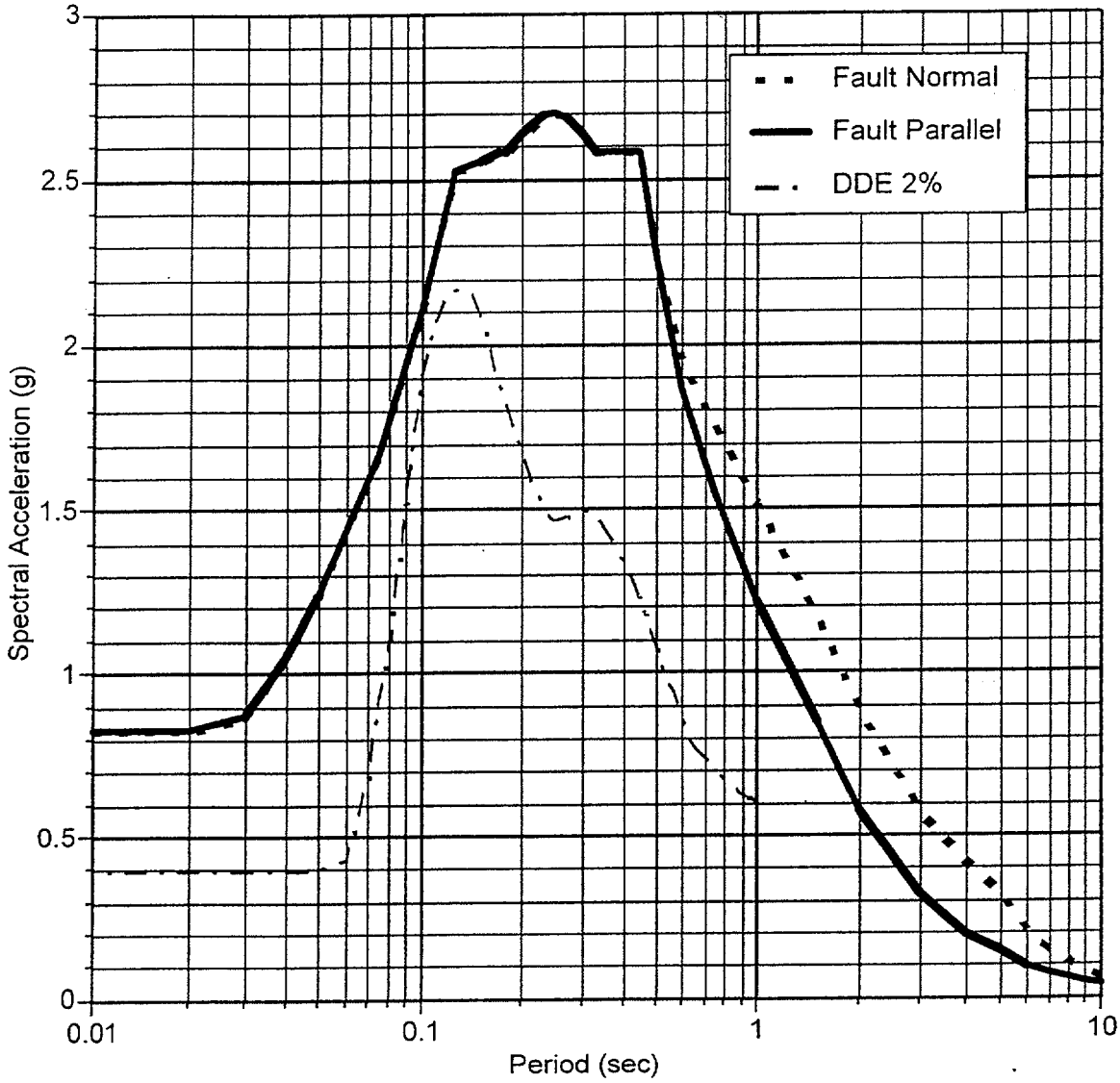

Figure 4. Comparison of the horizontal spectra at 2% damping .

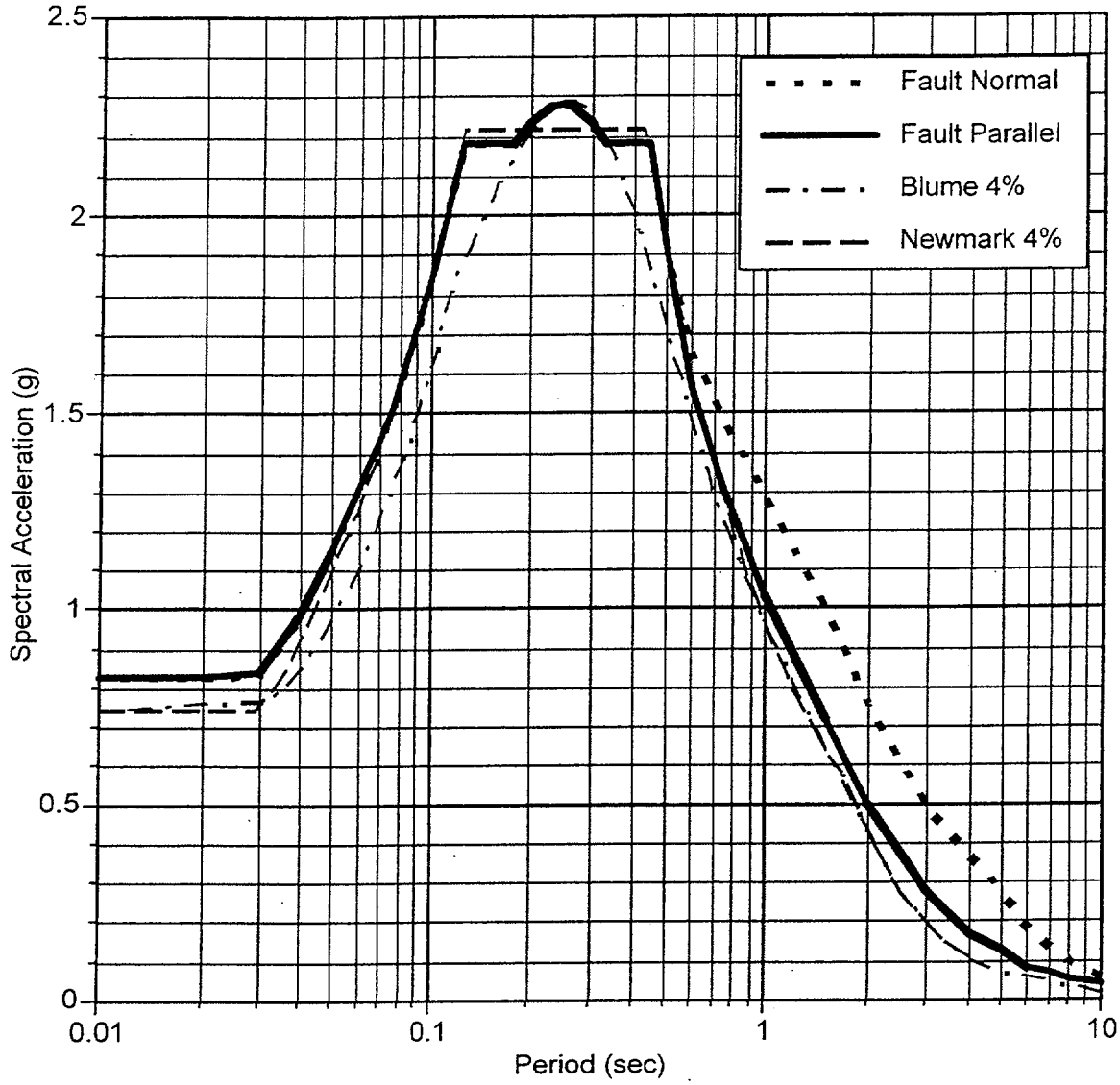

Figure 5. Comparison of the horizontal spectra at 4% damping .

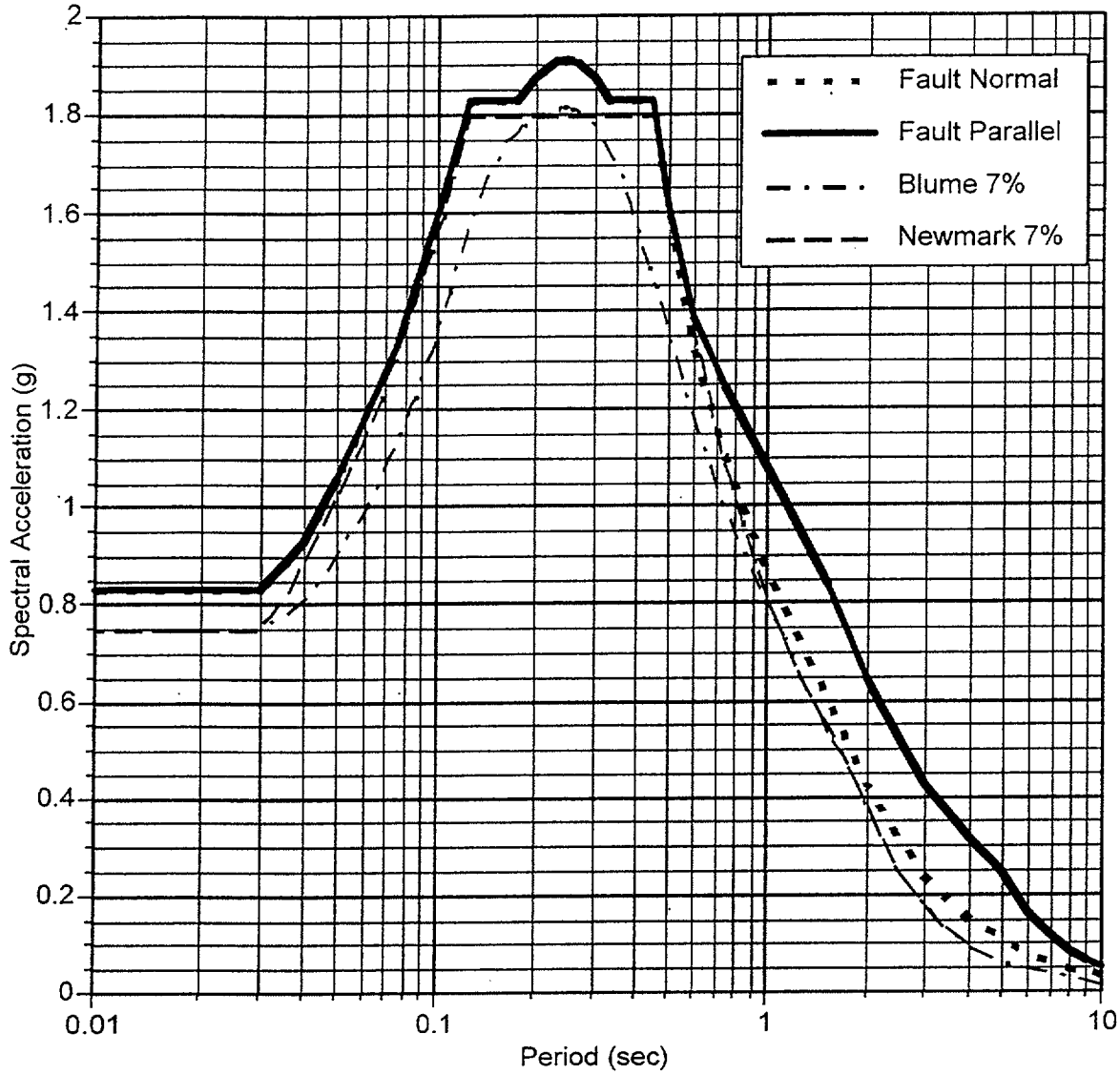

Figure 6. Comparison of the horizontal spectra at 7% damping .

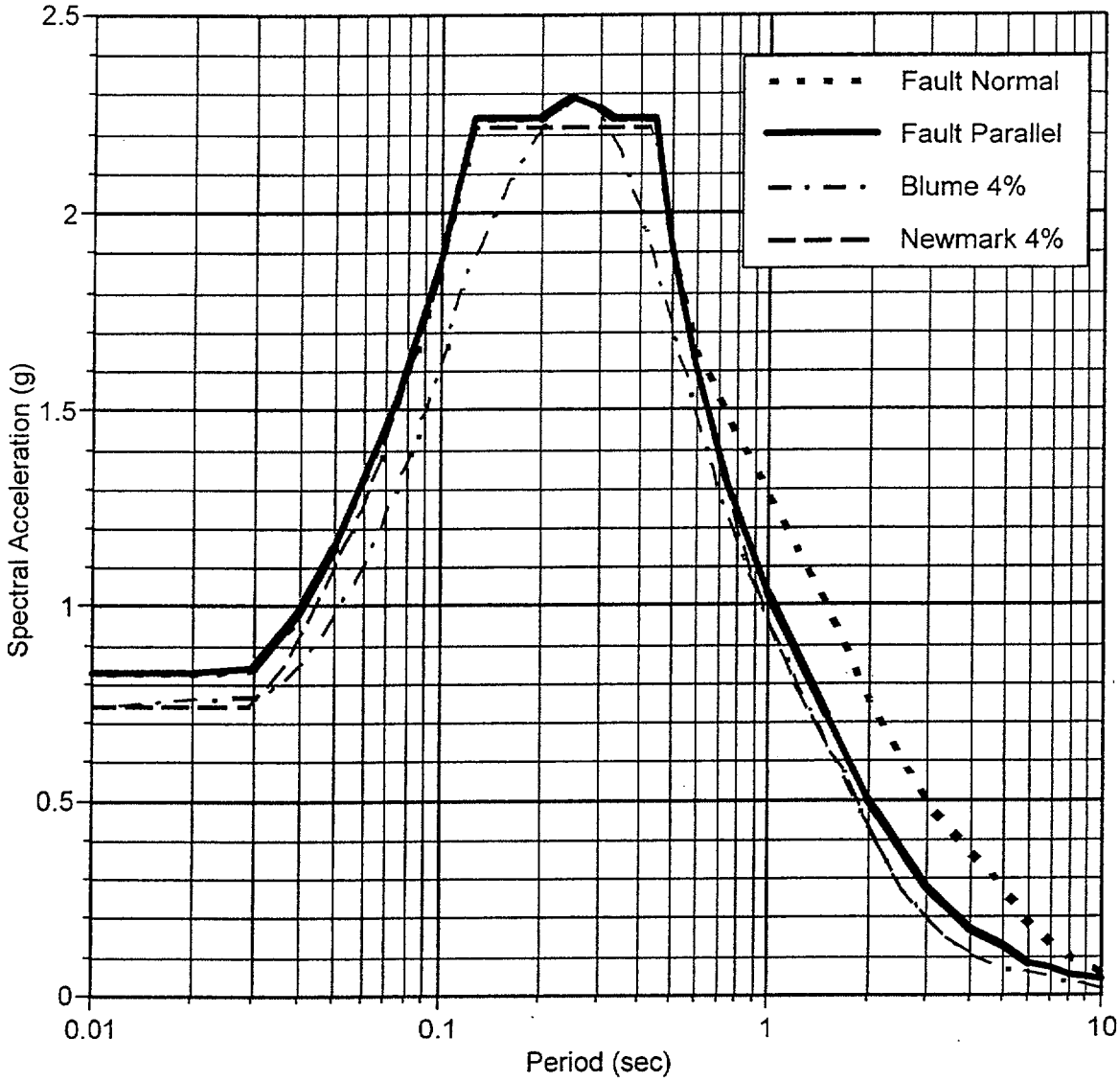

Figure 7. Comparison of the horizontal spectra at 4% damping after adjustment.

Table 6-13. 84th Percentile Final Spectra for the Fault Normal Component

Period (sec)	Frequency (Hz)	5%	2%	4%	7%
0.010	100.000	0.830	0.830	0.830	0.830
0.025	40.000	0.830	0.830	0.830	0.830
0.030	33.333	0.830	0.869	0.842	0.830
0.040	25.000	0.964	1.047	0.988	0.929
0.050	20.000	1.110	1.238	1.147	1.058
0.075	13.333	1.454	1.703	1.524	1.355
0.100	10.000	1.772	2.148	1.877	1.627
0.125	8.000	2.084	2.588	2.236	1.876
0.150	6.667	2.084	2.620	2.236	1.876
0.170	5.882	2.084	2.645	2.236	1.876
0.174	5.747	2.084	2.645	2.236	1.876
0.178	5.618	2.085	2.646	2.237	1.877
0.200	5.000	2.086	2.647	2.238	1.877
0.230	4.202	2.120	2.690	2.275	1.908
0.250	4.000	2.135	2.709	2.291	1.922
0.270	3.704	2.125	2.697	2.280	1.913
0.300	3.333	2.105	2.671	2.259	1.895
0.333	3.003	2.084	2.645	2.236	1.876
0.400	2.500	2.084	2.645	2.236	1.876
0.445	2.247	2.084	2.645	2.236	1.876
0.500	2.000	1.795	2.278	1.926	1.616
0.600	1.667	1.541	1.956	1.653	1.387
0.750	1.333	1.383	1.755	1.484	1.245
1.000	1.000	1.199	1.518	1.285	1.080
1.500	0.667	0.931	1.171	0.996	0.841
2.000	0.500	0.713	0.891	0.761	0.646
3.000	0.333	0.465	0.572	0.494	0.424
4.000	0.250	0.343	0.416	0.363	0.315
5.000	0.200	0.265	0.317	0.280	0.245
6.000	0.167	0.173	0.207	0.183	0.160
7.000	0.143	0.123	0.147	0.130	0.114
8.000	0.125	0.090	0.108	0.095	0.083
9.000	0.111	0.068	0.081	0.072	0.063
10.000	0.100	0.054	0.065	0.057	0.050

Table 6-14. 84th Percentile Final Spectra for the Fault Parallel Component.

Period (sec)	Frequency (Hz)	5%	2%	4%	7%
0.010	100.000	0.830	0.830	0.830	0.830
0.025	40.000	0.830	0.830	0.830	0.830
0.030	33.333	0.830	0.869	0.842	0.830
0.040	25.000	0.964	1.047	0.988	0.929
0.050	20.000	1.110	1.238	1.147	1.058
0.075	13.333	1.454	1.703	1.524	1.355
0.100	10.000	1.772	2.148	1.877	1.627
0.125	8.000	2.084	2.588	2.236	1.876
0.150	6.667	2.084	2.620	2.236	1.876
0.170	5.882	2.084	2.645	2.236	1.876
0.174	5.747	2.084	2.645	2.236	1.876
0.178	5.618	2.085	2.646	2.237	1.877
0.200	5.000	2.086	2.647	2.238	1.877
0.230	4.202	2.120	2.690	2.275	1.908
0.250	4.000	2.135	2.709	2.291	1.922
0.270	3.704	2.125	2.697	2.280	1.913
0.300	3.333	2.105	2.671	2.259	1.895
0.333	3.003	2.084	2.645	2.236	1.876
0.400	2.500	2.084	2.645	2.236	1.876
0.445	2.247	2.084	2.645	2.236	1.876
0.500	2.000	1.795	2.278	1.926	1.616
0.600	1.667	1.500	1.904	1.610	1.350
0.750	1.333	1.221	1.549	1.310	1.099
1.000	1.000	0.961	1.217	1.030	0.866
1.500	0.667	0.672	0.845	0.719	0.607
2.000	0.500	0.464	0.580	0.496	0.420
3.000	0.333	0.259	0.319	0.275	0.236
4.000	0.250	0.161	0.195	0.170	0.148
5.000	0.200	0.119	0.142	0.126	0.110
6.000	0.167	0.079	0.095	0.083	0.073
7.000	0.143	0.063	0.075	0.066	0.058
8.000	0.125	0.051	0.061	0.054	0.047
9.000	0.111	0.042	0.050	0.044	0.039
10.000	0.100	0.036	0.043	0.038	0.033

6B. Vertical Spectra

Step 1: Short and Moderate Period Envelope

The 5% damped vertical spectra for the DDE, Newmark Hosgri, Blume Hosgri, and LTSP/SSER 34 are plotted in Figure 8. Based on this figure, the spectra controlling the envelope spectrum over different period ranges are listed in Table 6-15. The resulting short and moderate period envelope vertical spectrum is listed in Table 6-16.

Table 6-15. Period ranges of controlling 5% damped 84th percentile vertical spectrum for the short-moderate period envelope

Period range (sec)	Controlling Vertical Spectrum
0.00 - 0.21 sec	LTSP
0.21 - 0.32 sec	Blume Hosgri
0.32 – 1.00 sec	Newmark Hosgri
1.00 - 1.50 sec	Blume Hosgri
1.50 - 2.00 sec	Newmark Hosgri

Table 6-16. Short and Moderate Period (T< 2 sec) Envelope for the 84th percentile Vertical Component for 5% damping

Period (sec)	Frequency (Hz)	Sa (g)	Spectrum
0.010	100.000	0.700	LTSP
0.025	40.000	0.700	LTSP
0.030	33.333	0.830	LTSP
0.040	25.000	1.109	LTSP
0.050	20.000	1.410	LTSP
0.075	13.333	1.727	LTSP
0.100	10.000	1.990	LTSP
0.120	8.333	1.890	LTSP
0.150	6.667	1.720	LTSP
0.170	5.882	1.610	LTSP
0.200	5.000	1.470	LTSP
0.250	4.000	1.424	Blume Hosgri
0.300	3.333	1.390	Blume Hosgri
0.400	2.500	1.361	Newmark Hosgri
0.450	2.222	1.361	Newmark Hosgri
0.500	2.000	1.203	Newmark Hosgri
0.600	1.667	1.012	Newmark Hosgri
0.750	1.333	0.819	Newmark Hosgri
1.000	1.000	0.602	Newmark Hosgri
1.500	0.667	0.413	Blume Hosgri
2.000	0.500	0.275	Newmark Hosgri

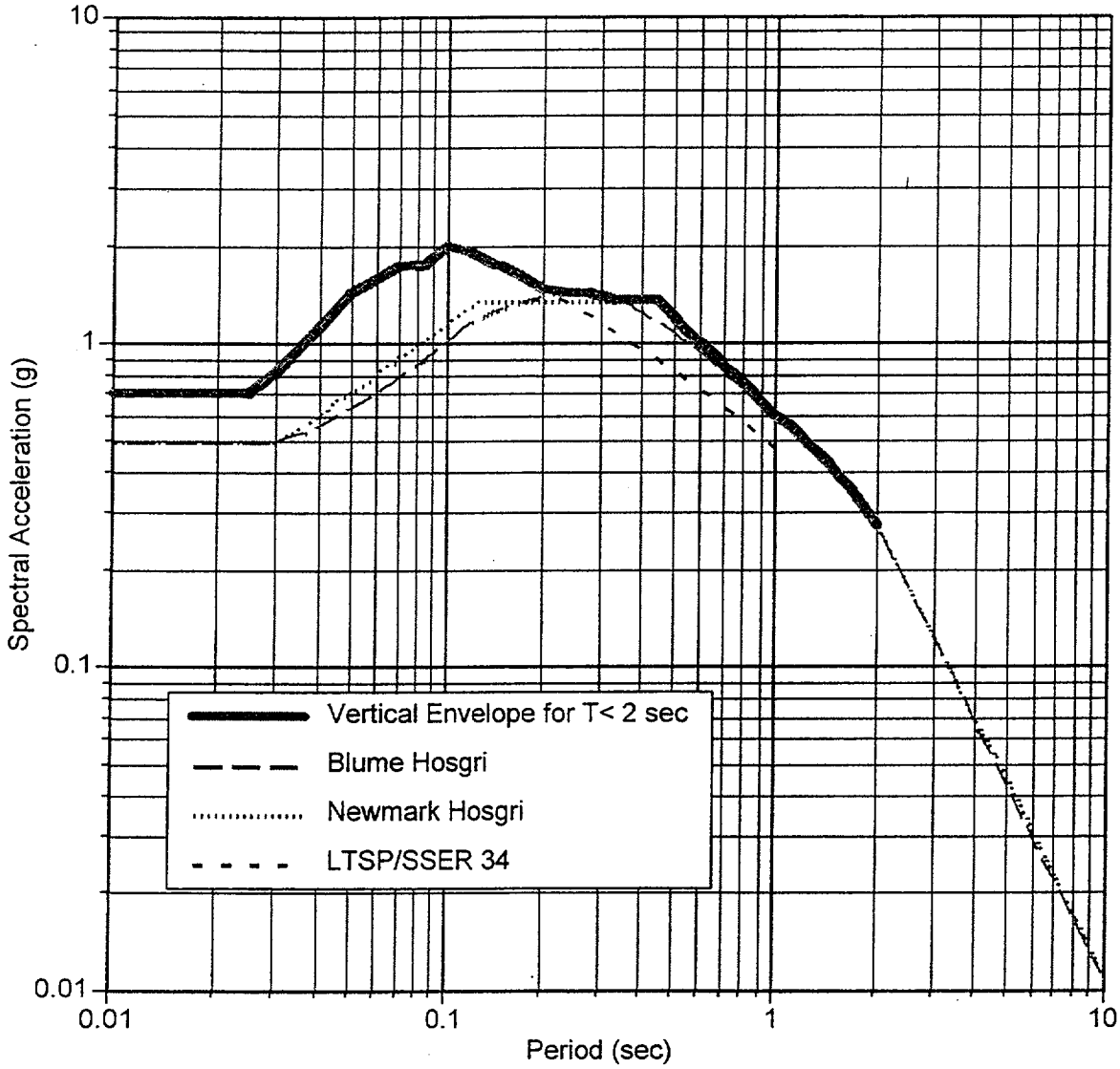

Figure 8. Vertical spectra for 5% damping.

Step 2. Empirical Evaluation of the V/H ratio at long periods

The median horizontal and vertical spectral acceleration were computed for the Abrahamson and Silva (1997) and for the Sadigh et al (1993,1997). The following inputs were used:

$M = 7.2$
$R_{Rup} = 4.5$ km
$R_{seis} = 4.9$ km
$D = 0$ km for Campbell depth to basement rock

These inputs were used in the following equations:

Eq 1 for Sadigh et al (1997) horizontal using R_{Rup}
Eq 6 for Sadigh et al (1993) vertical using R_{Rup}
Eq 4 for Abrahamson and Silva (1997) horizontal and vertical using R_{Rup}
Eq 16 for Campbell (1997) horizontal using R_{seis}
Eq 20 for Campbell (1997) vertical using R_{seis}

The results are listed in Table 6-17.

Table 6-17. Vertical/Horizontal ratio for long periods for empirical attenuation relations.

	Median Horizontal			Median Vertical			V/H ratio		
Period (sec)	Sadigh et al. (1997)	A&S (1997)	Campbell (1997)	Sadigh et al (1993)	A&S (1997)	Campbell (1997)	Sadigh et al (1993,1997)	A&S (1997)	Campbell (1997)
1	0.477	0.498	0.257	0.259	0.214	0.150	0.54	0.43	0.584
1.5	0.300	0.311	0.167	0.175	0.149	0.099	0.58	0.48	0.593
2	0.210	0.217	0.108	0.127	0.116	0.067	0.61	0.53	0.624
3	0.119	0.120	0.066	0.079	0.078	0.035	0.67	0.65	0.533
4	0.077	0.074	0.036	0.000	0.057	0.023		0.77	0.632
5		0.052		0.000	0.046			0.89	

At periods of 3 seconds or less, the V/H ratios are less than or equal to the commonly assumed value of 2/3. The Sadigh et al (1993) vertical model does not include coefficients for periods longer than 3 seconds. The ratios based on the Abrahamson and Silva model increase above 2/3 at periods greater than 3 seconds; however, these ratios are based on sparse data and are not very reliable. At period greater than 3 seconds, the V/H ratio is assumed to be 2/3. Using this ratio, the resulting vertical response spectral values at 5% damping are listed in Table 6-18. The horizontal spectrum values are from Table 6-5.

Table 6-18. 84th percentile long period vertical response spectral values (5% damping)

Period (sec)	V/H ratio	Horizontal Sa(g)	Vertical Sa(g)
2	0.67	0.411	0.275
3	0.67	0.235	0.157
4	0.67	0.149	0.100
5	0.67	0.106	0.071
6	0.67	0.079	0.053
7	0.67	0.063	0.042
8	0.67	0.051	0.034
9	0.67	0.042	0.028
10	0.67	0.036	0.024

Step 3: Envelop DCPP vertical spectra and the extended empirical vertical spectrum

The vertical spectra (5% damping) from the Newmark Hosgri, Blume Hosgri, and extended empirical model are shown in Figure 9. The extended empirical model controls the envelope for periods greater than 2 seconds.

The vertical spectrum is developed by combining Tables 6-16 and 6-18. The resulting spectrum is listed in Table 6-19.

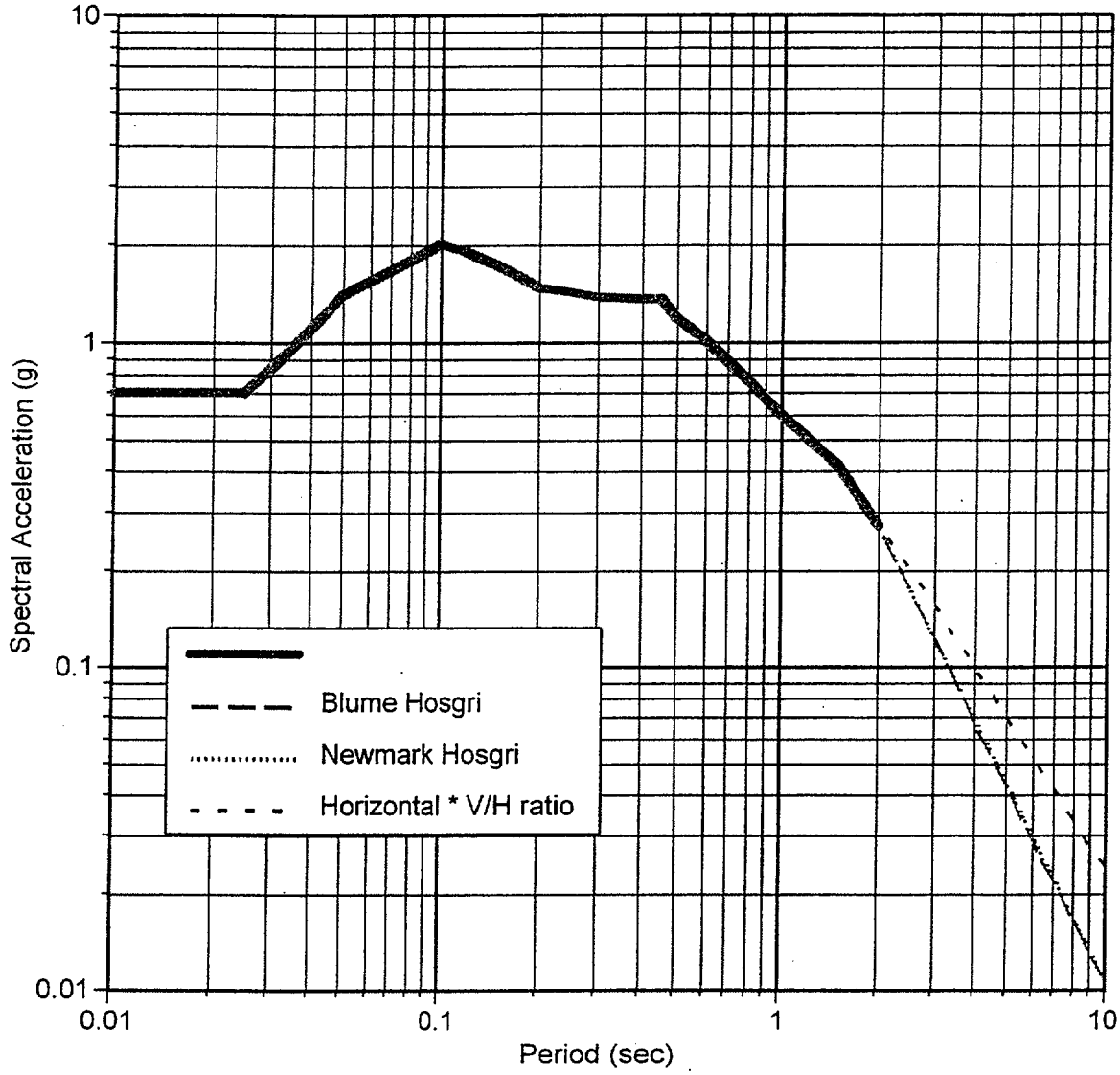

Figure 9. Long period vertical spectrum at 5% damping.

Table 6-19. 84th percentile Vertical Spectrum for 5% damping

Period (sec)	Frequency (Hz)	Sa (g)
0.010	100.000	0.700
0.025	40.000	0.700
0.030	33.333	0.830
0.040	25.000	1.109
0.050	20.000	1.410
0.075	13.333	1.727
0.100	10.000	1.990
0.120	8.333	1.890
0.150	6.667	1.720
0.170	5.882	1.610
0.200	5.000	1.470
0.250	4.000	1.424
0.300	3.333	1.390
0.400	2.500	1.361
0.450	2.222	1.361
0.500	2.000	1.203
0.600	1.667	1.012
0.750	1.333	0.819
1.000	1.000	0.602
1.500	0.667	0.413
2.000	0.500	0.275
3.000	0.333	0.157
4.000	0.250	0.100
5.000	0.200	0.071
6.000	0.167	0.053
7.000	0.143	0.042
8.000	0.125	0.034
9.000	0.111	0.028
10.000	0.100	0.024

Step 4: Vertical spectra at damping values of 2%, 4%, and 7%

The Abrahamson and Silva (1996) scale factors for the vertical component (eq 12, Tables 5-9a, 5-9b, and 5-9c) computed for a magnitude 7.2 earthquake are listed in Table 6-20. The Abrahamson and Silva scale factors are only defined for period up to 5 seconds. For periods greater than 5 seconds, the scale factor is assumed to be equal to the value at 5 seconds.

The scale factors were developed for 3% damping, but not 4% damping. To estimate the 4% damping scale factors, the square root of the 3% damping scale factor is used. This corresponds to assuming that the spectrum at 4% damping is given by the geometric mean of the 3% damping and 5% damping spectral values.

Using equation 13, the spectral values for dampings of 2%, 4% and 7% are computed by multiplying the 5% damped spectra (Table 6-19) by the scale factors listed in Table 6-20. The computed vertical spectra are listed in Table 6-21.

The spectra listed in Table 6-19 are compared to the DCPP spectra at 2%, 4%, and 7% damping in Figures 10, 11, and 12. For 2% and 7% damping, the vertical spectrum in Table 6-20 envelopes the DCPP spectra. For 4% damping, the Newmark Hosgri vertical spectrum slightly exceeds the vertical spectrum in Table 6-19 over the period range of 0.4 to 0.45 seconds. The 5% damped spectrum at periods of 0.4 and 0.45 seconds are increased to be equal to the spectrum at 0.3 seconds (Figure 13). The damping factors from Table 6-20 are then applied to the modified 5% damping spectral values to compute the modified spectra at 2%, 4%, and 7% damping. The resulting spectra are listed in Table 6-22. The final 4% damped spectrum is compared to the DCPP 4% damped spectra in Figure 13. With this modification, the vertical spectrum envelops the DCPP vertical spectra at 4% damping. Since the unadjusted spectra envelope the 2% and 7% DCPP spectra, then the adjusted spectra will also envelope the 2% and 7% DCPP spectra.

Table 6-20. Damping scale factors for the vertical component based on Abrahamson and Silva (1996)

Period (sec)	2%/5%	3%/5%	4%/5%	7%/5%
0.010	1.00	1.00	1.00	1.00
0.020	1.00	1.00	1.00	1.00
0.030	1.13	1.08	1.04	0.95
0.040	1.18	1.11	1.05	0.93
0.050	1.23	1.13	1.06	0.92
0.075	1.28	1.16	1.08	0.90
0.100	1.33	1.18	1.09	0.89
0.120	1.34	1.19	1.09	0.88
0.150	1.34	1.19	1.09	0.88
0.170	1.34	1.19	1.09	0.88
0.200	1.33	1.18	1.09	0.89
0.250	1.32	1.18	1.09	0.89
0.300	1.31	1.17	1.08	0.89
0.400	1.31	1.17	1.08	0.89
0.450	1.31	1.17	1.08	0.89
0.500	1.31	1.17	1.08	0.89
0.600	1.31	1.17	1.08	0.89
0.750	1.31	1.17	1.08	0.89
1.000	1.31	1.17	1.08	0.89
1.500	1.30	1.17	1.08	0.89
2.000	1.29	1.16	1.08	0.90
3.000	1.26	1.15	1.07	0.90
4.000	1.24	1.14	1.07	0.91
5.000	1.22	1.12	1.06	0.92
6.000	1.22	1.12	1.06	0.92
7.000	1.22	1.12	1.06	0.92
8.000	1.22	1.12	1.06	0.92
9.000	1.22	1.12	1.06	0.92
10.000	1.22	1.12	1.06	0.92

Table 6-21. Vertical spectra at various damping values (not adjusted)

Period (Sec)	Frequency (Hz)	5%	2%	4%	7%
0.01	100.000	0.700	0.700	0.700	0.700
0.025	40.000	0.700	0.700	0.700	0.700
0.03	33.333	0.830	0.938	0.863	0.789
0.04	25.000	1.109	1.309	1.164	1.031
0.05	20.000	1.410	1.734	1.495	1.297
0.075	13.333	1.727	2.211	1.865	1.554
0.1	10.000	1.990	2.647	2.169	1.771
0.12	8.333	1.890	2.533	2.060	1.663
0.15	6.667	1.720	2.305	1.875	1.514
0.17	5.882	1.610	2.157	1.755	1.417
0.2	5.000	1.470	1.955	1.602	1.308
0.25	4.000	1.424	1.880	1.552	1.267
0.3	3.333	1.390	1.821	1.501	1.237
0.4	2.500	1.361	1.783	1.470	1.211
0.45	2.222	1.361	1.783	1.470	1.211
0.5	2.000	1.203	1.576	1.299	1.071
0.6	1.667	1.012	1.326	1.093	0.901
0.75	1.333	0.819	1.073	0.885	0.729
1	1.000	0.602	0.789	0.650	0.536
1.5	0.667	0.413	0.537	0.446	0.368
2	0.500	0.275	0.355	0.297	0.248
3	0.333	0.157	0.198	0.168	0.141
4	0.250	0.100	0.124	0.107	0.091
5	0.200	0.071	0.087	0.075	0.065
6	0.167	0.053	0.065	0.056	0.049
7	0.143	0.042	0.051	0.045	0.039
8	0.125	0.034	0.041	0.036	0.031
9	0.111	0.028	0.034	0.030	0.026
10	0.100	0.024	0.029	0.025	0.022

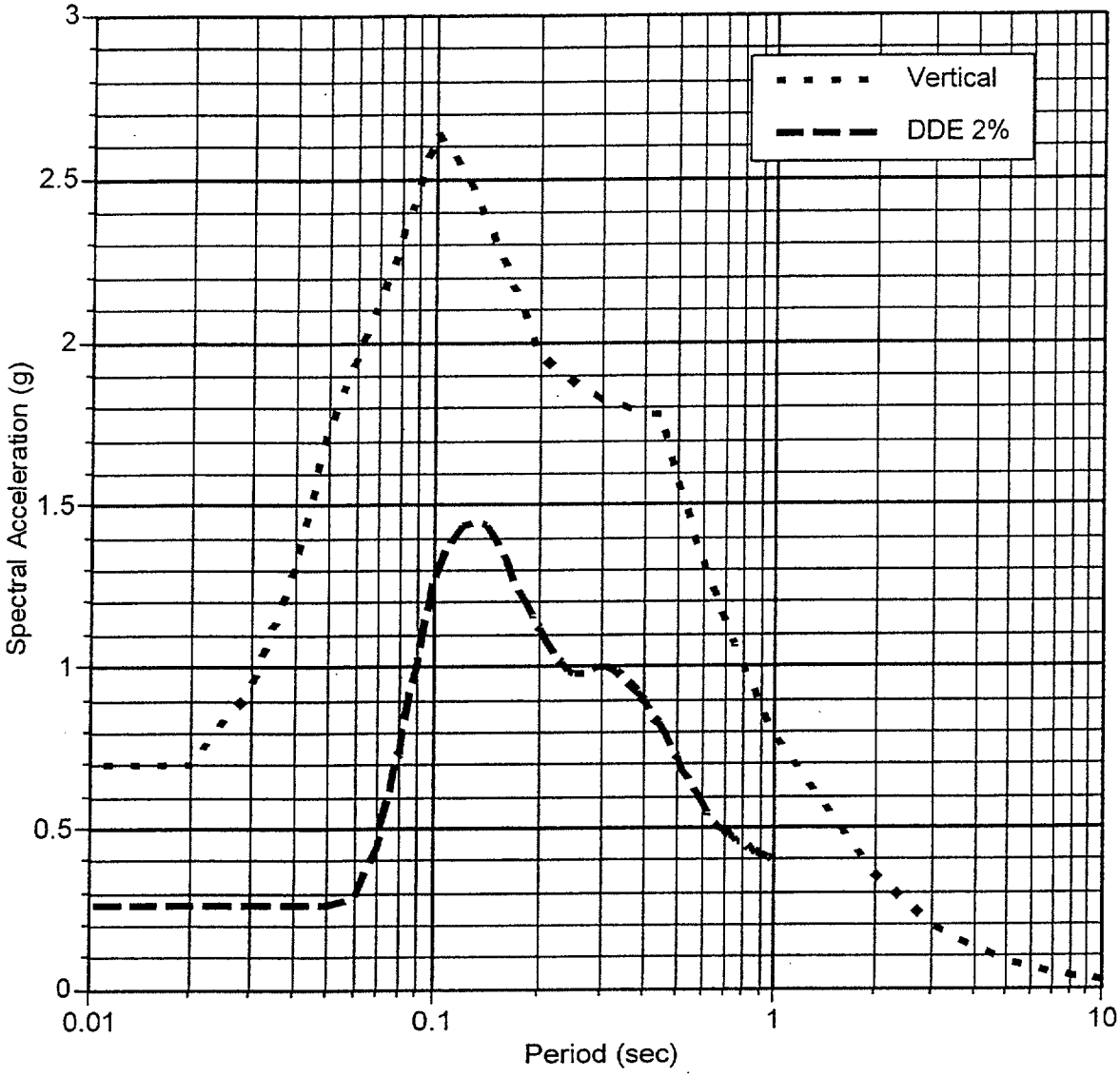

Figure 10. Comparison of the vertical spectra at 2% damping.

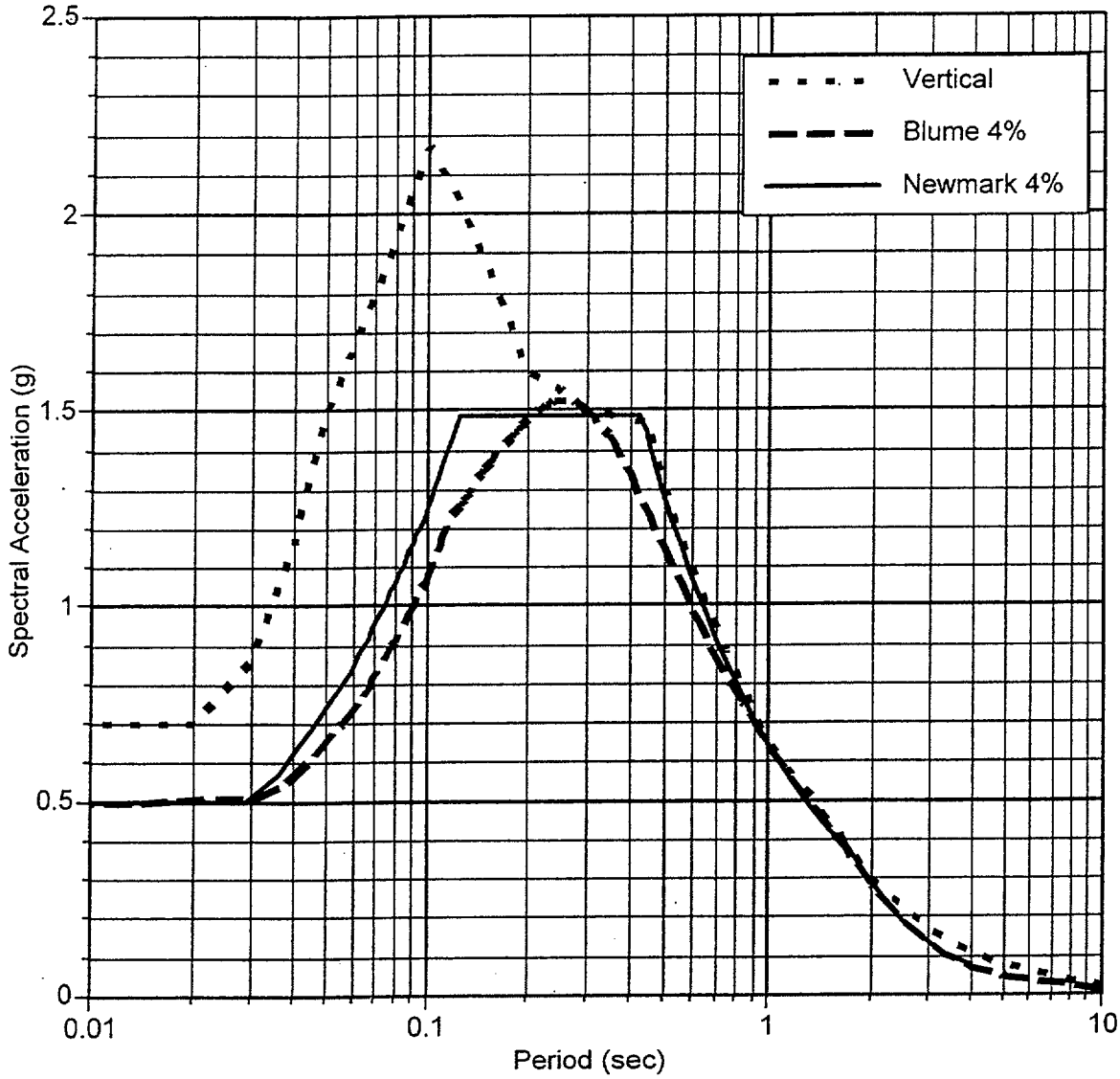

Figure 11. Comparison of the vertical spectra at 4% damping.

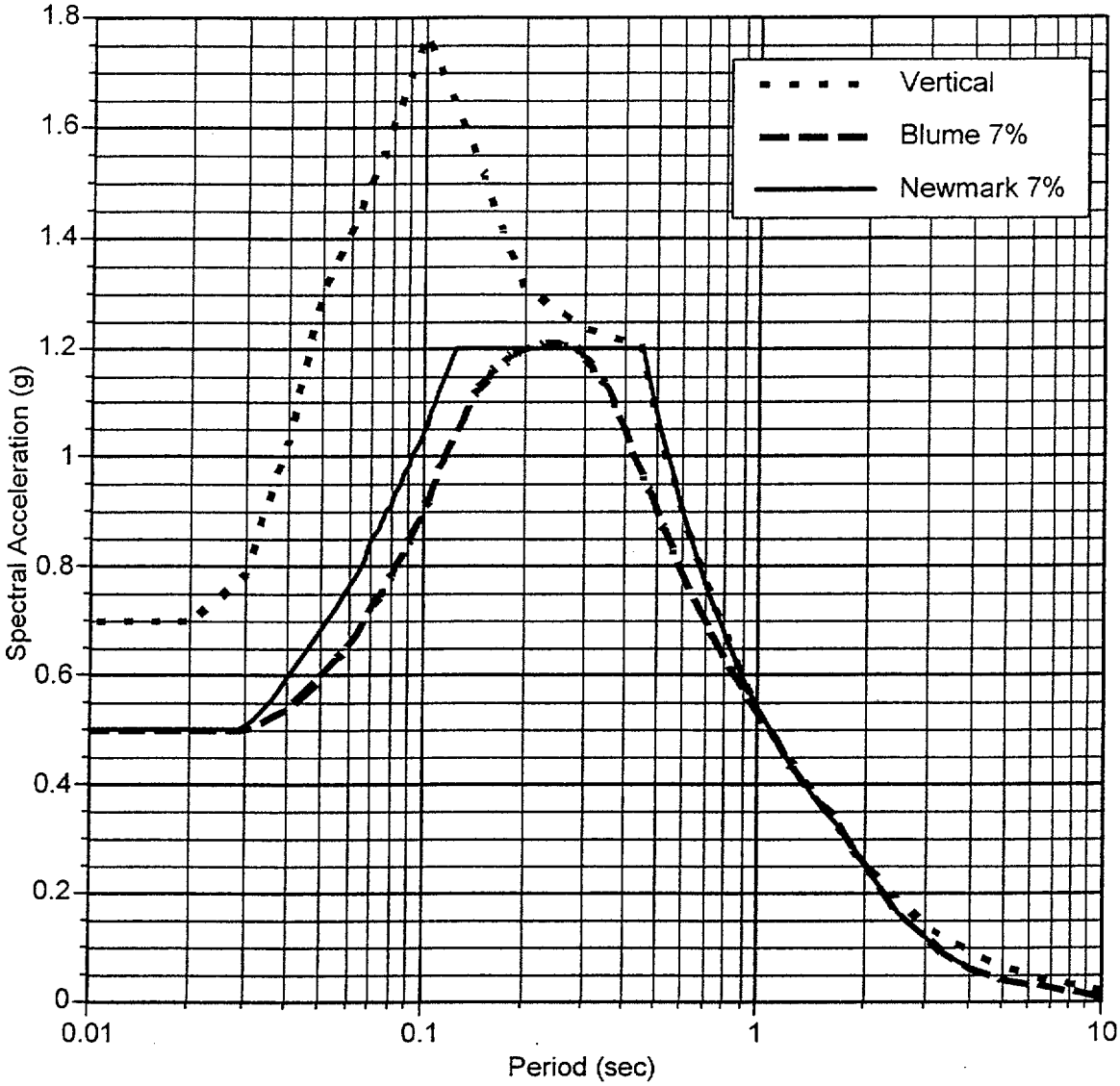

Figure 12. Comparison of the vertical spectra at 7% damping.

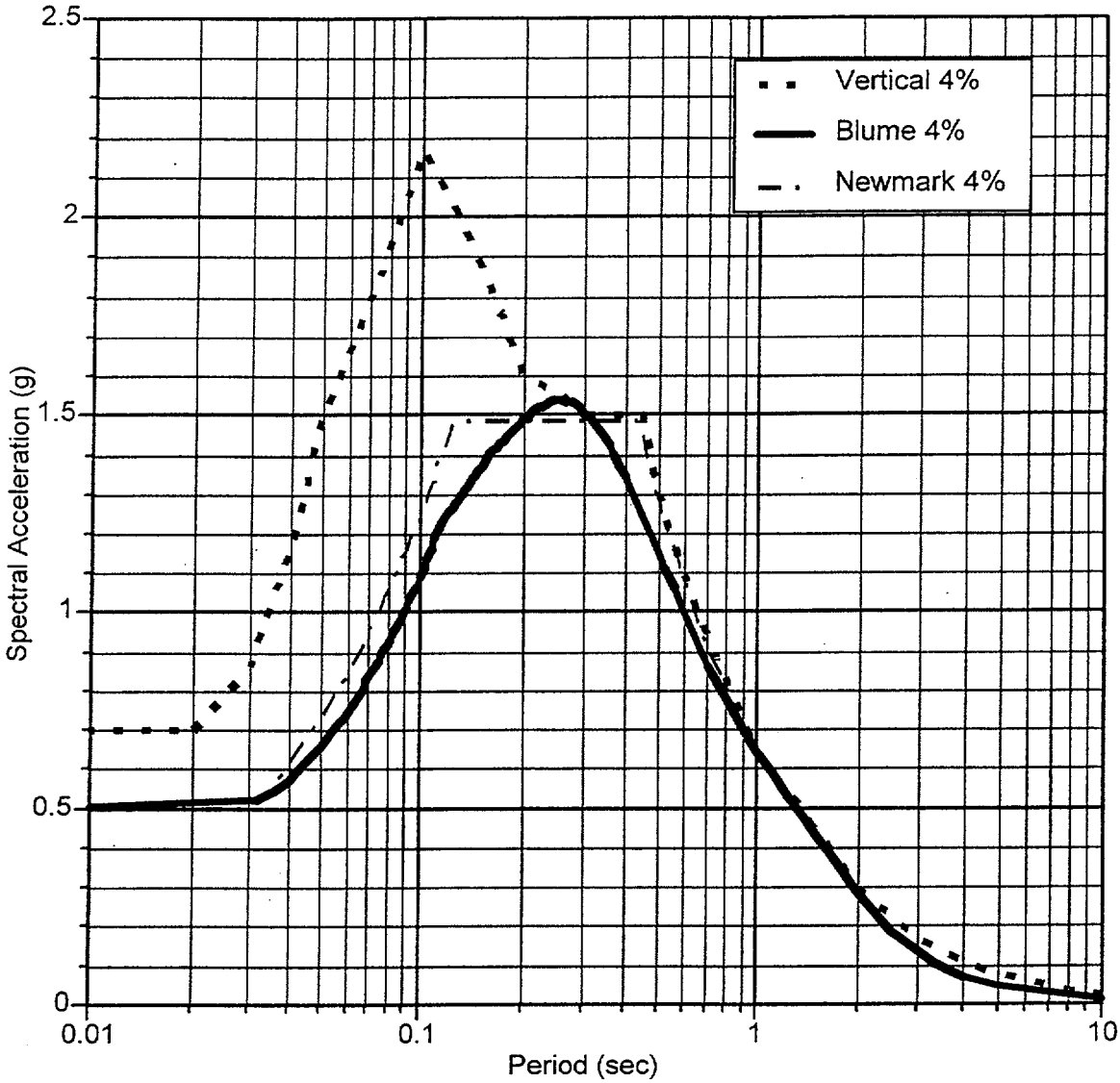

Figure 13. Comparison of the vertical spectra at 4% damping after the adjustment (increase) to the spectra.

Table 6-22. Final vertical spectra

Period (Sec)	Frequency (Hz)	5%	2%	4%	7%
0.01	100.000	0.700	0.700	0.700	0.700
0.02	40.000	0.700	0.700	0.700	0.700
0.03	33.333	0.830	0.938	0.863	0.789
0.04	25.000	1.109	1.309	1.164	1.031
0.05	20.000	1.410	1.734	1.495	1.297
0.075	13.333	1.727	2.211	1.865	1.554
0.1	10.000	1.990	2.647	2.169	1.771
0.12	8.333	1.890	2.533	2.060	1.663
0.15	6.667	1.720	2.305	1.875	1.514
0.17	5.882	1.610	2.157	1.755	1.417
0.2	5.000	1.470	1.955	1.602	1.308
0.25	4.000	1.424	1.880	1.552	1.267
0.3	3.333	1.390	1.821	1.501	1.237
0.4	2.500	1.390	1.821	1.501	1.237
0.45	2.222	1.390	1.821	1.501	1.237
0.5	2.000	1.203	1.576	1.299	1.071
0.6	1.667	1.012	1.326	1.093	0.901
0.75	1.333	0.819	1.073	0.885	0.729
1	1.000	0.602	0.789	0.650	0.536
1.5	0.667	0.413	0.537	0.446	0.368
2	0.500	0.275	0.355	0.297	0.248
3	0.333	0.157	0.198	0.168	0.141
4	0.250	0.100	0.124	0.107	0.091
5	0.200	0.071	0.087	0.075	0.065
6	0.167	0.053	0.065	0.056	0.049
7	0.143	0.042	0.051	0.045	0.039
8	0.125	0.034	0.041	0.036	0.031
9	0.111	0.028	0.034	0.030	0.026
10	0.100	0.024	0.029	0.025	0.022

7. RESULTS

The final response spectral accelerations at 2%, 4%, 5%, and 7% damping for the fault normal, fault parallel, and vertical components are given in Tables 6-13, 6-14, and 6-22, respectively.

8. CONCLUSIONS

The response spectral values referenced in section 7 should be used to define the ISFSI spectral accelerations for the three components (fault normal, fault parallel, and vertical) for the transient ground motion. These spectra should be used to develop time histories for the transient ground motion.

A limitation of the fault parallel spectrum is that it does not include the effects of fling. The fault parallel spectrum given here should not be used for engineering calculations. The fault parallel spectrum including fling effects is given in calculation GEO.DCPP.01.014.

9. REFERENCES

Abrahamson, N. A. and W. J. Silva (1996). Description and validation of the stochastic ground motion model, draft prepared by Pacific Engineering and Analysis for Engineering Research and Applications Div., Dept. of Nuclear Energy, contract no. 770573, appendix to Silva et al (1997).

Abrahamson, N. A. and W. J. Silva (1997). Empirical response spectral attenuation relations for shallow crustal earthquakes, Seism. Res. Let., vol. 68, 94-127.

Abrahamson, N. A. (2000). Effects of rupture directivity on probabilistic seismic hazard analysis, Proc. Sixth International Conference on Seismic Zonation, Palm Springs, CA. November 12-15, 2000.

Agbabian Associates, Inc. (1998). Geophysical investigations for the DCPP HLW-Dry Cask Storage Facility at the Diablo Canyon Power Plant, Report R9730-6676, July 31, 1998, revised September 25, 1998.

Boore D. M., W. Joyner, and T. Fumal (1997). Equations for estimating horizontal response spectra and peak acceleration from western North America earthquakes: a summary of recent work, Seism. Res. Let., 68, pp128-153.

Boore D. M., W. Joyner, and T. Fumal (1993). Estimation of response spectra and peak acceleration from western North American earthquakes: an interim report, USGS open file report 93-509.

Campbell, K. W. (1997). Empirical near-source attenuation relationships for horizontal and vertical components of peak ground acceleration, peak ground velocity, and pseudo absolute acceleration response spectra, Seism. Res. Let., 68, 154-179.

DCM C-17. Diablo Canyon Nuclear Power Plant Units 1 & 2, Hosgri response spectra, Design Criteria Memorandum C-17, Revision 18A.

DCM C-30. Double design earthquake response spectra for structures, systems and components, Design Criteria Memorandum C-30, Revision 7A.

Hanson, K. L., W. R. Lettis, J. R. Wesling, K. I. Kelson, and L. Mezger (1992). Quaternary marine terraces, south-central coastal California: Implications for crustal deformation and coastal evolution: in Quaternary Coasts of the United States: Marine and Lacustrine systems, *SEPM Special Publication* No. 48, p. 323-332.

Idriss, I. M. (1995). An overview of earthquake ground motions pertinent to seismic zonation, Proc. Fifth International Conference on Seismic Zonation, vol. III, 2111-2126.

Idriss, I. M. (1994). Updated standard error terms, Memo to Phalkun Tan, April 17, 1994.

Idriss, I. M. (1992). Empirical procedures for estimating earthquake ground motions, Proc. SEAOC conference, October 15, 1992.

Idriss. I. M. (1991). Selection of earthquake ground motions at rock sites, report prepared for the Structures Division, Building and Fire Research Laboratory, National Institue of Standard and Technology, Department of Civil Engineering, University of California, Davis, included in Idriss (1992).

McLaren, M. K., and W. U. Savage (in Press), Seismicity of South-central coastal California, October 1987 through January 1997, accepted for publication in *Bull. Seis. Soc. Amer.*

Pacific Gas and Electric Company (1988). Final report of the Diablo Canyon Long - Term-Seismic Program: U. S. Nuclear Regulatory Commission docket Nos. 50-275 and 50-323.

PG&E Calculation 72.2.7 (1993). LTSP 84% horizontal and vertical ground spectra. Sheet 21.

Sadigh K., C.Y. Chang, C. Y., Abrahamson, N. A., Chiou, S. J., and Power, M. S. (1993). Specification of long-period ground motions: Updated attenuation relationships for rock

site conditions and adjustment factors for near-fault effects. Proceedings of the seminar on seismic isolation, passive energy dissipation, and active control, Vol. 1, Applied Tech. Council, pp. 59-70.

Sadigh K., C.Y. Chang, J. A. Egan, F. Makdisi, R. R. Youngs (1997). Attenuation relationships for shallow crustal earthquakes based on California strong motion data, Seism Res. Let., vol. 68, 180-189.

Silva, W.J., N. Abrahamson, G. Toro, C. Costantino (1997). Description and validation of the stochastic ground motion model. Report Submitted to Brookhaven National Laboratory, Associated Universities, Inc. Upton, New York.

Somerville, P.G. (2001). Should near fault directivity be modeled in national ground motion mapping? Proceedings of the Second ATC-35 National Ground Mapping Workshop, San Francisco, May 10-11.

Somerville, P. G., N. F. Smith, R. W. Graves, N. A. Abrahamson (1997). Modification of empirical strong ground motion attenuation relations to include the amplitude and duration effects of rupture directivity, Seism. Res. Let., vol. 68, 199-222.

URS/Blume, (1977). Found on microfilm (starting at RLOC 02804-0332). Data are part of document transmittal ("Digitized Values of some spectra), that include the Diablo Canyon specification for seismic review of major structures for 7.5M Hosgri earthquake, February 8, 1977.

URS/Blume, (1982). Diablo Canyon Nuclear Power Plant- Criteria for development of floor response spectra in major structures for Design Earthquake (DE) and Double Design earthquake (DDE), Rev. 1, October 14, 1982.

U.S. Nuclear Regulatory Commission (1991). Safety Evaluation Report related to the operation of Diablo Canyon Nuclear Power Plant, Units 1 and 2, Docket Nos. 50-275 and 50-323, NUREG-0675, Supplement No. 34, June 1991.

U.S. Nuclear Regulatory Commission (1996). Standard review plan for spent fuel dry storage facilities, Final Report, NUREG-1567, March 2000.

1. CALCULATION COVER SHEET

PACIFIC GAS AND ELECTRIC COMPANY
GEOSCIENCES DEPARTMENT
CALCULATION DOCUMENT

Calc Number GEO.DCPP.01.12

Revision: 1
Date: September 26, 2001
Calc Pages: ~~51~~ 54
Appendix Pages: 33
Verification Method A
Verification Pages: 1

TITLE: Development of Fling Model for Diablo Canyon ISFSI

PREPARED BY: _____ DATE 9/28/01

Norman Abrahamson — Printed Name
Geoscience — Organization

VERIFIED BY: _____ DATE 9/29/01

William U. Savage — Printed Name
Geosciences — Organization

APPROVED BY: _____ DATE 10/5/01

Lloyd S. Cluff — Printed Name
Geosciences — Organization

REGISTERED GEOLOGIST
LLOYD S. CLUFF
No. EG767
CERTIFIED ENGINEERING GEOLOGIST
STATE OF CALIFORNIA

Expires 12/31/02

Rev. No.	Reason for Revisions	Revision Date
00	Initial Issue	07/27/01
01	- Editorial changes made per A. Tafoya's comments, dated 08/16/01. - Expanded discussion of the derivation of the standard deviation value of 0.19 $\log_{10}$ units was added to the paragraph describing Equation 5-6 (bottom of page 14 to top of page 15).	10/05/01

2. PURPOSE

The purpose of this calculation is to determine the 84th percentile fling at the ISFSI site. The fling is the ground motion due to tectonic deformation at the site. It will be incorporated into the time histories for the ISFSI in calculation GEO.DCPP.01.14.

3. ASSUMPTIONS

3.1 Functional form of the attenuation of fling with distance

The attenuation of the amplitude of the fling as a function of distance from the fault is assumed to follow the $\cot^{-1}$ model. The basis for this assumption is that $\cot^{-1}$ model is the theoretical form for attenuation of tectonic deformation (Stacey, 1969, page 77, equation 4.12). In this model, the amplitude of the fling is equal on the two sides of the fault, implying that the tectonic deformation is split equally to the two sides of the fault.

3.2 Functional form of the fling

The functional form of the fling in acceleration is assumed be a single cycle of a sine-wave (Figure 3-1) with the duration (rise-time) and amplitude of the sine-wave estimated empirically. The basis for this assumption is that this simple form provides an adequate fit to the fling for the few empirical recordings containing fling. As an example, the fling model is compared to the displacement from the 1999 Kocaeli earthquake in Figure 3-2. This model of the functional form of the fling time history is consistent with the displacement time histories.

3.3 Shear-Modulus

The shear-modulus of the crust is assumed to be 3×10^{11} dyne/cm^2. The basis for this assumption is that this is a generally accepted average value for the crust. (Kanamori and Anderson, 1975)

3.4 Form of the probability distribution of fling amplitude (displacement)

The amplitude of the fling in displacement (D_{site}) for a given fault displacement and distance is assumed to be lognormally distributed. The basis for this assumption is a evaluation of the transformation needed to make the data homoscedastic (Figure 3-3).

3.5 Form of the probability distribution of fling period

The period of the fling (T_{fling}) for a given earthquake magnitude is assumed to be lognormally distributed. The basis for this assumption is that the fling period is related to the rise-time of an earthquake and the rise-time is lognormally distributed (Somerville et al, 1999, page 74, figure 11).

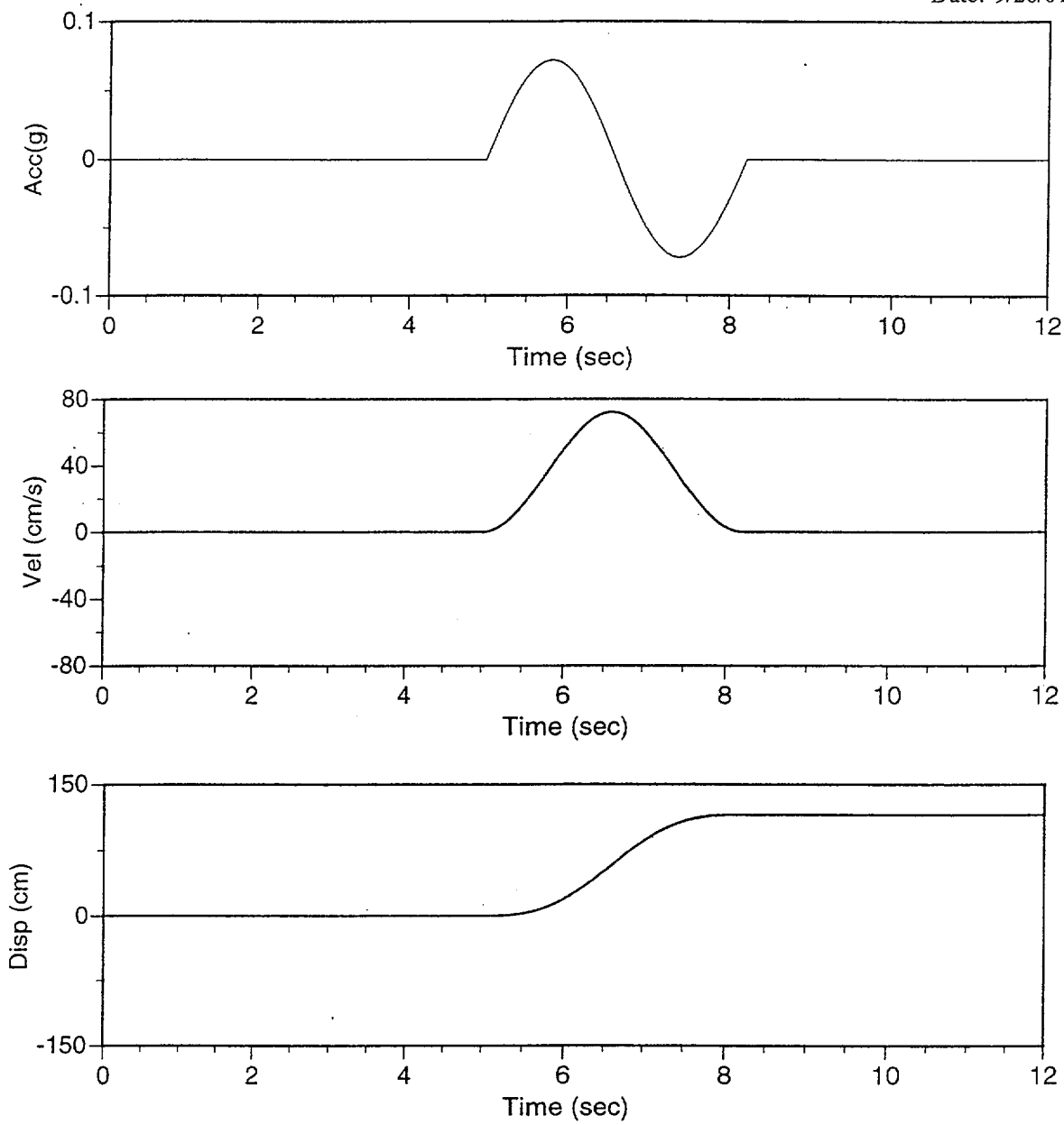

Figure 3-1. Example of the functional form of the fling time history. In this example, the duration of the fling (rise-time) is 3 seconds and the amplitude of the tectonic deformation at the site is 115 cm.

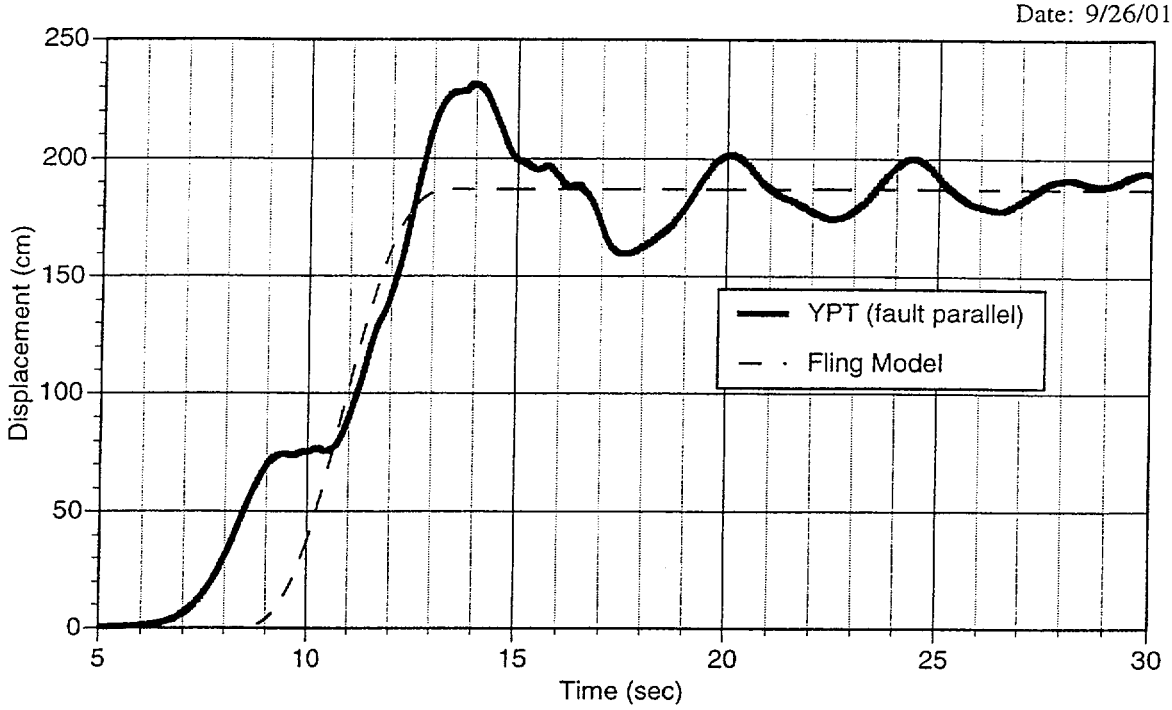

Figure 3-2. Example of the fling model for the YPT recording from the 1999 Kocaeli earthuake.

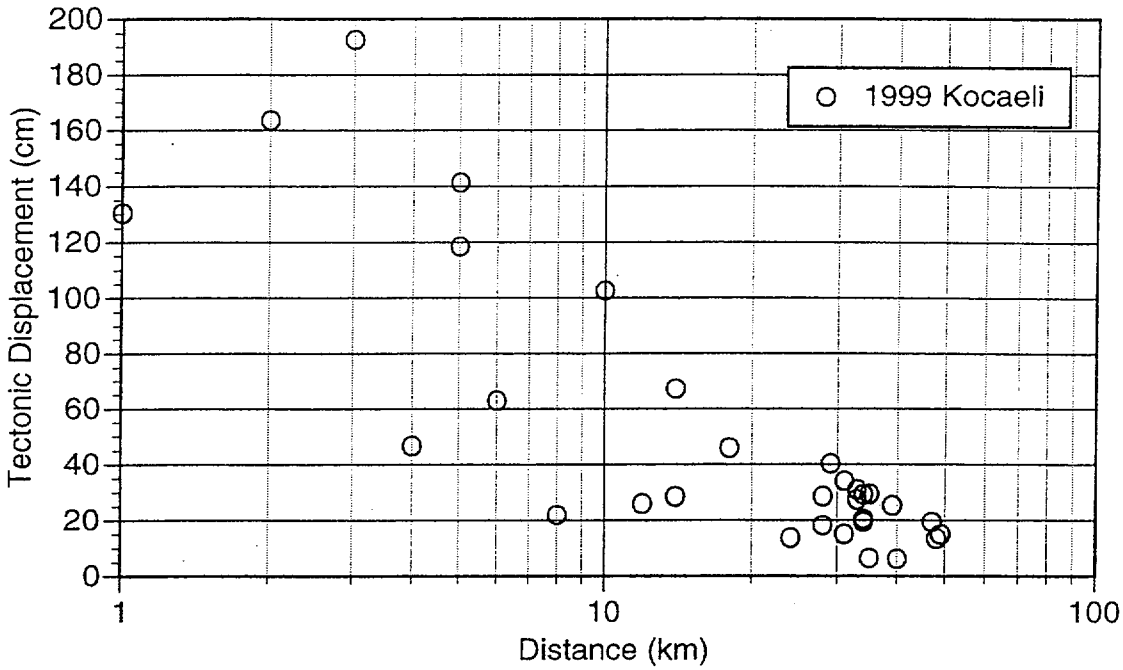

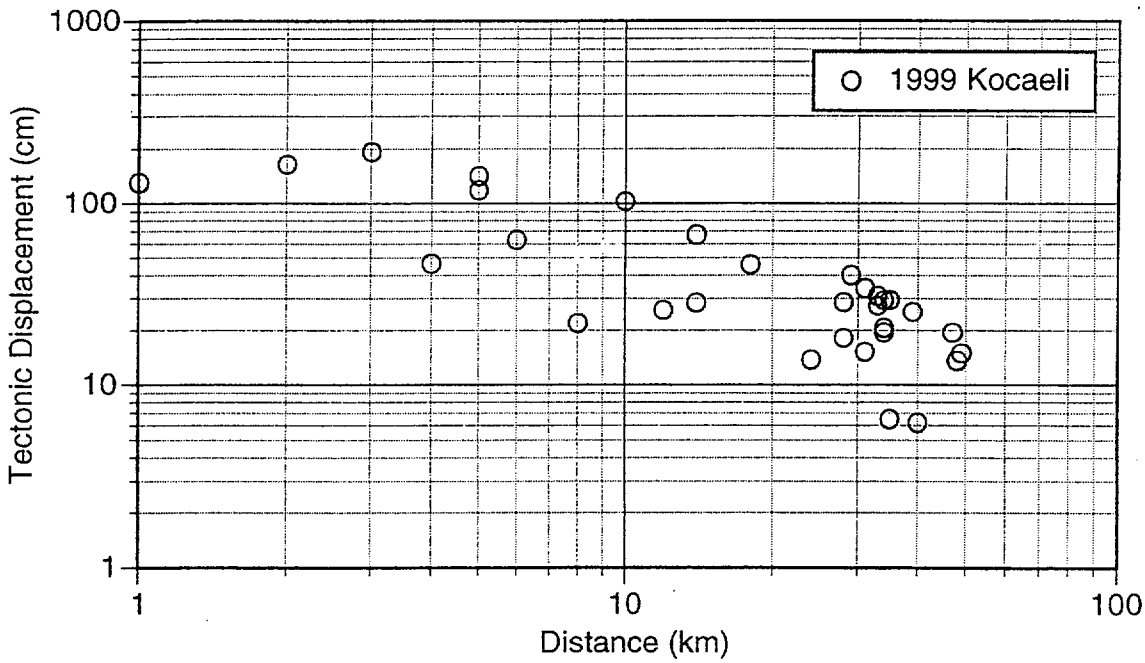

Figure 3-3. Evaluation of the distribution of the tectonic displacement. The top frame shows that the linear displacement is heteroscedastic. The lower frame shows that the log displacement is approximately homoscedastic.

4. DESIGN INPUTS

4.1 Data set of tectonic displacements

The model described in Section 5 for determining tectonic displacement as a function of distance from the fault was developed from an empirical database of measurements of permanent tectonic displacement using geodetic observations from four earthquakes. These earthquakes include the 1906 San Francisco Earthquake, 1940 Imperial Valley Earthquake, 1992 Landers Earthquake, and the 1999 Kocaeli Earthquake. These earthquakes were selected because they are large (M>=6.9) strike-slip earthquakes with readily available geodetic data on the tectonic deformation.

The earthquake magnitude ~~and rupture area~~ for each of the four earthquakes are listed in Table 4-1. JCY for NAA 10/18/01

Table 4-1. Magnitude ~~and rupture areas~~ for earthquakes JCY for NAA 10/18/01

Earthquake	Moment Magnitude	Reference
1906 San Francisco	7.9	Wells and Coppersmith (1994) Table 1
1940 Imperial Valley	6.92	Wells and Coppersmith (1994) Table 1
1992 Landers	7.34	Wells and Coppersmith (1994) Table 1
1999 Kocaeli	7.4	EERI (2000): page 3(mag), page 11(length=126 km), page 6 (width=16 km)

Norm Abramhamson concurred via telephone.

4.1.1 1906 San Francisco Earthquake

The tectonic displacements from the 1906 San Francisco earthquake were hand digitized from Figure 4.8 in Stacey (1969). These digitized values are listed in Table 4-2. As a check of the digitization, the digitized data are superimposed over the figure from Stacey in Figure 4-1.

4.1.2 1940 Imperial Valley Earthquake

The tectonic displacements from the 1940 Imperial Valley earthquake were hand digitized from Figure 2 in Byerly and Denoyer (1958). These digitized values are listed in Table 4-3. As a check of the digitization, the digitized data are superimposed over the figure from Byerly and Denoyer in Figure 4-2.

4.1.3 1994 Landers Earthquake

The tectonic displacements from the 1992 Landers earthquake were taken from Table 1 (page 627-628) in Hudnut et al. (1994). The location of the stations were taken from Table A-1 (page 640-641) of Hudnut et al (1994). These displacement values and locations are listed in Table 4-4. The coordinates of the rupture are taken from Wald and Heaton (1994) and are listed in Table 4-5.

The following stations listed in Table 1 of Hudnut et al (1994) did not have locations listed in Table A1: 0802, 0809, 0811, 1110, 1111, BOUC. Since a location was not available, these stations were excluded from this calculation. In addition, station LUCS appears to

have an error in either the location or the displacement and it was excluded.

4.1.4 1999 Kocaeli Earthquake

The tectonic displacements from the 1999 Kocaeli earthquake were taken from the online supplement to Reilinger et al. (2000). These displacement values are listed in Table 4-6. The coordinates of the rupture are measured from the regional Fault Rupture Map in EERI (2000) and are listed in Table 4-7.

4.2 Earthquake Magnitude

The magnitude of the earthquake on the Hosgri fault is 7.2 (SSER 34, page 2-43)

4.3 Distance from the Hosgri Fault

The closest rupture distance from the DCPP site to the Hosgri fault given in SSER 34 (page 2-43) is 4.5 km. Although the ISFSI is located east of DCPP (e.g. slightly further from the Hosgri fault), a rupture distance of 4.5 km is used.

Table 4-2. Horizontal displacements measured during 1906 San Francisco Earthquake (after Stacey, 1969, Figure 4.8).

Station	Distance from fault (km)	Displacement (cm)
1	0.2	158.0
2	0.5	158.0
3	1.1	204.0
4	1.2	155.0
5	1.8	136.0
6	2.1	136.0
7	1.9	145.0
8	2.1	157.0
9	2.0	187.0
10	2.7	177.0
11	3.8	87.0
12	3.9	83.0
13	4.9	98.0
14	6.4	64.0

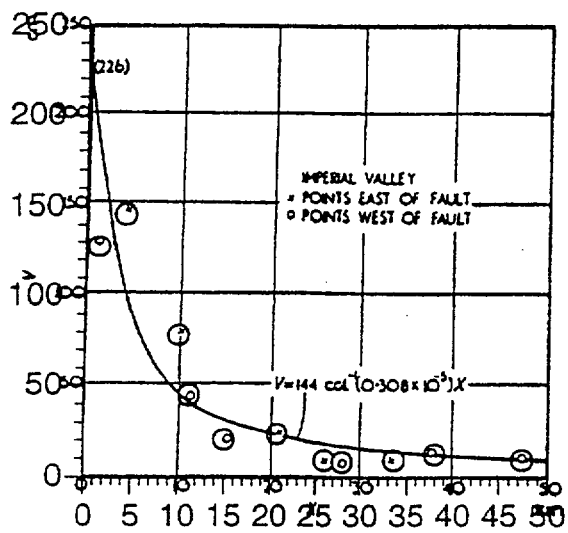

FIG. 2.

Figure 4-1. Check of digitized values (open circles) and the original plots from Stacey (1969).

Table 4-3. Horizontal displacements measured during 1940 Imperial Valley Earthquake (after Byerly and Denoyer, 1958, Page 19, Figure 2).

Station	Distance from fault (km)	Displacement (cm)
1	4.2	145.9
2	10.0	78.6
3	20.8	23.5
4	26.0	9.2
5	33.6	9.2
6	1.4	127.6
7	11.2	44.9
8	15.0	20.4
9	28.0	8.2
10	38.0	12.2
11	47.4	9.2

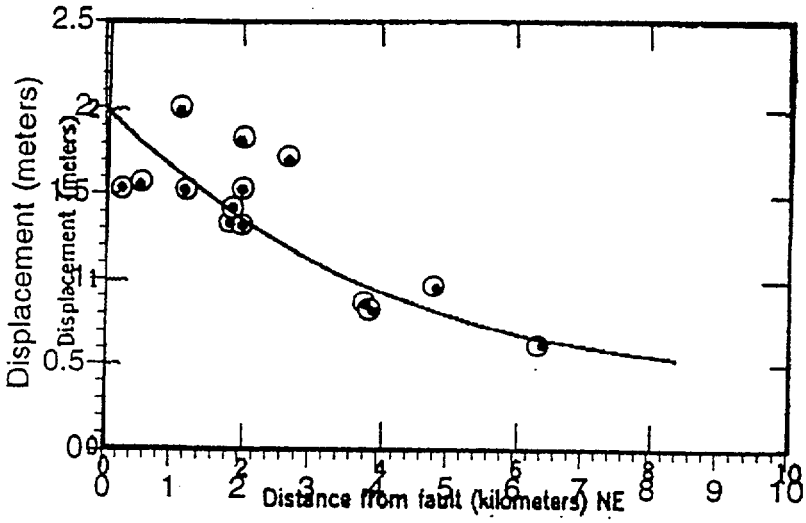

Figure 4-2. Check of digitized values (open circles) and the original plots from Byerly and Denoyer (1958).

Table 4-4. Horizontal displacements measured during the 1992 Landers Earthquake (from Hudnut et al., 1994 Tables 1 and A1).

Station Name	Longitude	Latitude	Horizontal Displacement	
			East (cm)	North (cm)
PIN1	-116.4582	33.6122	1.4	4.6
GOLD	-116.889	35.425	-0.8	-1.5
JPL1	-118.173	34.205	-1.5	0.3
SIO2	-117.252	32.867	1	1.3
VNDP	-120.6164	34.5561	-0.4	0.5
618	-118.8681	34.8253	-0.1	1.4
704	-118.54	34.4072	-5.4	0.4
705	-117.765	34.4928	-3	-1
803	-116.4147	35.0719	-1	-12
805	-117.5292	35.0072	-3.3	-0.3
806	-117.6142	35.3661	-1.5	-1.4
808	-115.9331	34.7278	-1.8	-9.8
818	-117.1042	34.0222	0.6	5.6
819	-117.5475	33.8842	-1.5	3.3
821	-116.5706	33.5614	2.3	5
1106	-116.8019	32.8444	-1.4	1.9
1107	-117.2769	33.1294	0.1	3
1108	-116.6933	33.2339	-4.3	3.1
1109	-116.2469	33.1597	-0.3	1
1112	-114.5122	33.2572	-0.5	-3
1113	-115.9639	33.6772	5.9	-5.5
1114	-115.2431	33.6808	2.5	-4.2
6050	-116.334	34.266	49.5	-48
6052	-116.84	34.516	-37.4	2.9
6054	-116.442	34.204	10.1	129.3
6056	-116.647	34.37	-9.7	66.3
6058	-116.585	34.04	13.6	33.3
6060	-116.3292	34.1356	42.9	-28.4
7000	-116.716	34.676	-95.5	15.4
7001	-116.469	34.56	38.3	-120.2
7002	-116.404	34.367	57.4	-115.8
7007	-116.225	34.705	1.7	-22.7
AMBO	-115.7422	34.5586	4.6	-7.4

Table 4.4 (cont'd)

Station Name	Longitude	Latitude	Horizontal Displacement	
			East (cm)	North (cm)
ANZA	-116.6618	33.556	-0.6	7.6
BEAR	-116.884	34.264	-4.2	9.9
BLAC	-115.72	33.664	2.1	-3.4
BRIN	-117.139	34.014	-1.8	3.5
CABA	-116.7755	33.9159	6.1	19.8
CAJO	-117.451	34.347	-6.1	-0.7
CHAP	-117.3089	34.1538	-0.1	-0.4
CHER	-116.9518	34.0028	4.1	15.4
COCH	-116.1583	33.7403	3.8	-1.8
CRAF	-117.0855	34.0614	2.7	6.6
CRIS	-115.2183	34.0442	2.7	-4.4
DASH	-117.0861	33.6356	1.8	5.1
DUMP	-116.663	34.793	-28.4	-10
EDM2	-116.43	33.87	5.4	5
ENDD	-114.4814	34.0441	0	-5
GAP	-116.174	33.747	3.2	-0.7
GARN	-116.5377	33.8978	-5.5	14.4
GODW	-115.9315	34.1846	9.8	-7.5
HECT	-116.421	34.785	-6.8	-32.4
HIGH	-117.1693	34.1339	0.6	3
INA5	-116.5154	34.0041	10.1	26.7
INDO	-116.777	33.7945	2.5	13.4
INYO	-117.8117	35.6475	-0.6	-1.6
JURU	-117.443	34.032	1.3	0.8
L290	-117.3286	35.9781	3.2	-1
LAST	-117.3092	33.8372	-0.5	3.4
LAZY	-116.5139	34.3439	-10.3	169.7
LIMP	-117.5489	33.9752	1.2	7.8
MATH	-117.4367	33.8566	-1.2	2.3
MAUM	-116.458	34.419	57.6	-166.7
MDAY	-117.7058	34.7429	-2.6	0.1
MEEK	-116.617	34.258	23.9	65.6
MILL	-117.0106	34.0907	5.8	5.7
MILU	-117.292	34.281	-4.3	0.4
NIGU	-117.7303	33.5145	-1.3	2
OCOT	-115.7961	32.79	-2.3	-0.3

Table 4-4. (cont'd)

Station Name	Longitude	Latitude	Horizontal Displacement	
			East (cm)	North (cm)
ONYX	-116.71	34.193	23.5	33.9
PARK	-116.3003	35.8669	1.2	-2.3
PAVE	-114.7468	33.4504	2.1	-3.4
PEAR	-117.9224	34.5121	-2.1	-0.9
PINY	-116.4588	33.6092	-1.3	5.1
POIN	-117.068	34.454	-14	-0.2
PORT	-118.1569	35.0872	1.6	-1.3
PVER	-118.4035	33.7438	-3.8	1.5
RESO	-116.392	33.688	3.1	4.6
ROCH	-116.61	33.608	3.2	5.6
ROD2	-114.828	35.113	2.1	-3.8
ROSA	-117.1889	33.5052	-1.7	6.6
ROUN	-118.4769	35.6417	6.8	-1.4
SAND	-116.2786	34.255	41.1	-30.9
SANO	-117.513	34.0182	3.5	2.2
SOAP	-116.981	34.904	-6.5	2.7
STIM	-117.2418	34.5341	-4	4.5
THOU	-116.2717	33.8893	11.7	-13.5
TOM2	-116.6337	33.9249	5	19.7
VIEW	-116.188	33.926	7	-9.5
WIDE	-116.4063	33.9314	4.3	8.9

Table 4-5. Fault rupture coordinates from 1992 Landers Earthquake (after Wald and Heaton (1994), figure 1)

Fault Name	Northern End		Southern End	
	Longitude	Latitude	Longitude	Latitude
Camp Rock	-116.721	34.696	-116.469	34.448
Emerson	-116.547	34.524	-116.417	34.306
Homestead	-116.454	34.362	-116.426	34.094

Table 4-6. Horizontal displacements measured during the 1999 Kocaeli Earthquake. (from Reilinger et al, 2000, online supplement)

Station	Longitude	Latitude	Displacement (mm) East	Displacement (mm) North
ANKR	32.75	39.88	-7.20	5.70
DEVR	31.90	41.18	21.40	21.70
KIBR	31.83	40.40	-28.40	14.30
SIVR	31.81	39.56	-21.20	19.80
ARDC	31.47	40.57	-54.10	29.30
NALL	31.45	40.14	-38.60	22.60
YIGI	31.43	40.93	41.60	49.60
ALAP	31.41	41.20	52.50	55.60
AKKO	31.19	41.04	101.30	112.20
CMLN	30.91	40.11	-64.80	40.00
DKMN	30.89	40.66	-217.60	-28.70
KDER	30.82	40.73	1129.40	654.60
TEB4	30.80	40.38	-195.80	64.50
AGOK	30.76	40.58	-251.00	-62.70
AGUZ	30.68	40.53	-278.00	57.70
KTOP	30.63	40.61	-460.90	71.00
PIRE	30.59	40.82	631.10	227.70
MHGZ	30.57	40.02	-56.20	29.60
SEYH	30.45	40.35	-181.70	71.50
KANR	30.29	41.04	274.20	107.50
SMAS	30.13	40.68	-1409.90	107.60
SISL	30.13	40.74	1635.30	-27.90
MEKE	30.02	40.46	-402.60	3.60
AKCO	29.97	41.03	289.60	44.40
IUCK	29.92	40.42	-303.10	-66.10
IGAZ	29.90	40.43	-331.30	-82.90
KPKL	29.88	40.06	-62.30	-30.20
GLCK	29.80	40.70	-1921.10	156.00
DERB	29.68	40.36	-190.30	-166.40
YUHE	29.63	40.80	936.30	-421.70
SILE	29.62	41.17	119.10	-90.30
OLU4	29.58	40.66	-1049.40	-551.00
AHMT	29.57	41.15	149.10	-124.70
TUBI	29.45	40.78	533.40	-333.20
DUMT	29.37	40.56	-337.50	-311.30
KRDM	29.36	41.01	210.70	-175.50
KUTE	29.28	40.48	-202.80	-201.80
CINA	29.14	40.63	-93.00	-100.60

Table 4-6. (cont.)

Station	Longitude	Latitude	Displacement (mm) East	Displacement (mm) North
BADA	29.12	40.85	149.00	-103.50
KILY	29.07	41.25	71.30	-65.80
KANT	29.06	41.06	104.80	-84.40
MUDA	28.94	40.30	-70.30	-66.80
FIS4	28.88	40.48	-81.90	-64.70
AVCI	28.72	40.98	44.00	-34.90
LTFY	28.41	39.99	-28.80	-13.30
YENI	28.37	40.39	-15.40	-22.00
SELP	28.36	41.05	18.60	-17.80
YALI	28.29	41.47	28.00	-13.80
MERT	27.96	40.96	10.00	-8.90
MADT	27.58	40.61	-1.70	-7.10

Table 4-7. Fault Rupture Coordinates from the 1999 Kocaeli Earthquake (after EERI 2000, Regional fault rupture map for the Izmit earthquake)

Rupture	West End of Rupture Segment		East End of Rupture Segment	
Segment	Longitude	Latitude	Longitude	Latitude
1	29.4000	40.7165	29.5407	40.7305
2	29.5485	40.7007	29.8293	40.7273
3	29.8465	40.7075	29.9397	40.7225
4	29.9410	40.7225	30.2730	40.7235
5	30.2808	40.7155	30.6110	40.6917
6	30.5945	40.6407	31.0237	40.7913
7	30.9543	40.7612	31.0757	40.7612

5. METHOD AND EQUATION SUMMARY

5.1 Methods

The method used to develop the parametric model of attenuation of the amplitude of the tectonic deformation displacement as a function of the rupture distance is non-linear least-squares regression.

The method used to develop the model of the period of the fling step is to estimate the duration of the fling by hand from strong motion accelerograms integrated to displacement.

5.2 Equations

5.2.1 Equation for average slip on fault

The seismic moment of an earthquake is defined as

$$M_0 = \mu \ \mathrm{Area}_{rup} \ D_{fault} \tag{5-1}$$

(Kanamori and Anderson, 1975, equation 5, page 1076), where μ is the shear-modulus of the crust, Area_{rup} is the area of the rupture in cm^2, and D_{fault} is the average displacement on the fault in cm. The seismic moment is related to magnitude by

$$M = 2/3 \log(M_0) - 10.7 \tag{5-2}$$

(Hanks and Kanamori, 1979, eq 7, page 2349). Solving for the seismic moment, eq. (5-2) becomes

$$M_0 = 10^{(1.5M+16.05)} \tag{5-3}$$

Substituting eq. (5-3) into eq. (5-1) and solving for D_{fault} gives

$$D_{fault} = \frac{10^{(1.5M+16.05)}}{\mu \ \mathrm{Area}_{rup}} \tag{5-4}$$

Taking the logarithm of eq. (5-4) leads to

$$\log(D_{fault}) = 1.5M + 16.05 - \log(\mu) - \log(\mathrm{Area}_{rup}) \tag{5-5}$$

The rupture area is related to the earthquake magnitude. The rupture area for large magnitude strike-slip earthquakes has been re-evaluated by the 1999 Working Group on Earthquake Probabilities in Northern California (Working Group, 1999). Using a self-similar scaling relation for Area_{rup}>500 km^2, the relation between magnitude and area is

$$M = 4.20 + \log(\mathrm{Area}_{rup}) - 10, \tag{5-6}$$

with a standard deviation of 0.12 $\log_{10}$ units (Working Group, 1999, Appendix C). The

−10 term is included to account for the difference in units of $Area_{rup}$. In the WG99 relation, the rupture area is in km^2, but eq. (5-5) uses cm^2. The WG99 estimate of the standard deviation is much smaller than the empirical estimates of 0.24 $\log_{10}$ units (Wells and Coppersmith, 1994, M vs RA for all source types). In this study, the standard deviation is computed using the average of the variances (square of the standard deviation) from the WG99 model and the Wells and Coppersmith (1994) models. This results in a standard deviation of 0.19 $\log_{10}$ units.

Substituting eq. (5-6) into eq. (5-5) and using assumption 3.3 ($\mu=3x10^{11}$ dyne/cm^2) leads to

$$\log(D_{fault}) = 0.5M - 1.23 \qquad (5\text{-}7)$$

Based on eq. (5-5), the standard deviation of $\log(D_{fault})$ is equal to the standard deviation of $\log(Area_{rup})$; and based on eq. (5-6), the standard deviation of $\log(Area_{rup})$ is equal to the standard deviation of M. Therefore, the standard deviation of the $\log(D_{fault})$ is 0.19 $\log_{10}$ units. To convert to natural log units, the standard deviation is multiplied by ln(10), resulting in a standard deviation of 0.44 natural log units.

Eq. (5-7) can be converted to natural log units as follows:

$$\ln(D_{fault}) = \ln(10)\ (0.5M - 1.23\ ) = 1.15M - 2.83 \qquad (5\text{-}8)$$

with a standard deviation

$$\sigma_{lnDfault} = 0.44 \qquad (5\text{-}9)$$

5.2.2 Tectonic displacement model as a function of distance

Using assumption 3.1, for a strike-slip fault, the basic form of the model for the amplitude of the fling displacement at the site is

$$D_{site} = 0.5\ D_{fault}\ \cot^{-1}(\alpha R)\ /\ (\pi/2) \qquad (5\text{-}10)$$

where D_{site} is the tectonic displacement at the site, D_{fault} is the average displacement on the fault plane, R is the rupture distance, and α is an unknown parameter to be determined. The 0.5 factor represents the assumption that half of the slip occurs on each side of a strike-slip fault (assumption 3.1). The ($\pi/2$) factor normalizes $\cot^{-1}$ because $\cot^{-1}(0)=2/\pi$ and the displacement at zero distance should be 0.5 D_{fault}.

5.2.3 Regression Equation for tectonic displacement

The JMP regression package does not include a built in function for $\cot^{-1}(x)$, so it is computed using the relation:

$$\cot^{-1}(x) = \pi/2 - \tan^{-1}(x) \qquad (5\text{-}11)$$

This is a standard trigonometric relation. Substituting eq. (5-6) into eq. (5-5) results in

$$D_{site} = D_{fault} \ (\pi/2 - \tan^{-1}(\alpha R)) / \pi \qquad (5\text{–}12)$$

A preliminary analysis of the distribution of D_{site} data indicated that it is approximately lognormally distributed (this is verified by an evaluation of the residuals later). Therefore, the for the regression model, $\ln(D_{site})$ is used as the dependent variable. The average fault slip, D_{fault}, for each earthquake is estimated from the earthquake magnitude and rupture area using eq. (5-4). Taking the natural logarithm of eq. (5-12) and using an event-specific D_{fault} term, the resulting regression equation is:

$$\ln(D_{site_{ij}}) = \ln((\Sigma_{k=1:N} c_k E_{jk}) + \ln(\pi/2 - \tan^{-1}(\alpha R_{ij})) - \ln(\pi) \qquad (5\text{-}13)$$

where $D_{site_{ij}}$ is the displacement from the ith point from the jth earthquake, $E_{jk} = 1$ for j=k, and 0 otherwise, c_k is the earthquake dependent mean fault slip determined from the regression, α is a constant coefficient, N is the total number of earthquakes and R is the distance in kilometers. The coefficient c_k corresponds to D_{fault}.

The standard deviation of D_{site} has two parts: the standard deviation of D_{fault} and the standard deviation of the regression (standard deviation of D_{site}, given D_{fault}). The total standard deviation is computed adding the variances of the two parts

$$\sigma_{\ln Dsite} = \sqrt{\sigma^2_{\ln Dfault} + \sigma^2_{\ln Dsitereg}} \qquad (5\text{-}14)$$

where $\sigma_{\ln Dsitereg}$ is the standard deviation from the regression analysis using eq (5-13).

5.2.4 Equation for the Fling in Acceleration

Using assumption 3.2, the fling acceleration time history is a sine wave when the time falls between t_1 and $t_1 + T_{fling}$, where t_1 is the arrival time of the fling and T_{fling} is the duration of the fling. Therefore, the equation for the fling in acceleration is

$$\begin{aligned} Acc_{fling}(t) &= 0 && \text{for } t < t_1 \\ Acc_{fling}(t) &= A \sin(\omega(t - t_1)) && \text{for } t_1 < t < t_1 + T_{fling} \\ Acc_{fling}(t) &= 0 && \text{for } t_1 + T_{fling} < t \end{aligned} \qquad (5\text{-}15)$$

where $\omega = 2\pi / T_{fling}$.

The amplitude of the fling in acceleration, A, is determined by setting the double integral of the fling acceleration equal to D_{site}. The velocity is the integral of acceleration:

$$v(t) = \int_0^t a(\tau) d\tau \qquad (5\text{-}16)$$

Substituting eq. (5-15) into eq. (5-16) leads to

$$v(t) = A\int_{t1}^{t}[\sin(\omega(\tau - t_1))]d\tau = \frac{A}{\omega}[1-\cos(\omega(t-t_1))] \tag{5-17}$$

The displacement is the integral of velocity:

$$d(t) = \int_0^t v(\tau)d\tau \tag{5-18}$$

Substituting eq. (5-17) into eq. (5-18) leads to:

$$d(t) = \int_{t1}^{t} v(\tau)d\tau = \frac{A}{\omega}\int_{t1}^{t}[1-\cos(\omega(\tau-t_1))]d\tau = \frac{At}{\omega} - \frac{A}{\omega^2}\sin(\omega(t-t_1)) \tag{5-19}$$

At the end of the fling ($t = t_1 + T_{fling}$), the fling displacement is equal to D_{site}. Using eq. (5-19) and setting $d(t_1 + T_{fling}) = D_{site}$, then

$$D_{site} = \frac{A\,T_{fling}}{\omega} = \frac{A\,T_{fling}^2}{2\pi} \tag{5-20}$$

Solving for A (in cm/s^2)

$$A(cm/s^2) = \frac{D_{site}\,2\pi}{T_{fling}^2} \tag{5-21}$$

Converting from cm/s^2 to g using 1g=981 cm/sec^2, then

$$A(g) = \frac{D_{site}\,2\pi}{981\,T_{fling}^2} \tag{5-22}$$

5.2.5 Standard Deviation of Fling Acceleration Amplitude

Taking the natural logarithm of eq. (22), results in

$$\ln(A) = \ln(D_{site}) - 2\ln(T_{fling}) + \ln(2\pi) - \ln(981) \tag{5-23}$$

Since $\ln(D_{site})$ and $\ln(T_{fling})$ are both assumed to be lognormally distributed (assumptions 3.4 and 3.5), and ln(A) is a linear combination of these two variables, then ln(A) is also lognormally distributed (Meyer, 1970, theorem 9.1, page 185).

Assuming that $\ln(D_{site})$ and $\ln(T_{fling})$ are uncorrelated, the variance of ln(A) is

$$\sigma^2_{\ln A} = \sigma^2_{\ln Dsite}\left(\frac{\partial \ln A}{\partial \ln D_{site}}\right)^2 + \sigma^2_{\ln Tfling}\left(\frac{\partial \ln A}{\partial \ln T_{fling}}\right)^2 \tag{5-24}$$

(Bevington, 1969, equation 4-9, page 60).

From eq. (5-23),

$$\left(\frac{\partial \ln A}{\partial \ln D_{site}}\right) = 1 \tag{5-25}$$

and

$$\left(\frac{\partial \ln A}{\partial \ln T_{fling}}\right) = -2 \tag{5-26}$$

Substituting eq. (5-25) and (5-26) into eq. (5-24) leads to

$$\sigma^2_{\ln A} = \sigma^2_{\ln Dsite} + 4\sigma^2_{\ln Tfling} \tag{5-27}$$

The standard deviation of ln(A) is given by the square root of the variance:

$$\sigma_{\ln A} = \sqrt{\sigma^2_{\ln Dsite} + 4\sigma^2_{\ln Tfling}} \tag{5-28}$$

(Meyer, 1970, page 134).

5.2.6 84th Percentile Acceleration Amplitude of the Fling

Since ln(A) is lognormally distributed (see Section 5.2.5), then the 84th percentile of ln(A) is given by

$$\ln(A)_{84th} = \ln(A)_{med} + \sigma_{\ln A} \tag{5-29}$$

This is based on the properties of a normal distribution (e.g. Meyer, 1970, page 343). Taking the exponential of both sides of eq. (5-28) leads to

$$A_{84th} = A_{med}\exp(\sigma_{\ln A}) \tag{5-30}$$

5.2.7 84th Percentile Displacement Amplitude of the Fling

Since $\ln(D_{site})$ is assumed to be lognormally distributed (assumption 3.4), then the 84th percentile of $\ln(D_{site})$ is given by

$$\ln(D_{site})_{84th} = \ln(D_{site})_{med} + \sigma_{\ln Dsite} \tag{5-31}$$

This is based on the properties of a normal distribution (e.g. Meyer, 1970, page 343).

Taking the exponential of both sides of eq. (5-31) leads to

$$D_{site\ 84th} = D_{site\ med} \exp(\sigma_{lnDsite}) \tag{5-32}$$

5.2.8 Fling Period for the 84th percentile acceleration amplitude and 84th percentile displacement amplitude

There are two parts to the fling: amplitude of the displacement (D_{site}) and the period of the fling (T_{fling}). Both D_{site} and T_{fling} have variability. To develop the 84th percentile ground motion, requires consideration of the variability of both terms. There is not a unique combination of D_{site} and T_{fling} to define an 84th percentile ground motion. Here, the 84th percentile ground motion is developed using the 84th percentile displacement (D_{site}) and the fling period that leads to an 84th percentile of the fling acceleration (A).

Using eq. (5-22) and (5-30), the 84th percentile fling acceleration is given by

$$A_{84} = \frac{D_{site\ med}\, 2\pi}{981\ T^2_{fling\ med}} \exp(\sigma_{\ln A}) \tag{5-33}$$

The 84th percentile acceleration can also be reached using the 84th percentile displacement and an appropriate fling period (T_{fling1}).

$$A_{84} = \frac{D_{site\ 84}\, 2\pi}{981\ T^2_{fling\ 1}} \tag{5-34}$$

Substituting eq. (5-33) into eq. (5-34) leads to

$$\frac{D_{site\ med}\, 2\pi}{981\ T^2_{fling\ med}} \exp(\sigma_{\ln A}) = \frac{D_{site\ 84}\, 2\pi}{981\ T^2_{fling\ 1}} \tag{5-35}$$

Solving eq. (5-35) for T_{fling1},

$$T_{fling\ 1} = \sqrt{\frac{D_{site\ 84}\, T^2_{fling\ med}}{D_{site\ med} \exp(\sigma_{lnA})}} \tag{5-36}$$

Substituting eq. (5-32) into eq. (5-36) leads to

$$T_{fling\ 1} = \sqrt{\exp(\sigma_{\ln Dsite} - \sigma_{\ln A})}\, T_{fling\ med} \tag{5-37}$$

5.2.9 Vector Amplitude

For some of the data, the tectonic deformation is given in terms of the slip in the east-west and north-south directions separately. The vector amplitude of the tectonic deformation is computed using the square root of the sum of the squares of the orthogonal displacements:

$$D = \sqrt{D_{EW}^2 + D_{NS}^2} \tag{5-38}$$

where D_{EW} is the tectonic deformation in the EW direction and D_{EW} is the tectonic deformation in the NS direction. This is a well known equation.

5.2.10 Distance from the station to the fault

The distance from the station to the site is computed using a flat earth approximation:

$$R = \sqrt{(A\,\Delta\lambda)^2 + (B\Delta\phi)^2} \tag{5-39}$$

where $\Delta\lambda$ and $\Delta\phi$ are the differences in longitude and latitude between the site and the point on the rupture closest to the site (Richter, 1958, page 701). The value of B is 1.85 km/minute of latitude (Richter, 1958, page 704) and the value of A is 1.86/cos(ϕ) km/minute of longitude (Richter, 1958, page 702). Multiplying by 60 minutes/degree results in B= 111.0 km/degree and A = 111.6/cos(ϕ) km/degree.

5.3 Computer Software

A commercial statistical analysis computer program was used to conduct the regression analysis. This program is describe below:

a. Program Name: JMP
b. Program Version: 3.1
c. Program Revision: N/A
d. Computer platform program designed to run on: Macintosh
e. Capabilities and limitations based on its intended use: The program has the capability to run a non-linear least-squares regression based on user defined parametric functions. A limitation is that the JMP non-linear regression cannot determine the α parameter. This parameter must be varied by hand to find the minimum variance solution.
f. Test plans and test cases required to demonstrate the programs capabilities and limitations: None
g. Instructions for use based on the programs capabilities and limitations: no special instructions
h. Program author/owner: SAS Institute Inc.
i. Identification of individual responsible for controlling the software code or executables: unknown, but acceptable, see Item k.
j. Change control: unknown, but acceptable, see Item k.
k. Verification methods used: Test the program using an artificial data set with a known solution.

5.3.1 Verification of JMP for nonlinear regression using Method B

An artificial data set was developed for four earthquakes based on the following parameters:

Eqk 1: $D_{fault} = 1.0$ m
Eqk 2: $D_{fault} = 2.0$ m
Eqk 3: $D_{fault} = 3.0$ m
Eqk 4: $D_{fault} = 4.0$ m
$\alpha = 0.30$
Standard deviation of ln(D) = 0.4

For each earthquake, 250 data point were developed for distances of 1 to 50 km. The displacement from the ith point from the jth earthquake is computed using the natural logarithm of eq. (5-12):

$$Ln(D_{ij}) = \ln(D_{fault_j} (\pi/2 - \tan^{-1}(\alpha R_{ij}) / \pi)) + \varepsilon_{ij}$$

and ε_{ij} are normally distributed with mean zero and standard deviation of 0.4.

The output from the nonlinear regression for a fixed value of α=0.3 is shown on page 22. The estimated coefficients are close to the values for the artificial data set (see Table 5-1)

Nonlinear Fitting Control Panel

Go | Step | Stop | Reset

- Second Deriv. Method
- Continuous Update
- Iteration Log
- Loss is -LogLikelihood

Confid Limits

Report
Converged in the Gradient

	Current	Limit	Alpha
Iteration	3	60	0.050
Shortening	0	15	
O Criterion	2.173475e-11	0.0000001	
D Criterion	0.0000019718	0.0000001	
G Criterion	0.0000000036	0.000001	
CL Criterion	.	0.00001	

Parameter	Current Value	Lock	SSE
c1	0.9927347632		165.77235035
c2	1.9726814604		.
c3	2.9482780122		
c4	4.0105950685		
alpha	0.3		

Formulas

$$\ln(c1)\cdot E1+\ln(c2)\cdot E2+\ln(c3)\cdot E3+\ln(c4)\cdot E4+\ln\left(\frac{\pi}{2}-\arctan(dist\cdot alpha)\right)-\ln(\pi)$$

Mo

$\frac{1}{(c1)}\cdot E1$	c1
$\frac{1}{(c2)}\cdot E2$	c2
$\frac{1}{(c3)}\cdot E3$	c3
$\frac{1}{(c4)}\cdot E4$	c4
0	alpha

Solution

SSE	DFE	MSE	RMSE
165.77235035	996	0.1664381	0.4079683

Parameter	Estimate	ApproxStdErr	Lower CL	Upper CL
c1	0.9927347632	0.02561487	.	.
c2	1.9726814604	0.05089938	.	.
c3	2.9482780122	0.07607185	.	.
c4	4.0105950685	0.1034819	.	.
alpha	0.3	0	.	.

Correlation of Estimates

Figure 5-1. Output from the JMP program validation run with alpha fixed at 0.30.

Table 5-1. Test 1 for non-linear regression (fixed α=0.3)

Parameter	Actual value	Estimated Value
$D_{fault\ 1}$	1.0	0.99
$D_{fault\ 2}$	2.0	1.97
$D_{fault\ 3}$	3.0	2.95
$D_{fault\ 4}$	4.0	4.01
Standard deviation	0.40	0.41

In the second test, the α term was also estimated using the non-linear regression. The output from the best α is shown below on this page, and the results are listed in Table 5-2. The differences between the actual and estimated values are larger for test 2 due to error in estimation of the α term.

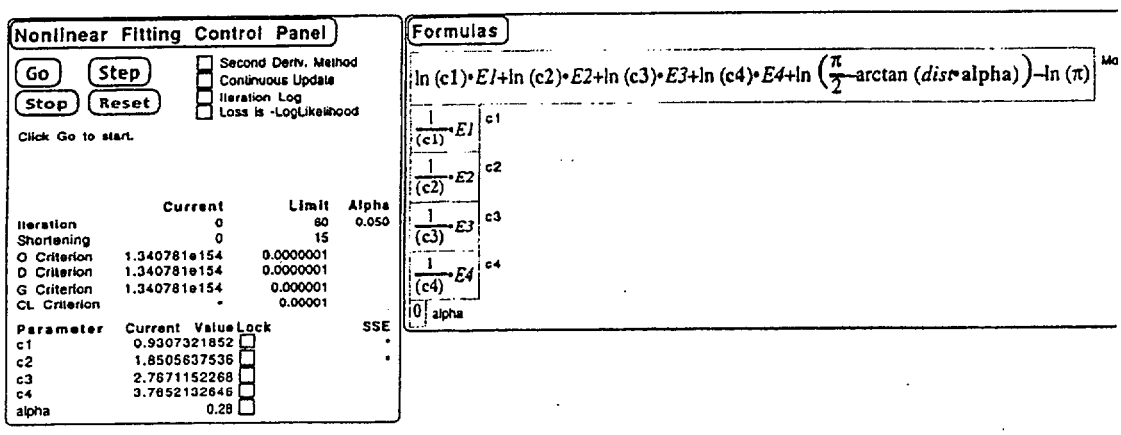

Figure 5-2. Output from the JMP program validation run with alpha determined by the regression.

Table 5-2. Test 2 for non-linear regression

Parameter	Actual value	Estimated Value
$D_{fault\ 1}$	1.0	0.93
$D_{fault\ 2}$	2.0	1.85
$D_{fault\ 3}$	3.0	2.77
$D_{fault\ 4}$	4.0	3.76
α	0.30	0.28
Standard deviation	0.40	0.41

The results of these test cases indicate that the non-linear regression program is working properly.

6. BODY OF CALCULATIONS

6.1 Determination of Distances and Vector Amplitudes for the Displacement Data

The perpendicular distances from the sites with the geodetic measurements to the fault ruptures were not given for the 1992 Landers and 1999 Kocaeli earthquakes. The distances for the Landers earthquake data were computed using the site coordinates (Table 4-4) and the fault coordinates (Table 4-5) assuming vertically dipping faults with eq. (5-39). The resulting distances are listed in Table 6-1.

The amplitudes of the displacements listed in Table 4-4 are given separately for the East and North directions. The amplitudes of the displacement vectors are computed using eq. (5-38) and are listed in Table 6-1.

Similarly, distances for the Kocaeli earthquake data were computed using the site coordinates and the fault coordinates in Tables 4-6 and 4-7. The results are listed in Table 6-2.

The amplitudes of the displacements listed in Table 4-6 are given separately for the East and North directions. The amplitudes of the displacement vectors are computed using eq. (5-38) and are listed in Table 6-2.

Table 6-1. Distances and horizontal vector amplitudes of displacement for the Landers earthquake.

Station Name	Distance from fault (km)	Displacement (cm)
PIN1	53.6	4.8
GOLD	82.4	1.7
JPL1	144.2	1.5
SIO2	156.6	1.6
VNDP	356.8	0.6
0618	196.4	1.4
0704	169.8	5.4
0705	98.2	3.2
0803	50.2	12.0
0805	81.3	3.3
0806	110.0	2.1
0808	58.0	10.0
0818	63.0	5.6
0819	106.1	3.6
0821	60.7	5.5
1106	143.2	2.4
1107	133.3	3.0
1108	98.8	5.3
1109	105.2	1.0
1112	200.7	3.0
1113	63.0	8.1
1114	118.6	4.9
6050	8.8	69.0
6052	21.2	37.5
6054	0.4	129.7
6056	15.8	67.0
6058	15.8	36.0
6060	9.3	51.4
7000	1.1	96.7
7001	8.0	126.2
7002	4.1	129.2
7007	35.4	22.8
AMBO	67.6	8.7

Table 6-1 (cont'd)

Station Name	Distance from fault (km)	Displacement (cm)
ANZA	63.7	7.6
BEAR	40.3	10.8
BLAC	80.9	4.0
BRIN	66.3	3.9
CABA	37.8	20.7
CAJO	77.4	6.1
CHAP	80.2	0.4
CHER	49.5	15.9
COCH	46.4	4.2
CRAF	60.8	7.1
CRIS	111.3	5.2
DASH	79.5	5.4
DUMP	12.0	30.1
EDM2	24.9	7.4
ENDO	179.1	5.0
GAP	45.0	3.3
GARN	24.1	15.4
GODW	46.2	12.3
HECT	27.4	33.1
HIGH	67.7	3.1
INA5	13.0	28.5
INDO	46.5	13.6
INYO	144.5	1.7
JURU	93.9	1.5
L290	152.6	3.4
LAST	86.4	3.4
LAZY	5.7	170.0
LIMP	104.3	7.9
MATH	96.9	2.6
MAUM	2.2	176.4
MDAY	90.1	2.6
MEEK	15.9	69.8
MILL	53.6	8.1
MILU	69.8	4.3
NIGU	136.9	2.4
OCOT	156.4	2.3

Table 6-1. (cont'd)

Station Name	Distance from fault (km)	Displacement (cm)
ONYX	25.1	41.2
PARK	135.5	2.6
PAVE	171.3	4.0
PEAR	111.9	2.3
PINY	54.0	5.3
POIN	41.6	14.0
PORT	137.6	2.1
PVER	186.8	4.1
RESO	45.2	5.5
ROCH	56.6	6.4
ROD2	166.5	4.3
ROSA	96.3	6.8
ROUN	190.2	6.9
SAND	13.9	51.4
SANO	100.5	4.1
SOAP	33.1	7.0
STIM	51.0	6.0
THOU	26.8	17.9
TOM2	26.8	20.3
VIEW	28.8	11.8
WIDE	18.2	9.9

Table 6-2. Distances and vector amplitudes of displacement for the Kocaeli earthquake.

Station	Distance from fault (km)	Displacement (cm)
ANKR	173.1	0.9
DEVR	83.2	3.0
KIBR	75.4	3.2
SIVR	147.6	2.9
ARDC	39.5	6.2
NALL	76.0	4.5
YIGI	35.2	6.5
ALAP	55.7	7.6
AKKO	31.0	15.1
CMLN	64.8	7.6
DKMN	8.5	21.9
KDER	1.0	130.5
TEB4	33.6	20.6
AGOK	12.0	25.9
AGUZ	14.2	28.4
KTOP	4.4	46.6
PIRE	14.0	67.1
MHGZ	69.0	6.4
SEYH	34.5	19.5
KANR	35.2	29.5
SMAS	4.8	141.4
SISL	1.9	163.6
MEKE	29.2	40.3
AKCO	34.2	29.3
IUCK	32.6	31.0
IGAZ	31.2	34.2
KPKL	72.0	6.9
GLCK	2.7	192.7
DERB	38.9	25.3
YUHE	10.1	102.7
SILE	49.3	14.9
OLU4	4.8	118.5
AHMT	46.7	19.4
TUBI	6.5	62.9
DUMT	17.6	45.9

Table 6-2. (cont)

Station	Distance from fault (km)	Displacement (cm)
KRDM	32.8	27.4
KUTE	28.2	28.6
CINA	23.9	13.7
BADA	27.8	18.1
KILY	65.4	9.7
KANT	47.6	13.5
MUDA	60.5	9.7
FIS4	51.2	10.4
AVCI	64.1	5.6
LTFY	116.7	3.2
YENI	94.4	2.7
SELP	94.7	2.6
YALI	124.7	3.1
MERT	123.8	1.3
MADT	154.0	0.7

6.2 Derivation of displacement model as a function of distance from fault

Step 1: Inputting data

The distance and measured displacement data from Section 4 are entered into the JMP program as the independent and dependent variables, respectively. The JMP data file used in the regression analysis is listed in Table 6-3. The earthquakes listed in Table 6-3 are 1 (Landers, 1992), 2 (Imperial Valley, 1940), 3 (San Francisco, 1906), and 4 (Kocaeli,1999). Since the focus of this analysis is to model the tectonic deformation at short distances, only stations at distances less than 50 km were included in the regression analysis.

Table 6-3 Data file used in JMP

Rows	Eqk	dist	displac	logDisp	E1	E2	E3	E4	model	resid
1	1	9	69.0	4.233	1	0	0	0	3.987	0.247
2	1	21	37.5	3.625	1	0	0	0	3.175	0.450
3	1	0	129.7	4.865	1	0	0	0	5.122	-0.257
4	1	16	67.0	4.205	1	0	0	0	3.457	0.747
5	1	16	36.0	3.583	1	0	0	0	3.456	0.127
6	1	9	51.4	3.941	1	0	0	0	3.944	-0.003
7	1	1	96.7	4.572	1	0	0	0	5.022	-0.450
8	1	8	126.2	4.838	1	0	0	0	4.070	0.787
9	1	4	129.2	4.862	1	0	0	0	4.557	0.305
10	1	35	22.8	3.125	1	0	0	0	2.671	0.454
11	1	40	10.8	2.375	1	0	0	0	2.543	-0.168
12	1	38	20.7	3.031	1	0	0	0	2.606	0.425
13	1	49	15.9	2.769	1	0	0	0	2.339	0.430
14	1	46	4.2	1.436	1	0	0	0	2.402	-0.966
15	1	12	30.1	3.405	1	0	0	0	3.713	-0.308
16	1	25	7.4	1.996	1	0	0	0	3.018	-1.022
17	1	45	3.3	1.187	1	0	0	0	2.432	-1.246
18	1	24	15.4	2.735	1	0	0	0	3.049	-0.314
19	1	46	12.3	2.513	1	0	0	0	2.408	0.105
20	1	27	33.1	3.500	1	0	0	0	2.925	0.574
21	1	13	28.5	3.352	1	0	0	0	3.643	-0.292
22	1	46	13.6	2.612	1	0	0	0	2.402	0.211
23	1	6	170.0	5.136	1	0	0	0	4.340	0.796
24	1	2	176.4	5.173	1	0	0	0	4.847	0.325
25	1	16	69.8	4.246	1	0	0	0	3.450	0.796
26	1	25	41.2	3.720	1	0	0	0	3.011	0.708
27	1	42	14.0	2.639	1	0	0	0	2.510	0.129
28	1	45	5.5	1.713	1	0	0	0	2.429	-0.715
29	1	14	51.4	3.940	1	0	0	0	3.576	0.364
30	1	33	7.0	1.951	1	0	0	0	2.738	-0.786
31	1	27	17.9	2.883	1	0	0	0	2.944	-0.062
32	1	27	20.3	3.012	1	0	0	0	2.944	0.067
33	1	29	11.8	2.468	1	0	0	0	2.874	-0.406
34	1	18	9.9	2.291	1	0	0	0	3.324	-1.033
35	2	4	145.9	4.983	0	1	0	0	4.354	0.629
36	2	10	78.6	4.364	0	1	0	0	3.695	0.669
37	2	21	23.5	3.157	0	1	0	0	3.010	0.147
38	2	26	9.2	2.219	0	1	0	0	2.793	-0.574
39	2	34	9.2	2.219	0	1	0	0	2.540	-0.321
40	2	1	127.6	4.849	0	1	0	0	4.788	0.061
41	2	11	44.9	3.804	0	1	0	0	3.594	0.211
42	2	15	20.4	3.016	0	1	0	0	3.324	-0.308
43	2	28	8.2	2.104	0	1	0	0	2.720	-0.616
44	2	38	12.2	2.501	0	1	0	0	2.419	0.083
45	2	47	9.2	2.219	0	1	0	0	2.199	0.020
46	3	0	158.0	5.063	0	0	1	0	5.225	-0.162
47	3	1	158.0	5.063	0	0	1	0	5.184	-0.121
48	3	1	204.0	5.318	0	0	1	0	5.095	0.223
49	3	1	155.0	5.043	0	0	1	0	5.079	-0.036
50	3	2	136.0	4.913	0	0	1	0	4.984	-0.072
51	3	2	136.0	4.913	0	0	1	0	4.940	-0.027
52	3	2	145.0	4.977	0	0	1	0	4.969	0.008
53	3	2	157.0	5.056	0	0	1	0	4.937	0.120
54	3	2	187.0	5.231	0	0	1	0	4.953	0.279
55	3	3	177.0	5.176	0	0	1	0	4.842	0.335
56	3	4	87.0	4.466	0	0	1	0	4.673	-0.207
57	3	4	83.0	4.419	0	0	1	0	4.659	-0.240
58	3	5	98.0	4.585	0	0	1	0	4.517	0.068
59	3	6	64.0	4.159	0	0	1	0	4.325	-0.167
60	4	40	6.2	1.816	0	0	0	1	2.750	-0.934
61	4	35	6.5	1.867	0	0	0	1	2.864	-0.997
62	4	31	15.1	2.716	0	0	0	1	2.990	-0.274
63	4	8	21.9	3.089	0	0	0	1	4.206	-1.117
64	4	1	130.5	4.872	0	0	0	1	5.220	-0.348
65	4	34	20.6	3.026	0	0	0	1	2.910	0.116
66	4	12	25.9	3.253	0	0	0	1	3.901	-0.648
67	4	14	28.4	3.346	0	0	0	1	3.745	-0.399
68	4	4	46.6	3.842	0	0	0	1	4.696	-0.853
69	4	14	67.1	4.206	0	0	0	1	3.758	0.448
70	4	34	19.4	2.963	0	0	0	1	2.884	0.079
71	4	35	29.4	3.383	0	0	0	1	2.864	0.518

Table 6-3 . (cont) Data file used in JMP

lows	Eqk	dist	dispiac	logDisp	E1	E2	E3	E4	model	resid
72	4	5	141.4	4.952	0	0	0	1	4.640	0.312
73	4	2	163.6	5.097	0	0	0	1	5.078	0.019
74	4	29	40.3	3.695	0	0	0	1	3.049	0.647
75	4	34	29.3	3.378	0	0	0	1	2.893	0.485
76	4	33	31.0	3.435	0	0	0	1	2.940	0.495
77	4	31	34.1	3.531	0	0	0	1	2.983	0.547
78	4	3	192.7	5.261	0	0	0	1	4.951	0.310
79	4	39	25.3	3.230	0	0	0	1	2.765	0.465
80	4	10	102.7	4.632	0	0	0	1	4.056	0.576
81	4	49	14.9	2.705	0	0	0	1	2.530	0.175
82	4	5	118.5	4.775	0	0	0	1	4.640	0.135
83	4	47	19.4	2.967	0	0	0	1	2.584	0.383
84	4	6	62.9	4.141	0	0	0	1	4.423	-0.281
85	4	18	45.9	3.827	0	0	0	1	3.541	0.285
86	4	33	27.4	3.311	0	0	0	1	2.934	0.377
87	4	28	28.6	3.354	0	0	0	1	3.083	0.271
88	4	24	13.7	2.617	0	0	0	1	3.245	-0.628
89	4	28	18.1	2.898	0	0	0	1	3.097	-0.199
90	4	48	13.5	2.600	0	0	0	1	2.565	0.035

Step 2: Setting up regression model
The model in eq. (5-13) is set up as the regression model in the JMP regression. A screen print of the model set up in JMP is shown below:

$$\ln(\mathbf{c1})\bullet E1+\ln(\mathbf{c2})\bullet E2+\ln(\mathbf{c3})\bullet E3+\ln(\mathbf{c4})\bullet E4+\ln\left(\frac{\pi}{2}-\arctan(dist\bullet\mathbf{alpha})\right)-\ln(\pi)$$

Step 3: Running regression analyses
The non-linear least-squares regression analysis function is invoked using the data and model from steps 1 and 2. Since the regression software could not determine α, this value was varied manually. The root mean square error (RMSE) for a range of α values is shown in Table 6-4. The output screens from the final run is given on page 35.

Table 6-4. Determination of α.

α	RMSE (std dev)
0.21	0.4977
0.22	0.49752
0.23	0.49755

Output from JMP non-linear regression.

Nonlinear Fitting Control Panel

Go | Step | Stop | Reset | Confid Limits

- [ ] Second Deriv. Method
- [ ] Continuous Update
- [ ] Iteration Log
- [ ] Loss is -LogLikelihood

Report
Converged in the Gradient

	Current	Limit	Alpha
Iteration	1	60	0.050
Shortening	0	15	
O Criterion	1.668972e-16	0.0000001	
D Criterion	1.654025e-11	0.0000001	
G Criterion	1.475513e-25	0.000001	
CL Criterion	•	0.00001	

Parameter	Current Value	Lock	SSE
c1	355.49755384	[ ]	21.286832959
c2	296.22924735	[ ]	•
c3	384.37238888	[ ]	
alpha	0.22	[ ]	
c4	428.77359782	[ ]	

Formulas

Solution

SSE	DFE	MSE	RMSE
21.286832959	86	0.2475213	0.4975151

Parameter	Estimate	ApproxStdErr	Lower CL	Upper CL
c1	355.49755384	30.3321684	•	•
c2	296.22924735	44.4363003	•	•
c3	384.37238888	51.1086566	•	•
alpha	0.22	0	•	•
c4	428.77359782	38.3136466	•	•

Correlation of Estimates

The α value that results in the minimum RMSE is α =0.22. The coefficients for this run are listed in Table 6-5.

Table 6-5. Regression Coefficients.

Earthquake	Parameter	Estimate
Landers	C_1	355.5
Imperial Valley	C_2	296.2
San Francisco	C_3	384.4
Kocaeli	C_4	428.8

alpha = 0.22

σ = 0.50 (from Table 6-4)

Figures 6-1, 6-2, 6-3, and 6-4 compare the data for each individual earthquake along with their corresponding models (event specific c value). Figure 6-5 shows the data for all the earthquakes combined, with the displacement normalized by the c coefficient for the particular earthquake. Residuals from the regression are shown in Figure 6-6. As shown, there are no biases in the residuals with distance.

The estimated D_{fault} values listed in Table 6-5 are plotted versus magnitude in Figure 6-7. These values are compared to the model of D_{fault} from eq. (5-7). There are only four data points, but in general they are consistent with the model from eq. (5-7). The model (eq. 5-7) yields a median displacement for a magnitude 7.2 earthquake of about 2 m. This is consistent with the 1.8-2m displacements found in trenching studies at San Simeon (PG&E, 1988)

The total standard deviation of D_{site} is computed using eq. (5-14) with the following values:

$\sigma_{\ln Dsite\ reg} = 0.50$

$\sigma_{\ln Dfault} = 0.44$ (from eq. 5-9)

Using these values in eq. (5-14) gives

$$\sigma_{\ln Dsite} = \sqrt{0.44^2 + 0.50^2} = 0.67 \qquad (6\text{-}1)$$

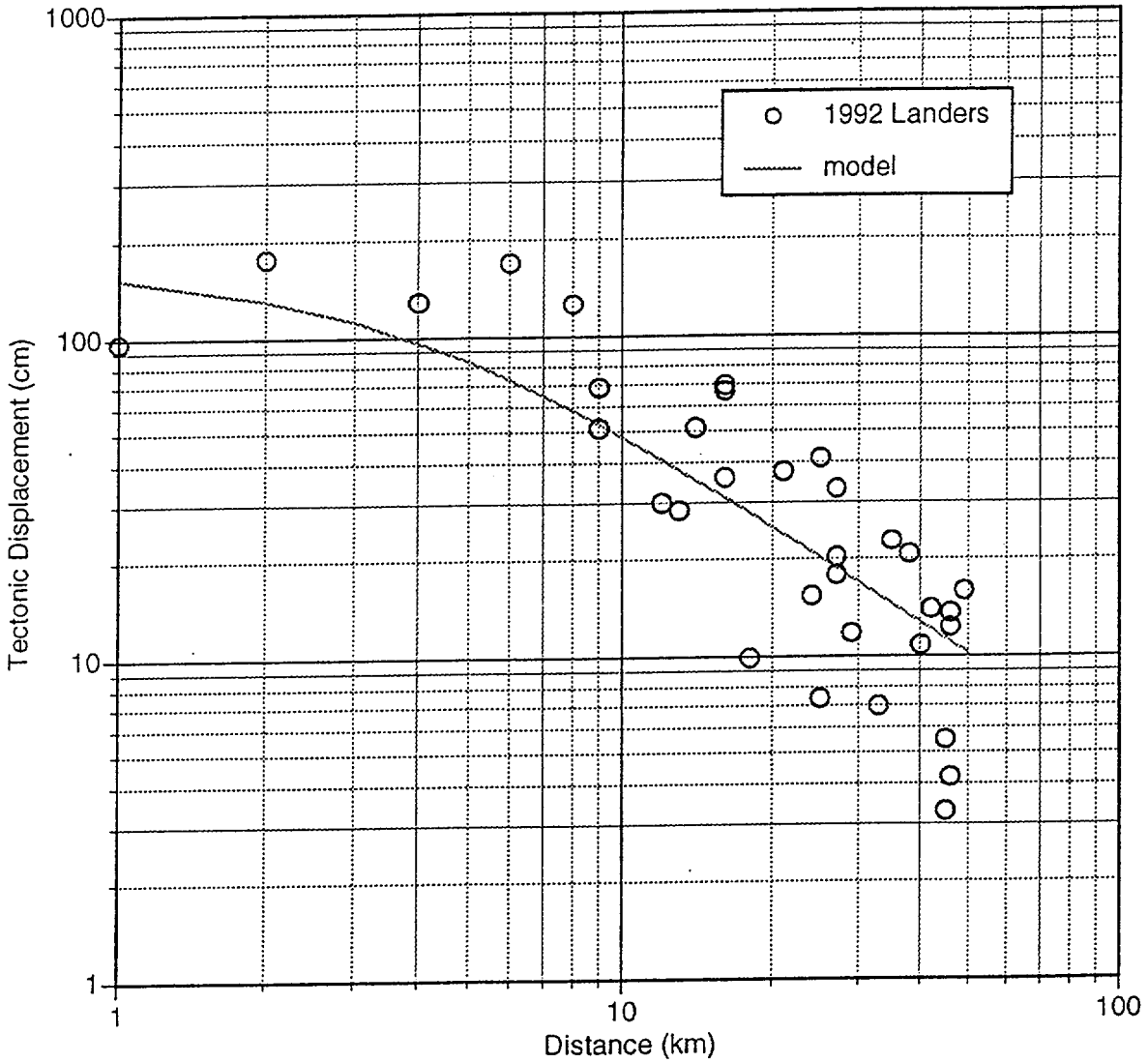
1992 Landers
model
Tectonic Displacement (cm)
1000
100
10
1
1
10
100
Distance (km)

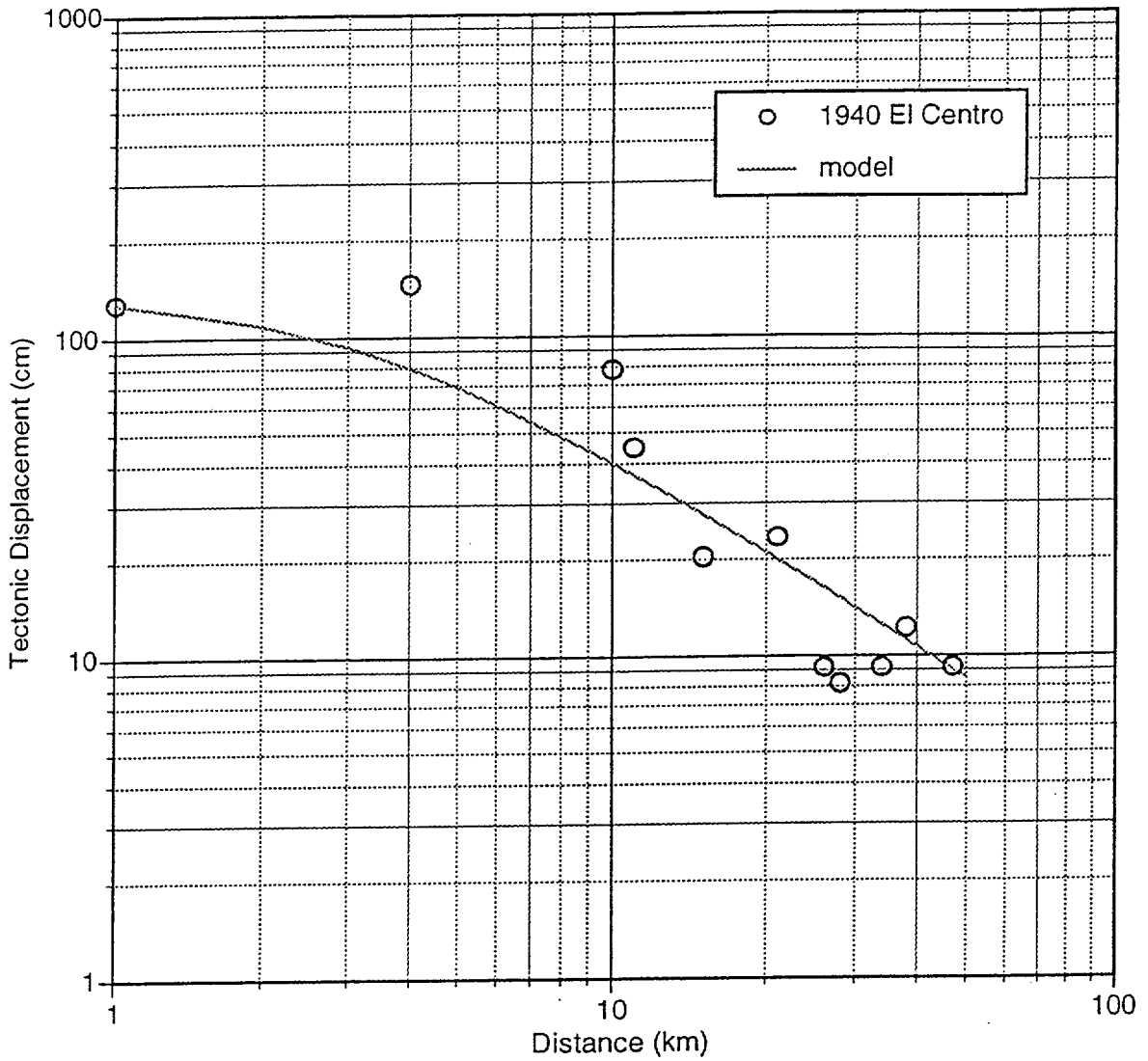
1940 El Centro
model
Tectonic Displacement (cm)
1000
100
10
1
1
10
100
Distance (km)

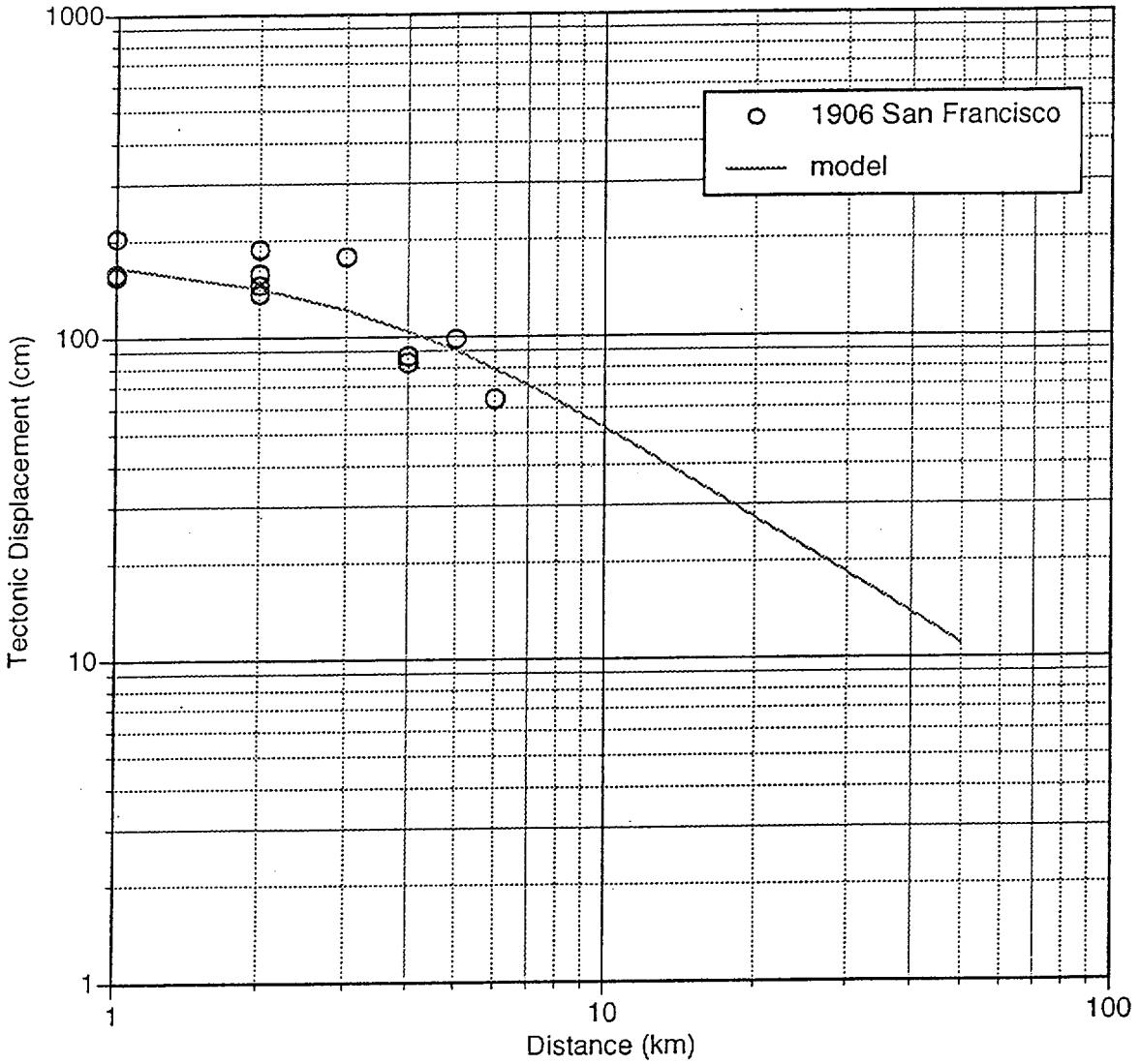
1906 San Francisco
model
Tectonic Displacement (cm)
1000
100
10
1
1
10
100
Distance (km)

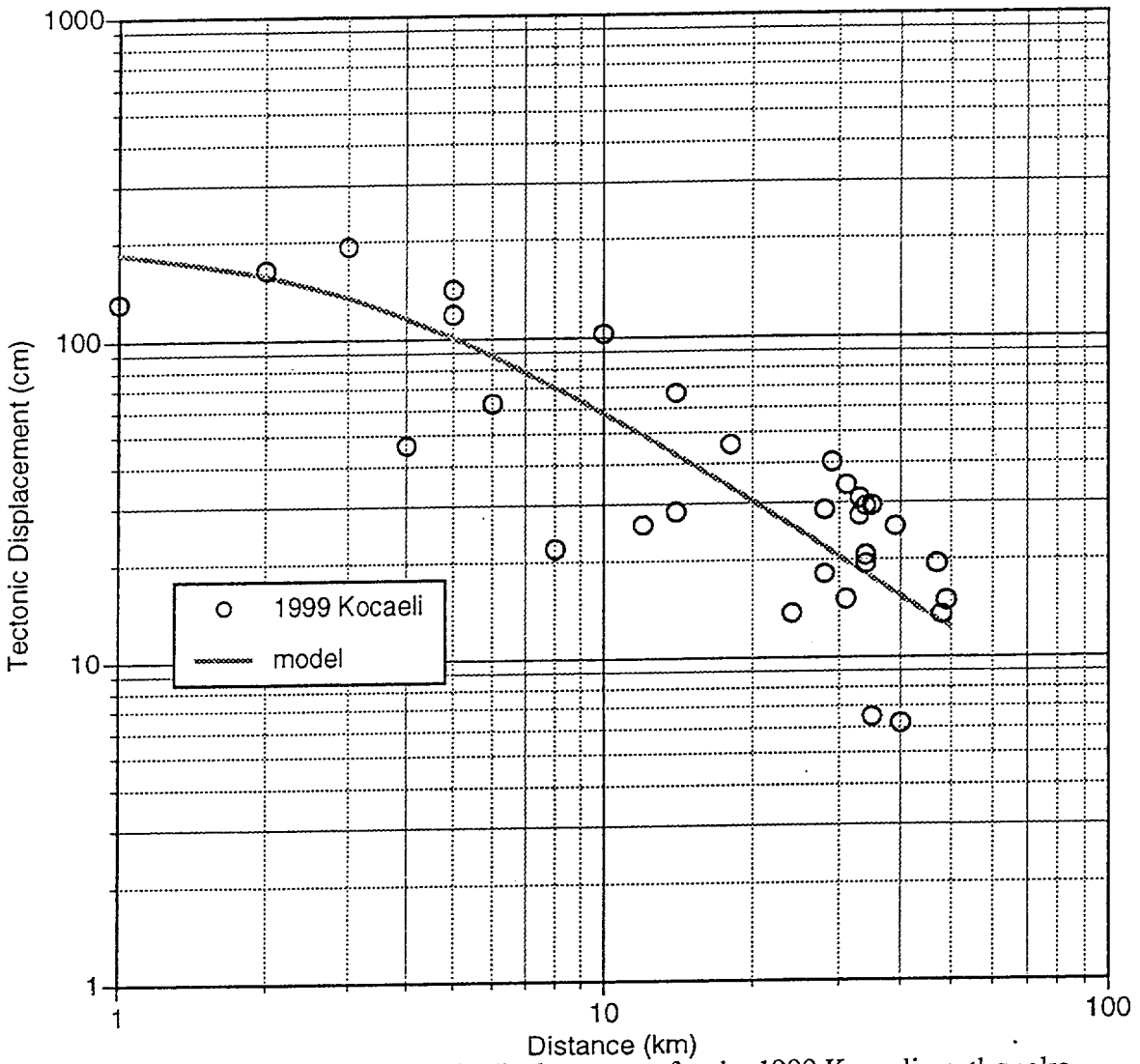

Figure 6-4. Comparison of the tectonic displacements for the 1999 Kocaeli earthquake with the model from the regression.

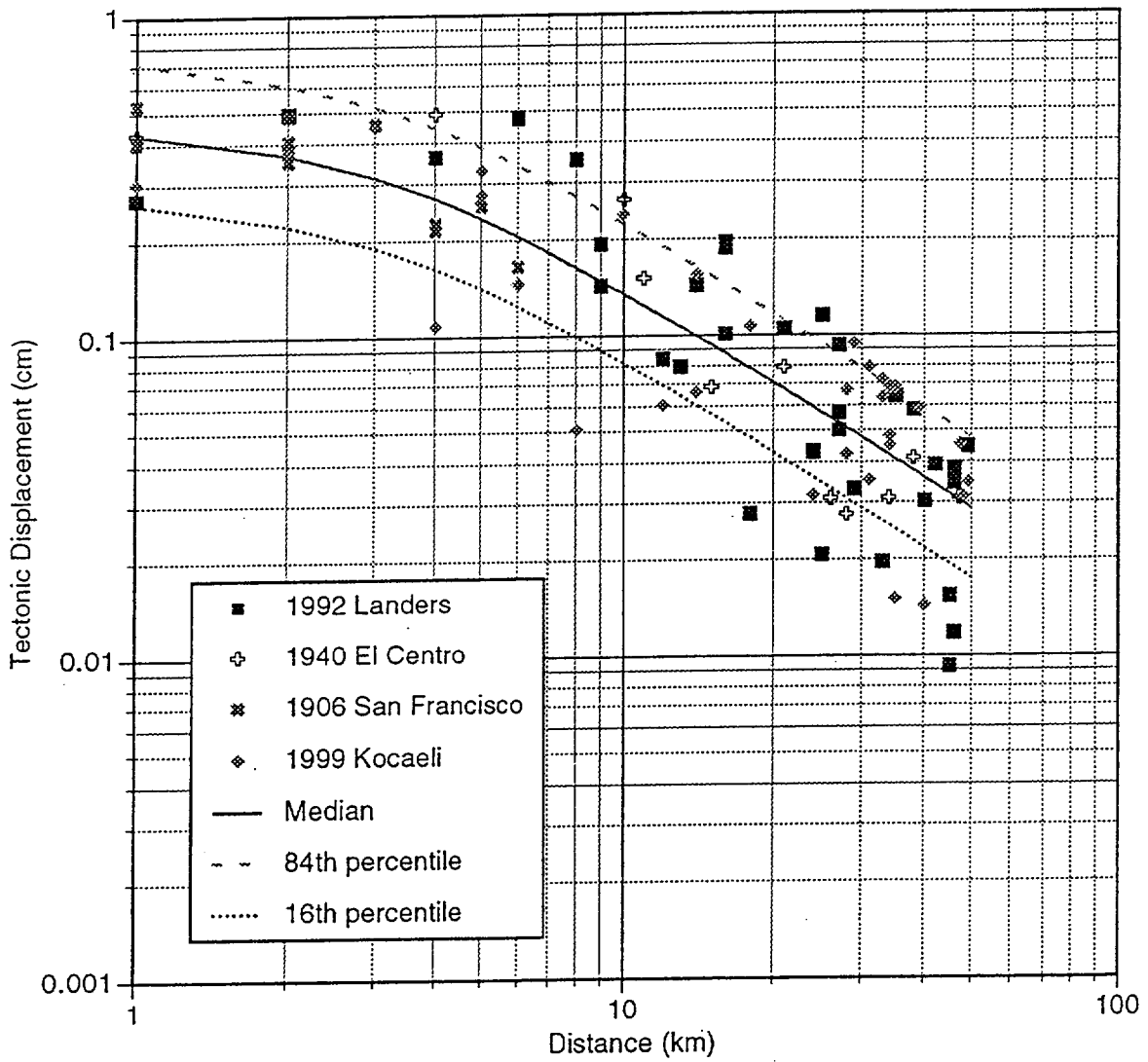

Figure 6-5. Comparison of the normalized displacements (normalized by the estimated fault displacement) with the model prediction.

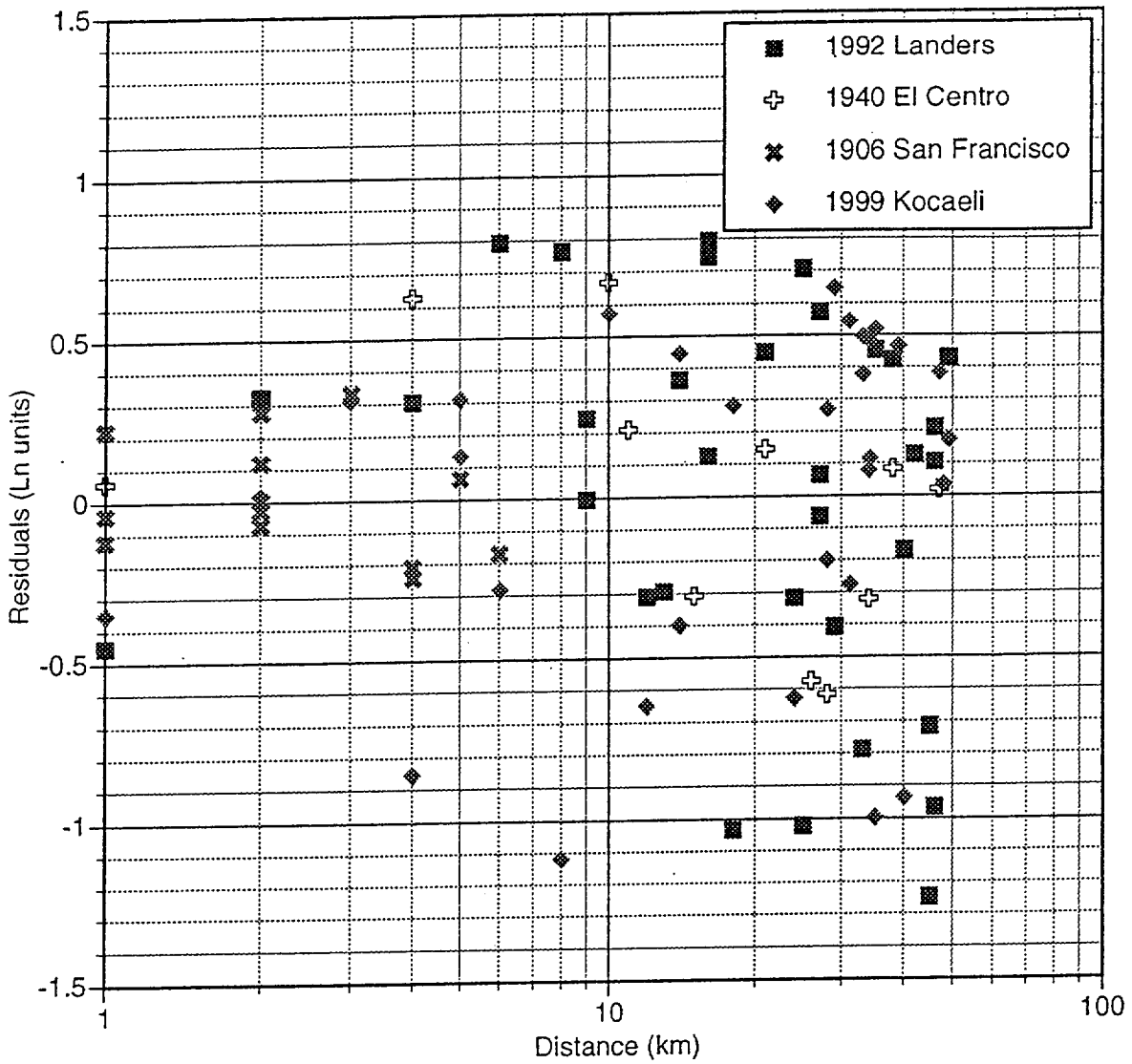

Figure 6-6. Residuals of the regression.

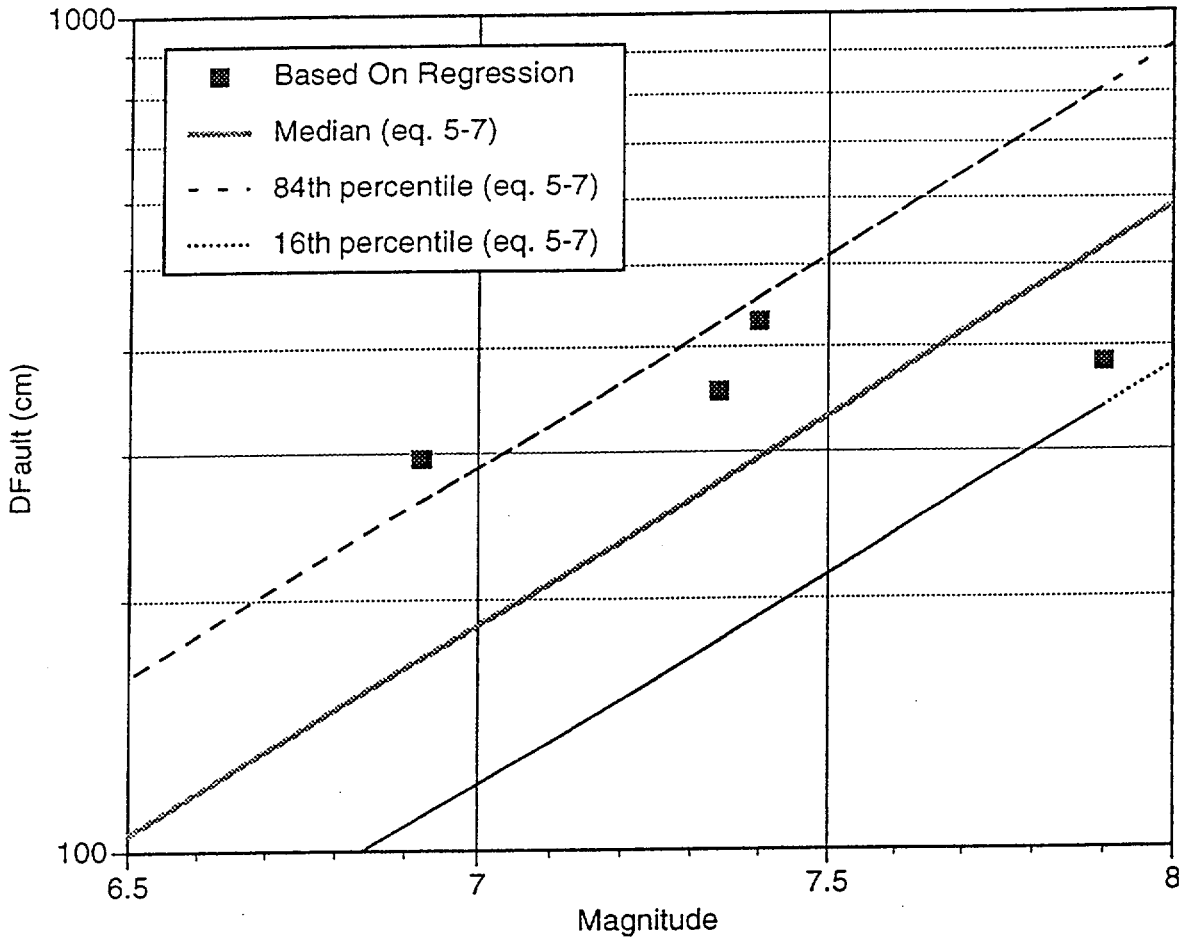

Figure 6-7. Comparison of the fault displacements estimated from the regression (Table 6-5) with the model of the fault displacement derived from the magnitude-area relation (eq. 5-7).

Development of the Fling Period Model:
The strong motion data near large earthquakes that contain permanent displacement were examined visually to estimate the duration of the fling. A simple straight line was fit to the displacement. This does not include the curved start and stop of the fling model (Figure 6-8). The ratio of the fling period (T_{fling}) to the duration from the straight line, t_2, is approximately 1.78.

Three earthquakes have well defined permanent displacements that can be determined from the strong motion data: 1992 Landers, 1999 Kocaeli, and 1999 Chi-Chi. The strong motion recordings that are closer to the fault slip direction for records with permanent displacements are listed in Table 6-6. The Landers data are from Chen (1995); the Kocaeli data are from Rathjie (2001); and the Chi-Chi data are from Lee et al. (1999). For the Kocaeli and Chi-Chi data, the component closest to parallel to the fault slip is used.

Table 6-6 also lists the estimated start and stop times defining the straight-line fits. The displacements from the strong motion data on which these estimates are based are shown in the appendix to this calculation package.

For the Landers Lucerne recording, the permanent displacement is larger on the component perpendicular to the fault strike. There are two reasons for this. First, there are large bends in the strike of the rupture of the Landers earthquake resulting in tectonic deformation that is not parallel to the strike of the section of the fault near the Lucerne recording. Second, the processing of the recorded ground motions appears to have removed much of the permanent displacement on the fault parallel component. The fault parallel component of the Lucerne recording shown by Somerville et al (1997) has a larger displacement, but this is based on the geodetic observations and not on strong motion data. (The strong motion data were modified by Somerville et al (1997) to be consistent with the geodetic data.) Therefore, for this recording, the empirically derived fling duration is computed from 285 component.

The median value of t_2 for each earthquake is listed in Table 6-7. The standard deviation of $\ln(t_2)$ from the well-recorded Chi-Chi earthquake is 0.31. This value is assumed to be representative of the within-earthquake variability of $\ln(t_2)$.

The fling period, T_{fling}, is computed by scaling the median value of t_2 by 1.78. The resulting estimates of T_{fling} are also listed in Table 6-7. Since T_{fling} is simply a scale factor time t_2, then the standard deviation of $\ln(T_{fling})$ is equal to the standard deviation of $\ln(t_2)$. That is

$$\sigma_{(\ln Tfling)} = 0.31 \qquad (6\text{-}2)$$

The estimated values of T_{fling} are plotted as a function of magnitude in Figure 6-9. These three data points were fit to the form:

$$\ln(T_{fling}) = c1 + \ln(10)\ 0.5M \qquad (6\text{-}3)$$

The resulting equation is

$$\ln(T_{fling}) = -6.96 + 1.15\ M \qquad (6\text{-}4)$$

with a standard deviation of 0.13 natural log units. This standard deviation represents the between-earthquake variability of $\log(T_{fling})$. Combining the standard deviations of the within-earthquake and between-earthquake variability of $\ln(T_{fling})$, the total standard deviation of $\ln(T_{fling})$ is

$$\sigma_{\ln(T_{fling})} = \sqrt{0.31^2 + 0.13^2} = 0.34 \qquad (6\text{-}5)$$

Table 6-6. Time and amplitude values for the near fault fling dataset of strong ground motion time histories.

Earthquake	Station	t_1 (sec)	$t_1 + t_2$ (sec)	t_2 (sec)	Amplitude (cm)
Landers	LCN285	7.6	10.0	2.4	191.0
Kocaeli	YPT-Long	9.5	12.6	3.1	189.1
	SKR-Tran	32.3	35.2	2.9	176.1
Chi-Chi	TCU048E	30.4	33.7	3.3	37.0
	TCU049E	31.8	33.4	1.6	65.7
	TCU050E	29.3	32.3	3.0	50.1
	TCU051E	29.6	32.6	3.0	49.7
	TCU052-150	33.0	37.4	4.4	-838.7
	TCU053E	31.0	34.0	3.0	77.0
	TCU054E	30.0	32.9	2.9	41.2
	TCU055E	12.2	15.2	3.0	91.0
	TCU056E	28.5	31.8	3.3	51.7
	TCU057E	28.4	31.4	3.0	50.7
	TCU060E	28.1	31.1	3.0	44.7
	TCU063E	28.0	31.3	3.3	51.4
	TCU064E	31.0	33.4	2.4	15.3
	TCU067E	29.0	30.5	1.5	124.5
	TCU068N	33.8	37.5	3.7	843.5
	TCU070E	29.8	33.0	3.2	29.9
	TCU075E	27.5	28.5	1.0	128.8
	TCU076E	26.2	28.1	1.9	103.8
	TCU082E	29.2	32.5	3.3	71.2
	TCU100E	29.5	32.8	3.3	47.6
	TCU101E	11.5	15.7	4.2	156.2
	TCU104E	29.8	32.7	2.9	27.7
	TCU105E	30.2	33.1	2.9	28.2
	TCU106E	28.0	31.3	3.3	36.3
	TCU109E	28.7	30.8	2.1	33.0
	TCU116E	24.8	27.9	3.1	44.6
	TCU120E	26.0	29.0	3.0	71.8
	TCU122E	25.0	28.0	3.0	56.1
	TCU123E	27.8	30.8	3.0	49.9

Table 6-7. Estimated fling durations from strong motion data

Earthquake	Magnitude	Number of Recordings	Median straight line duration (t_2) (sec)	Standard deviation of $\ln(t_2)$	Median T_{fling} (sec)
1992 Landers	7.34	1	2.40	-	4.27
1999 Kocaeli	7.4	2	3.00	0.05	5.34
1999 Chi-Chi	7.6	29	3.00	0.31	5.34

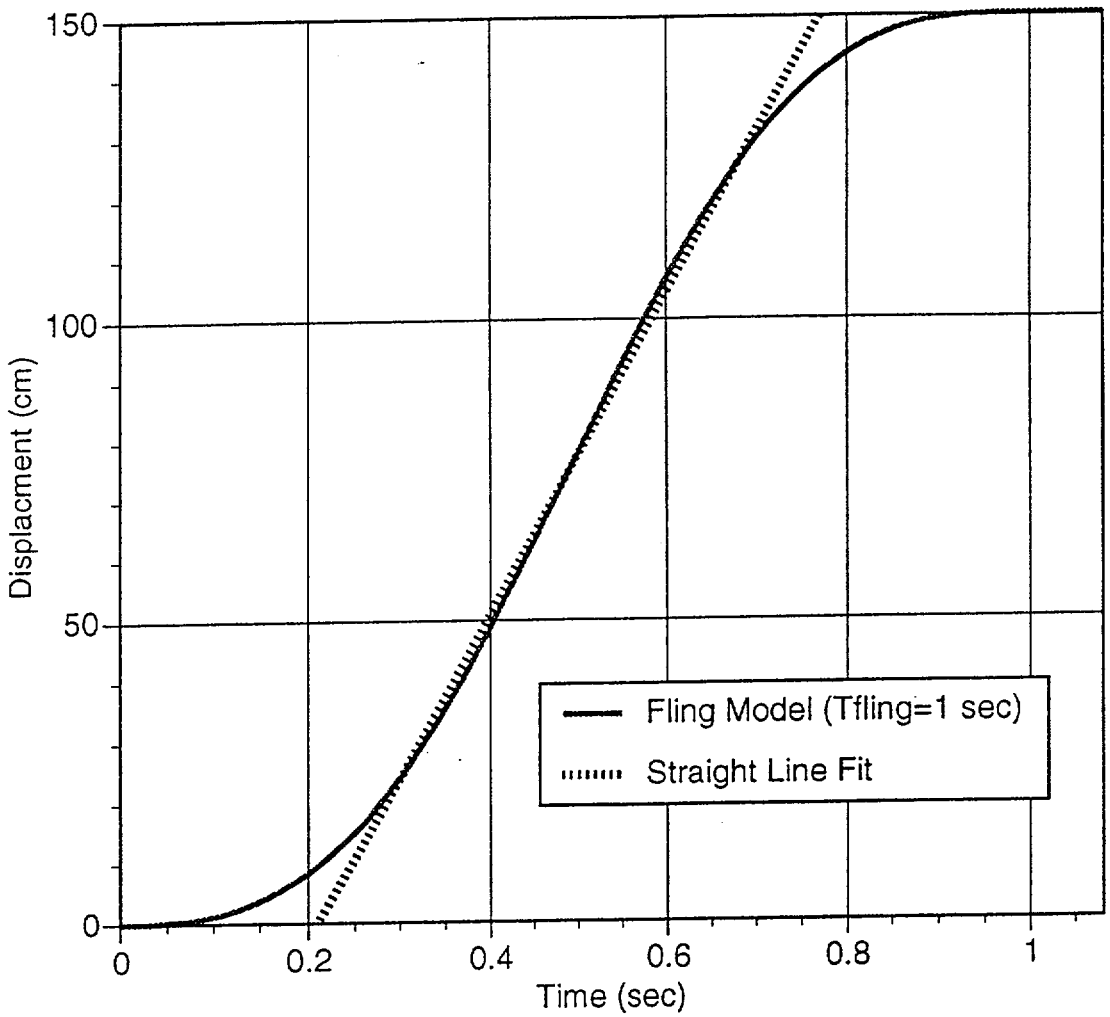

Figure 6-8. Comparison of time of the fling from a straight line fit and the sine-wave fling model. The ratio is about 1.78.

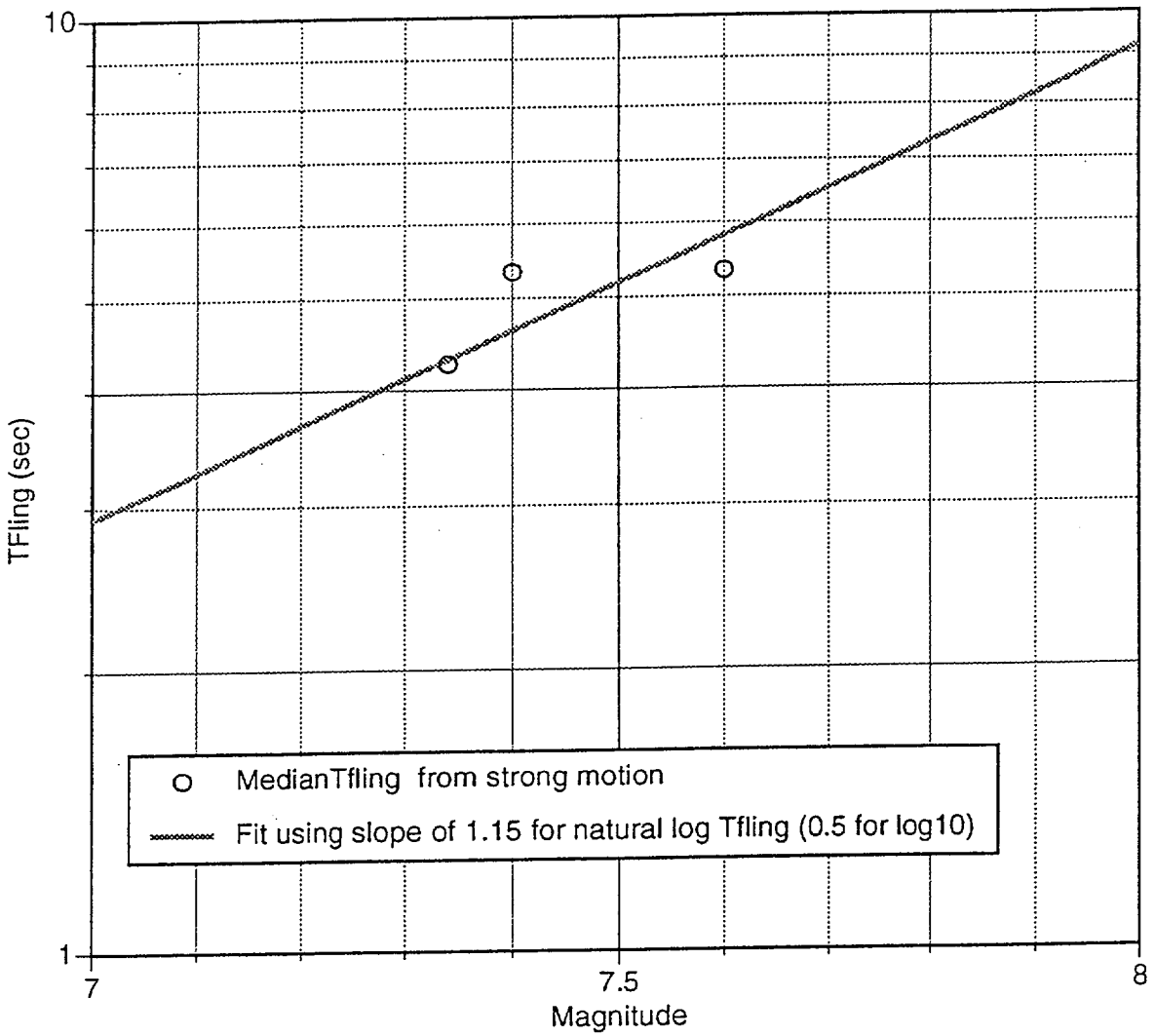

Figure 6-9. Fit of the period of the fling as a function of magnitude.

Estimation of the fling amplitude at the ISFSI site

The average slip on the fault, D_{fault}, is computed using eq. (5-8), with the following inputs:

$M = 7.2$

The resulting value is

$D_{fault} = 233$ cm

The median displacement at the site is computed using eq. (5-12) with α=0.22 from Table 6-5 and R=4.5 km:

$$D_{site\ med} = D_{fault}\ (\pi/2\text{-}\tan^{-1}(\alpha\ 4.5))/\pi = 233\ \text{cm}\ (\pi/2\text{-}\tan^{-1}(\alpha\ 4.5))/\pi = 59\ \text{cm} \qquad (6\text{-}6)$$

The 84th percentile displacement at the site is computed using eq. (5-32). The 84th percentile fling amplitude is

$$D_{site\ 84th} = D_{site\ med} * \exp(\sigma_{lnDsite}) = 59\ \text{cm} * \exp(0.67) = 115\ \text{cm} \qquad (6\text{-}7)$$

The median Fling period is computed using

$$T_{fling\ med} = \exp(-6.96 + 1.15\ M) = \exp(-6.96 + 1.15\ (7.2)) = 3.7\ \text{sec} \qquad (6\text{-}8)$$

The median acceleration amplitude of fling is computed using eq. (5-22):

$$A_{med}(g) = \frac{D_{site\ med}\,2\pi}{981\ T^2_{fling\ med}} = \frac{59cm * 2\pi}{981 cm/s^2/g * (3.7\sec)^2} = 0.028g \qquad (6\text{-}9)$$

The standard deviation of ln(A) is computed using eq. (5-28):

$$\sigma_{\ln A} = \sqrt{\sigma^2_{\ln Dsite} + 4\sigma^2_{\ln Tfling}} = \sqrt{0.67^2 + 4(0.34)^2} = 0.95 \qquad (6\text{-}10)$$

The 84th percentile of the acceleration amplitude of fling is computed using eq. (5-30):

$$A_{84th} = A_{med} * \exp(\sigma_{lnA}) = 0.028\ g * \exp(0.95) = 0.072\ g \qquad (6\text{-}11)$$

The amplitude of the 84th percentile fling time history is computed using eq. (5-37) :

$$T_{fling\,1} = \sqrt{\exp(\sigma_{\ln Dsite} - \sigma_{\ln A})}\, T_{med} = \sqrt{\exp(0.67 - 0.95)}\;\; 3.7\,\text{sec} = 3.2\,\text{sec} \qquad (6\text{-}12)$$

The corresponding angular frequency of the fling pulse (in acceleration) is

$$\omega = 2\pi/T_{fling1} = 1.96 \text{ radians/sec.} \qquad (6\text{-}13)$$

7. RESULTS

The 84th percentile fling at the ISFSI site from a magnitude 7.2 earthquake on the Hosgri fault has a displacement amplitude of 115 cm and an acceleration amplitude of 0.072g. The corresponding period of the fling is 3.2 sec.

The acceleration time history of the fling is given by

$$Acc_{fling}(t) = 0 \qquad \text{for } t < t_1$$
$$Acc_{fling}(t) = A \sin(\omega(t - t_1)) \qquad \text{for } t_1 < t < t_1 + T_{fling}$$
$$Acc_{fling}(t) = 0 \qquad \text{for } t_1 + T_{fling} < t$$

with $A = 0.072g$, and $\omega = 1.96$ radians/sec. t_1 is the arrival time of the fling at the site.

8. CONCLUSIONS

The derived fling model is appropriate for estimating the fling at the ISFSI site due to a strike-slip earthquake on the Hosgri fault.

Limitations:

If a style of faulting other than strike-slip is considered for the Hosgri, then this model is not applicable.

The duration of the fling is estimated using only the data from three earthquakes. The magnitudes of these are range from 7.3 to 7.6. The extrapolation of this model to earthquakes less than magnitude 7 is very poorly constrained. Care should be taken before extrapolating these models to moderate magnitudes.

9. REFERENCES

Bevington, P. R. (1969). Data reduction and error analysis for the physical sciences, McGraw-Hill Book Company,

Byerly, P., and DeNoyer, J. (1958). "Energy in earthquakes as computed from geodetic observations," *Contributions in Geophysics, In Honor of Beno Gutenberg*, New York: Pergamon Press.

Chen, X. D. (1995). Near field ground motion from the Landers earthquake, EERL 95-02, California Institute of Technology Report.

EERI (2000). 1999 Kocaeli, Turkey, Earthquake Reconnaissance Report, Earthquake Engineering Research Institute, Oakland, CA.

Hanks, T. and H. Kanamori (1979). A moment magnitude scale, J. Geopy. Res., 84, 2348-2350.

Hudnut, K.W., Bock, Y., Cline, M., Fang, P., Feng, Y., Freymueller, J., Ge, X., Gross, W.K., Jackson, D., Kim, M. King, N.E., Langbein, J., Larsen, S.C., Lisowski, M., Shen, Z.-K., Svarc, J., and Zhang, J. (1994). "Co-seismic displacements of the 1992 Landers earthquake sequence," *Bull. Seism. Soc. America*, 84(3), 625-645.

Kanamori, H. and D. L. Anderson (1975). Theoretical basis of some empirical relations in seismology, Bull. Seism. Soc. Am., 65, 1073-1095.

Lee, W. H. K, T. C. Shin, K. W. Kuo, and K. C. Chen (1999). Digital acceleration data from the 1999 Chi-Chi Taiwan earthquake, Compact Disk produced by the Taiwan Central Weather Bureau, December 13, 1999.

Meyer, P. L. (1970). Introductory probability and statistical applications, second ed. Addison-Wesley Publication Company.

PG&E (1988). Final Report of the Long Term Seismic Program, Pacific Gas and Electric Company, Diablo Canyon Power Plant, Docket Nos. 50-275 and 50-323, July 1988.

Rathjie, E. (2001). Processing of the strong motion data from the 1999 Kocaeli earthquake, Report to PG&E.

Reilinger, R.E., Ergintav, S., Burgmann, R., McClusky, S., Lenk, O., Barka, A., Gurkan, O., Hearn, L., Feigl, K.L., Cakmak, R., Aktug, B., Ozener, H., Toksoz, M.N. (2000). "Coseismic and postseismic fault slip for the 17 August 1999, M = 7.5, Izmit, Turkey Earthquake," *Science*, 289, 1519-1524.

Reilinger, R.E., Ergintav, S., Burgmann, R., McClusky, S., Lenk, O., Barka, A., Gurkan, O., Hearn, L., Feigl, K.L., Cakmak, R., Aktug, B., Ozener, H., Toksoz, M.N. (2000). Online supplement to "Coseismic and postseismic fault slip for the 17 August 1999, M = 7.5, Izmit, Turkey Earthquake," *Science*, 289, 1519-1524. The on-line supplement is available via the Science web site: www.aaas.org

Richter, C. F. (1958). Elementary Seismology. Freeman, San Francisco, 570 pp.

Somerville, P. G., K. Irikura, R. Graves, S. Sawada, D. Wald, N. Abrahamson, Y. Iwasaki, T. Kagawa, N. Smith, and A. Kowada. "Characterizing crustal slip models for the prediction of strong ground motion", Seism. Res. Let., 70, 59-80.

Stacey, F.D., (1969). Physics of the Earth, John Wiley & Sons, Inc., New York.

Wald, D. J and T. H. Heaton (1994). Spatial and temporal distribution of slip for the 1992 Landers, California, Earthquake, Bull. Seism. Soc. Am., 84, 668-691.

Wells, D. L. and K. J. Coppersmith (1994). New empirical relationships among magnitude, rupture length, rupture width, rupture area, and surface displacement, Bull. Seism. Soc. Am., 84, 974-1002.

Working Group on California Earthquake Probabilities (1999). Earthquake probabilities in the San Francisco Bay Region: 2000 to 2030 – A summary of Findings. U. S. Geological Survey Open File Report 99-157.

Appendix for Calculation Number GEO.DCPP.01.12

Revision Number 1

September 26, 2001

Plots of Time Histories Used to Measure Fling Period

Landers Earthquake: Station LCN, Comp 285, Fling Model

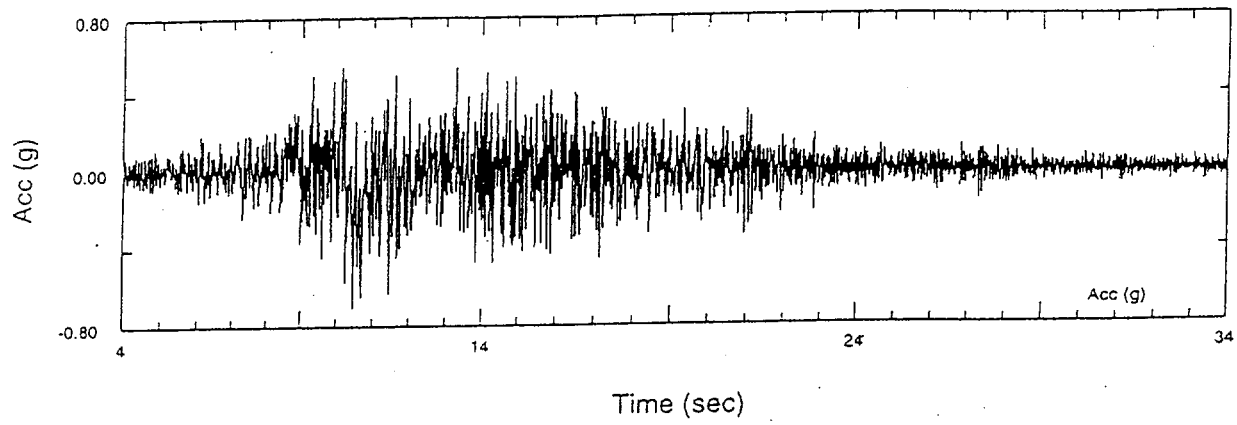

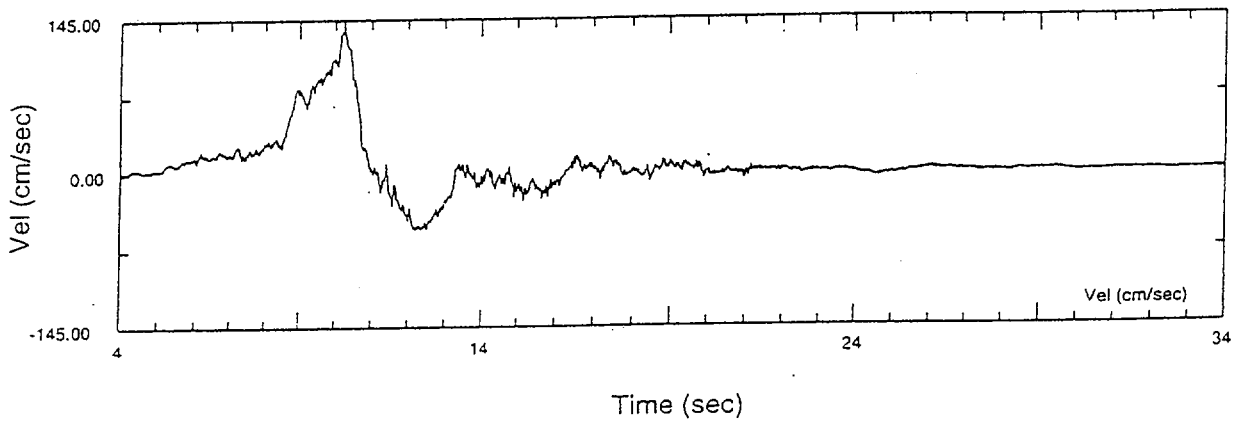

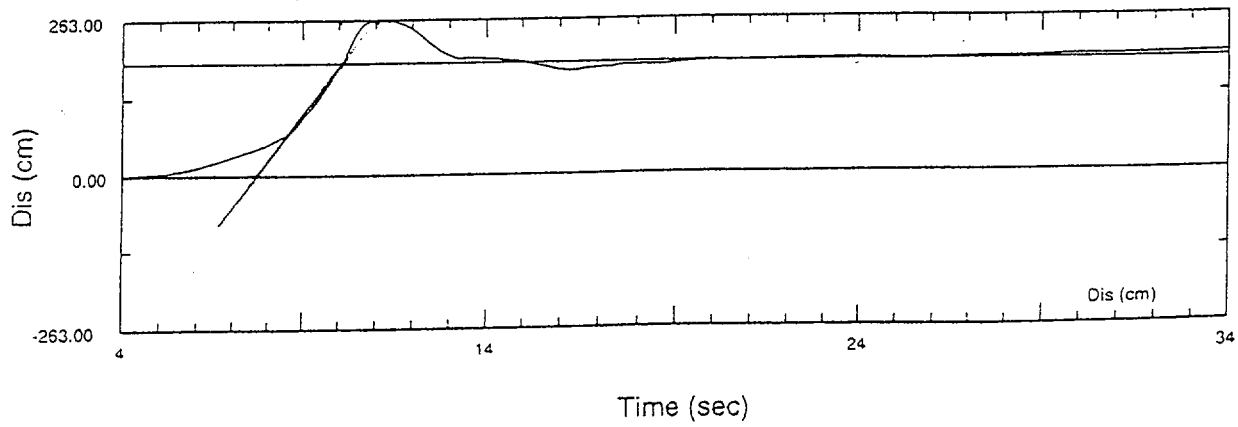

Izmit Earthquake: Station YPT, Fault ~~Normal~~ Parallel, Fling Model

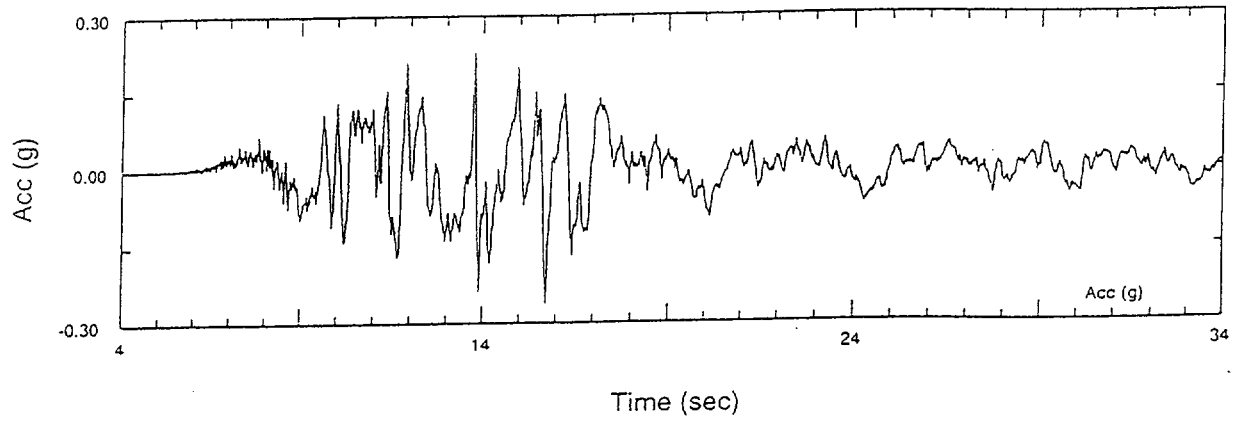

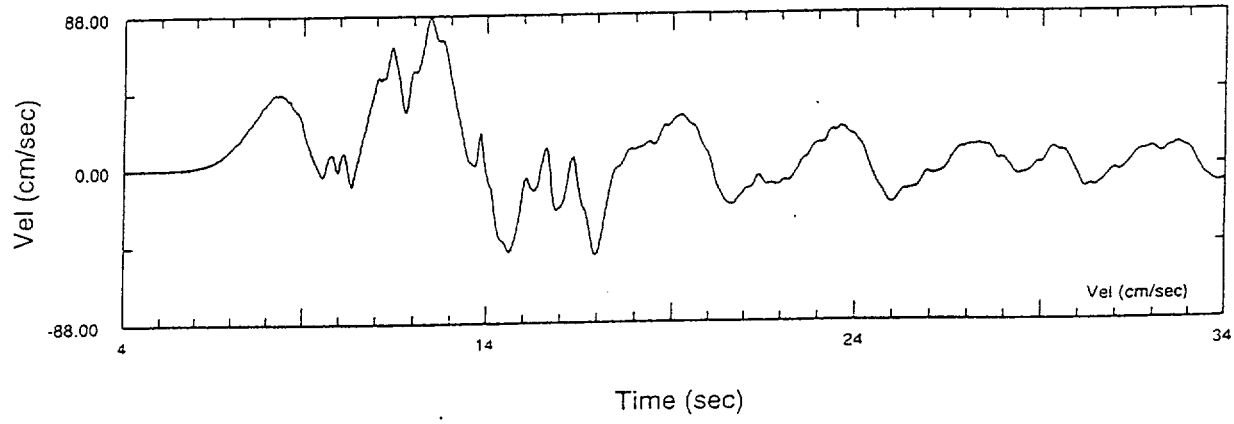

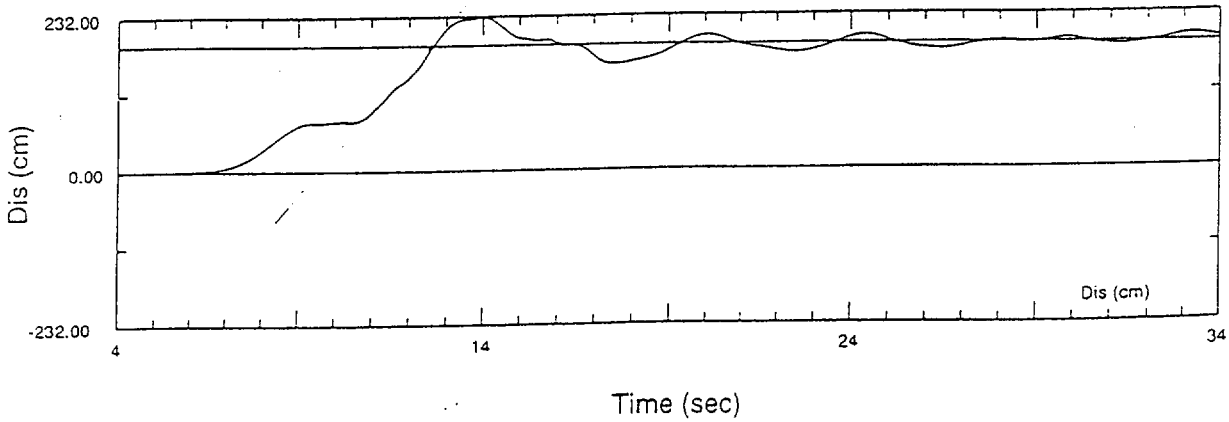

Izmit Earthquake: Station SKR, Fault ~~Normal~~ Parallel, Fling Model

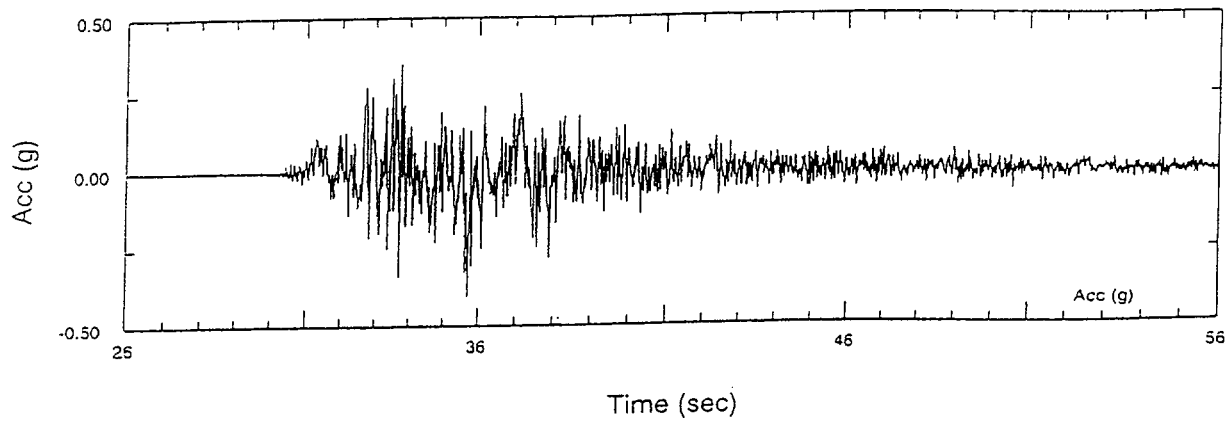

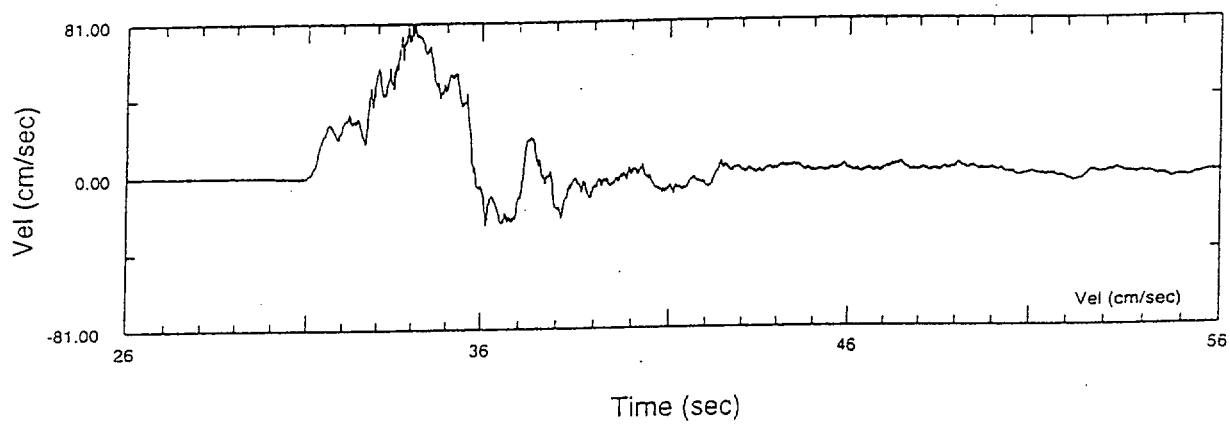

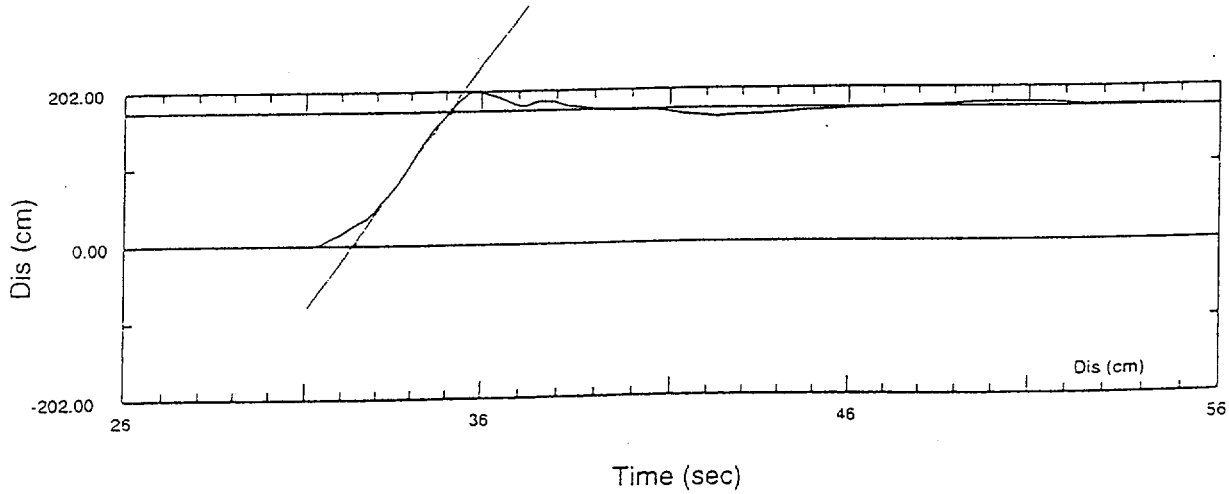

Chi-Chi Earthquake: Station TCU048, East, Fling Model

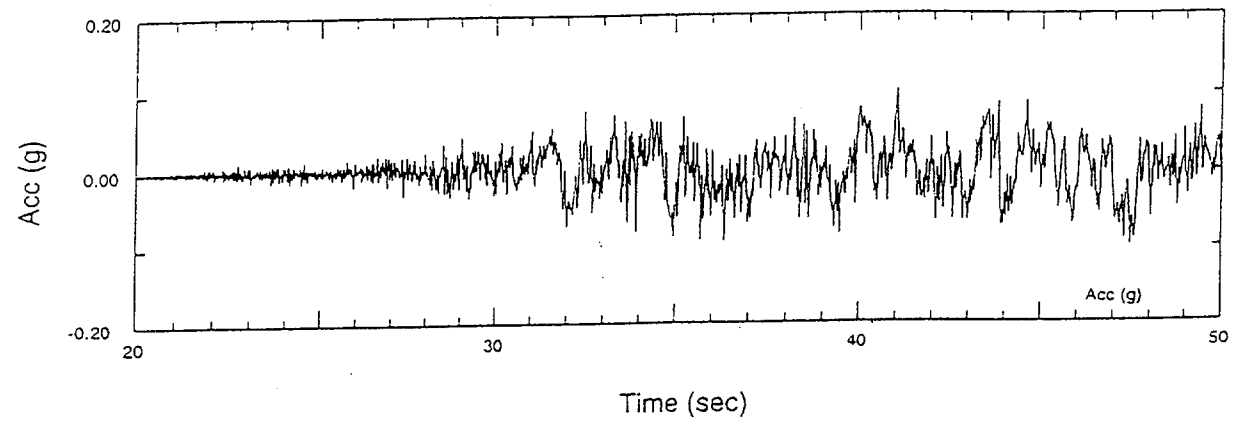

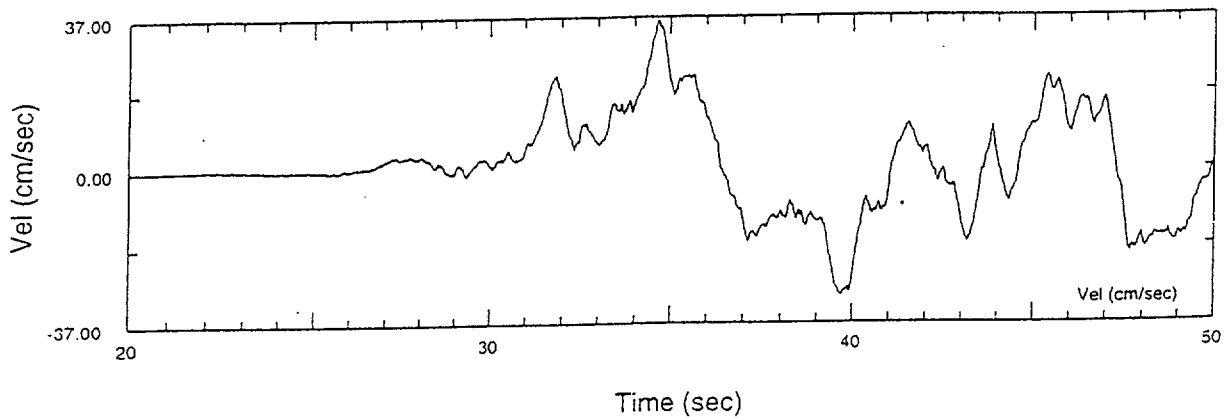

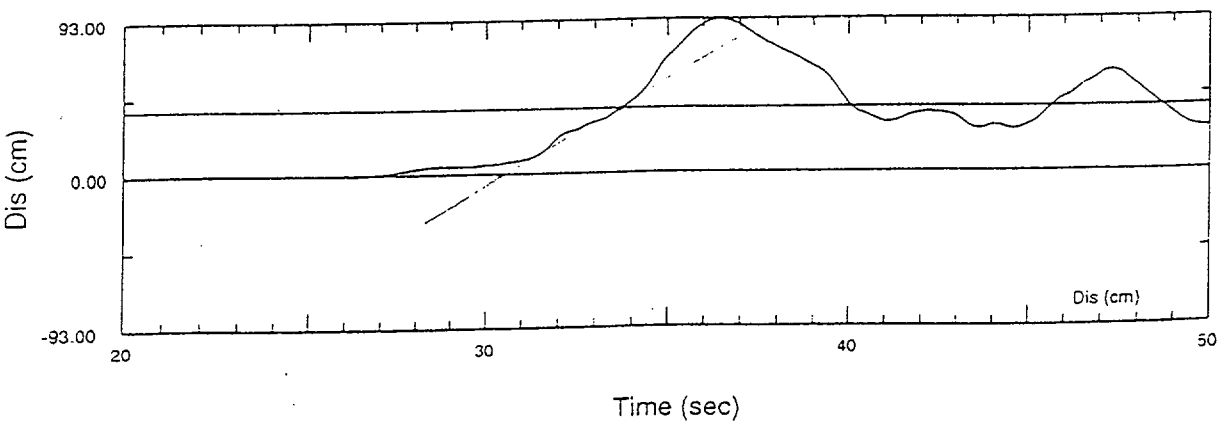

Chi-Chi Earthquake: Station TCU049, East, Fling Model

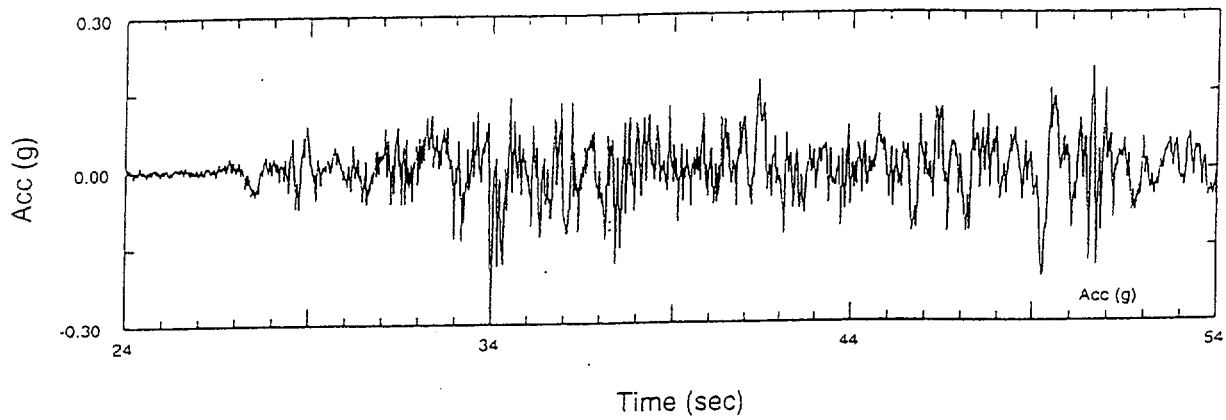

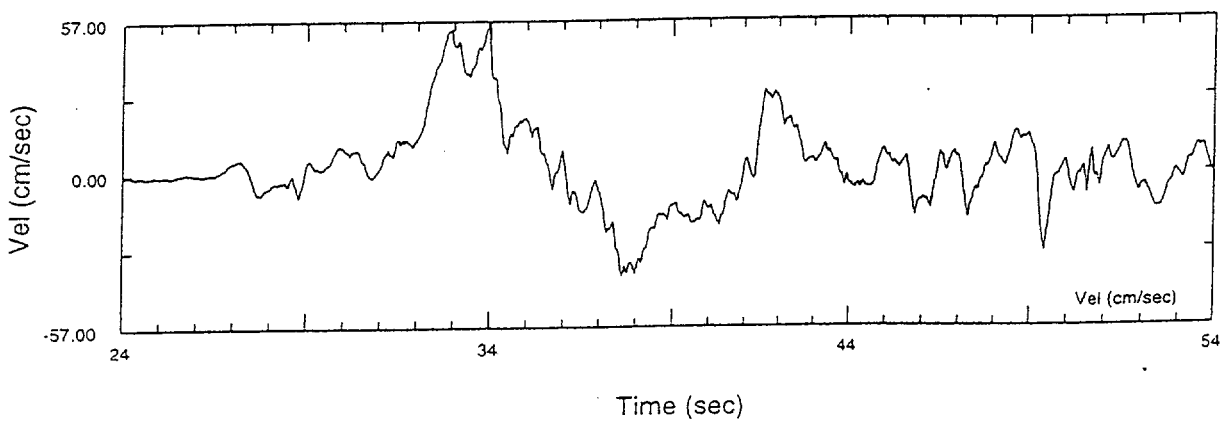

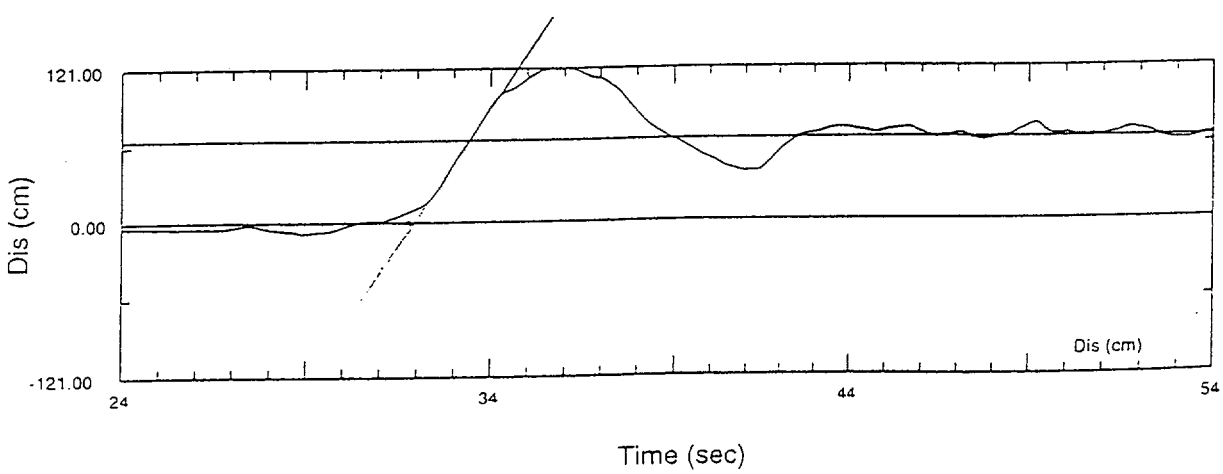

Chi-Chi Earthquake: Station TCU050, East, Fling Model

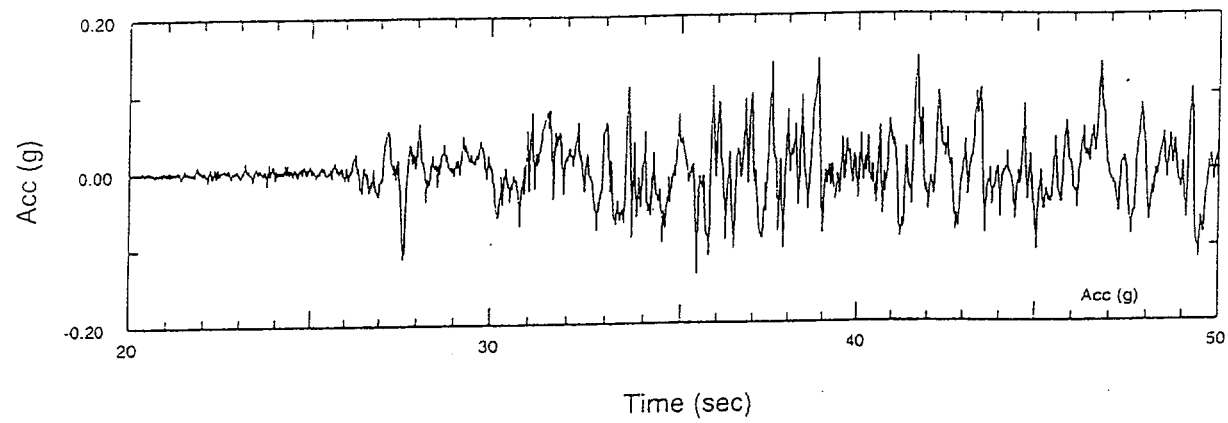

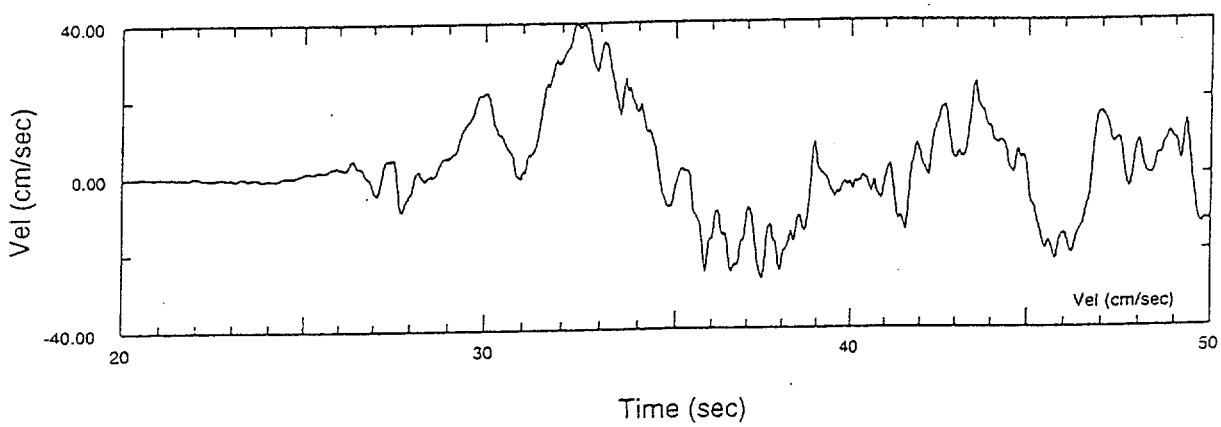

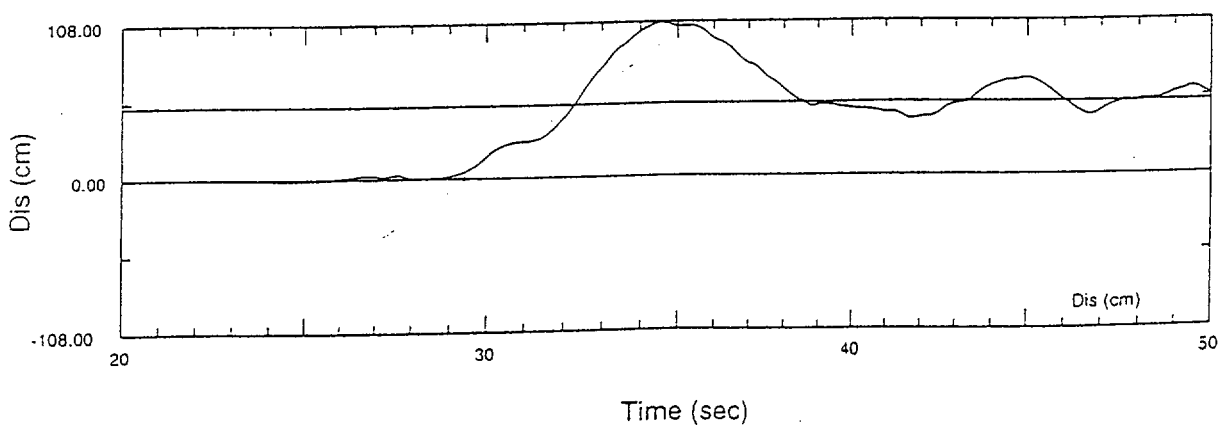

Chi-Chi Earthquake: Station TCU051, East, Fling Model

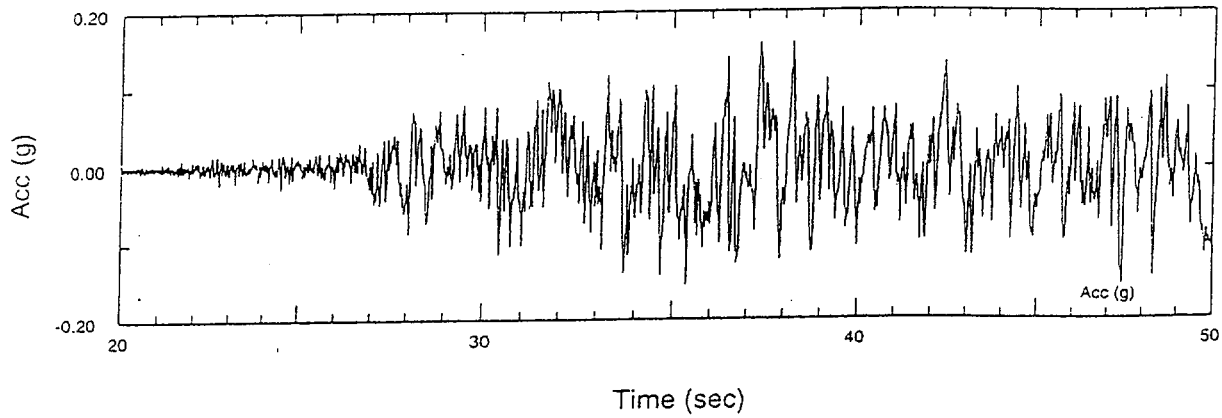

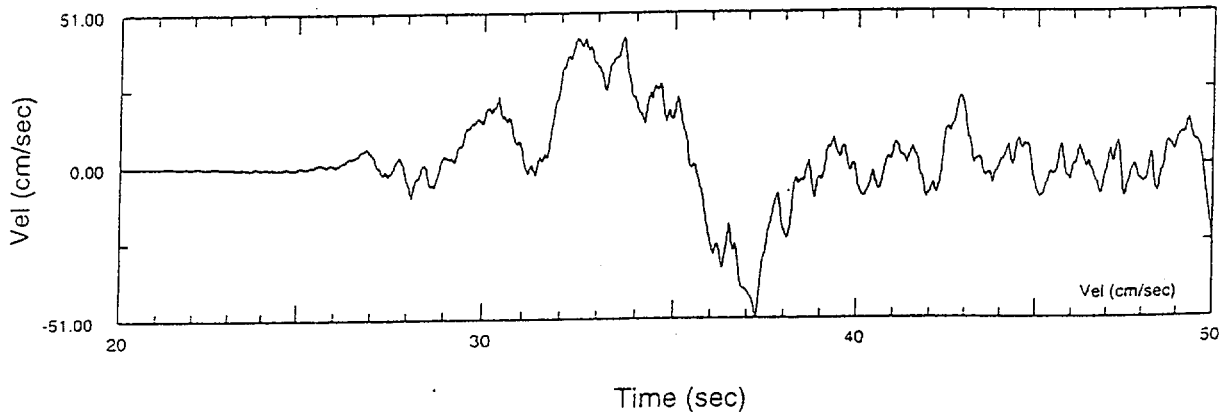

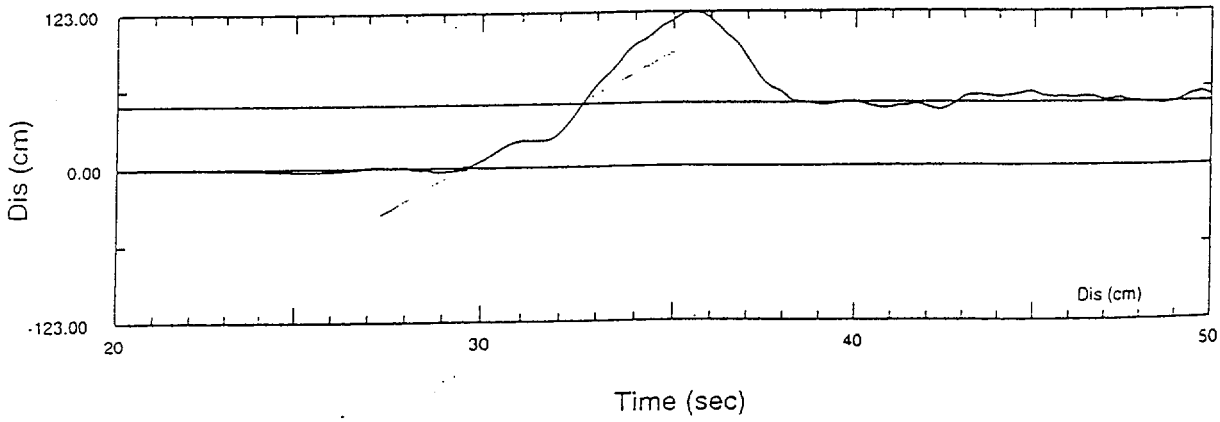

Chi-Chi Earthquake: Station TCU052, Comp 150, Fling Model

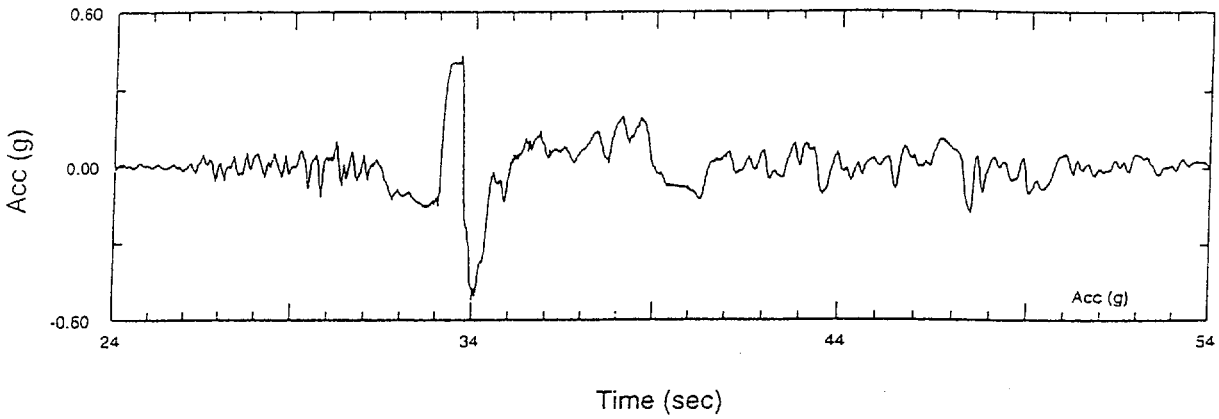

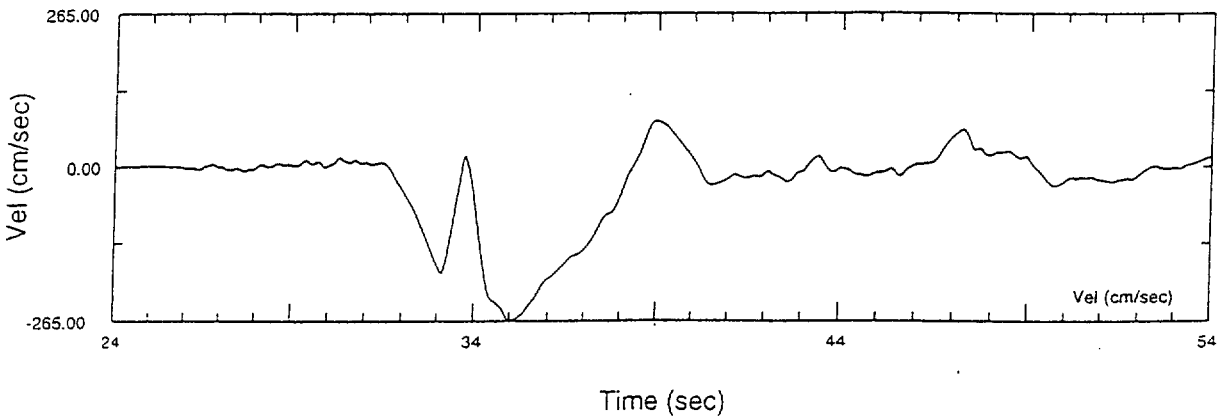

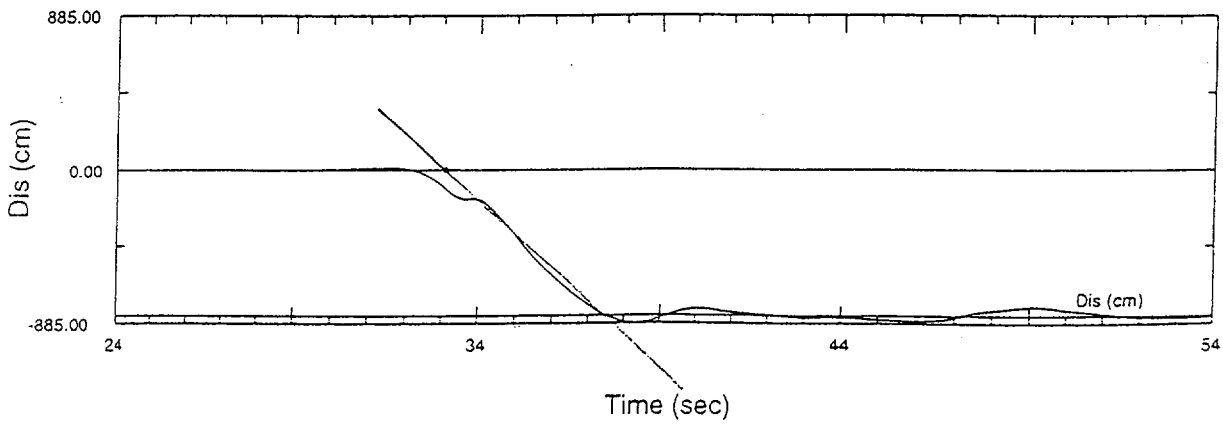

Chi-Chi Earthquake: Station TCU053, East, Fling Model

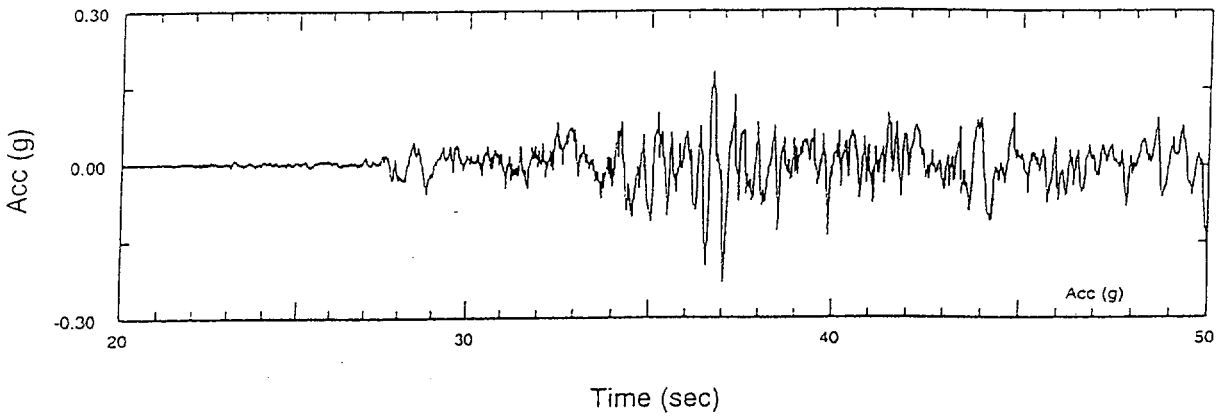

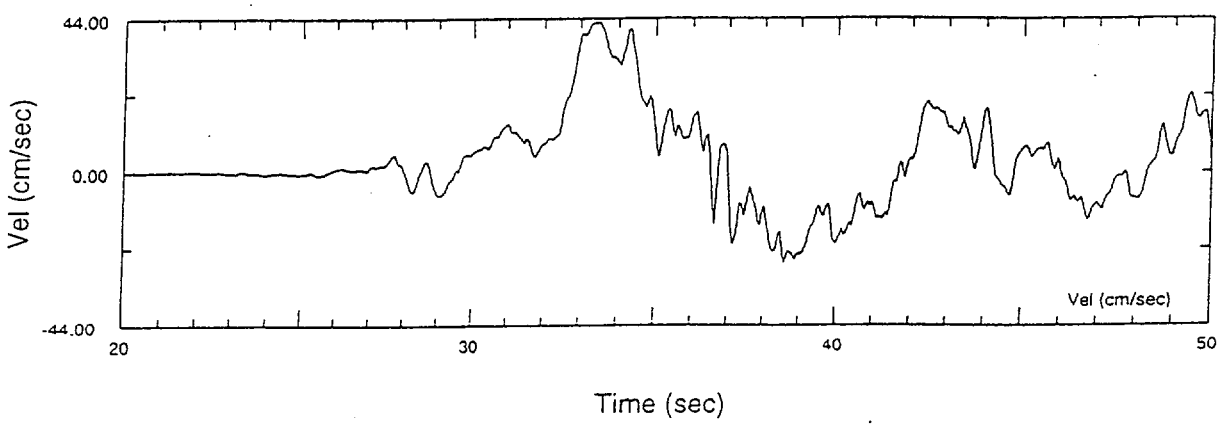

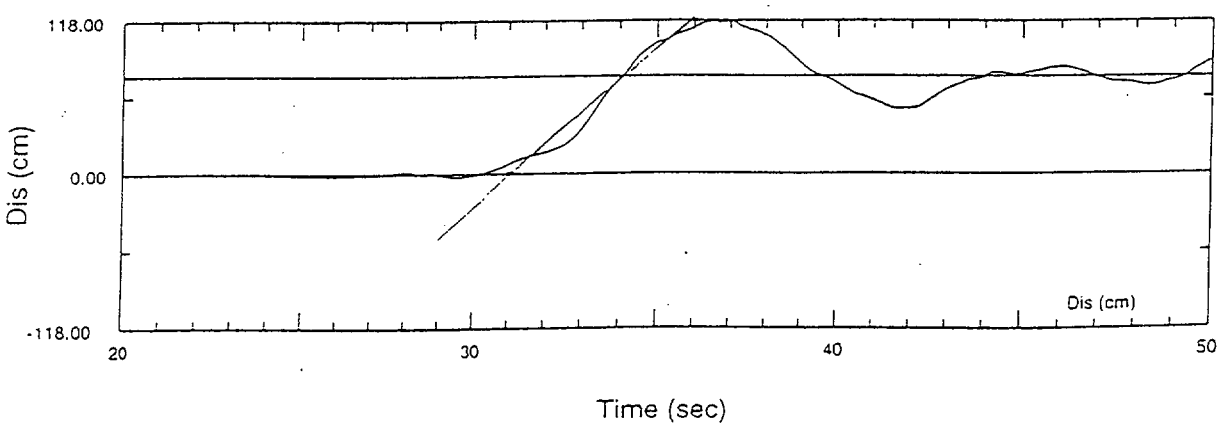

Chi-Chi Earthquake: Station TCU054, East, Fling Model

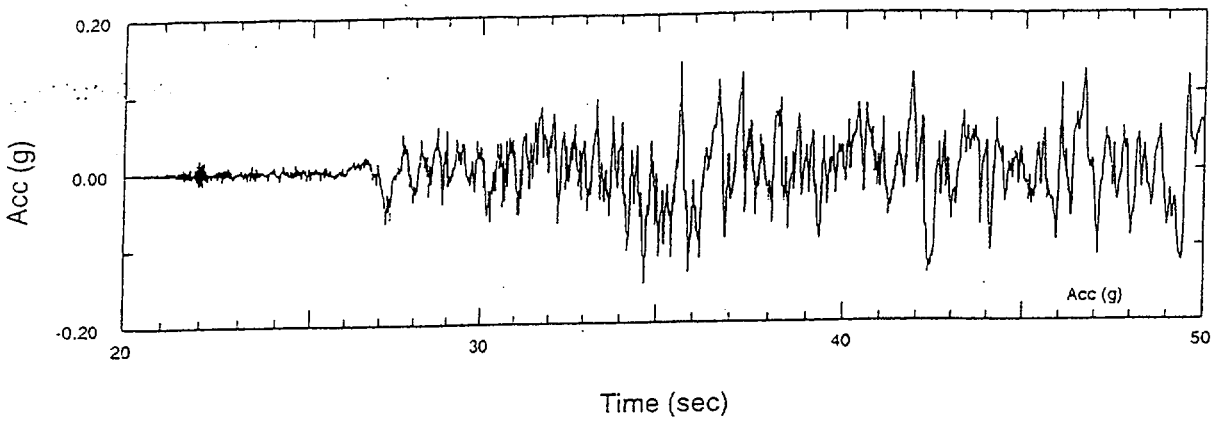

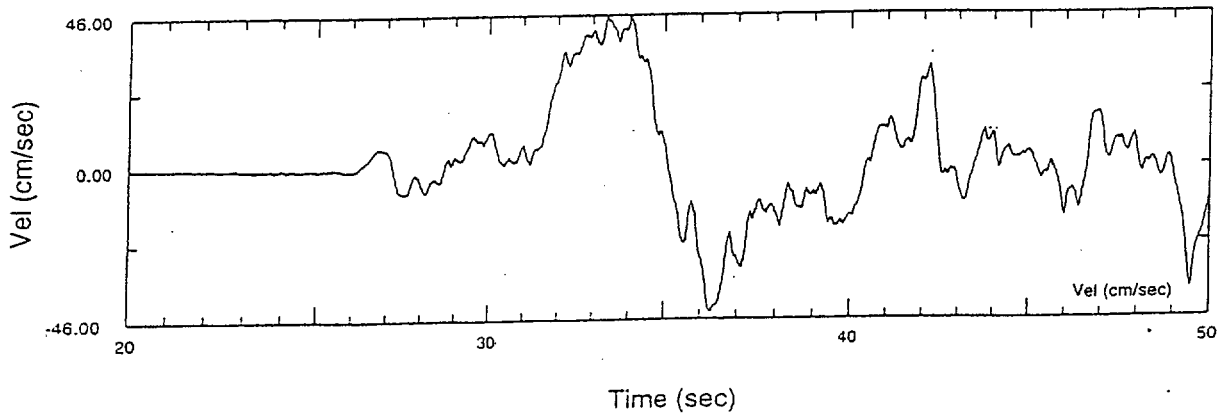

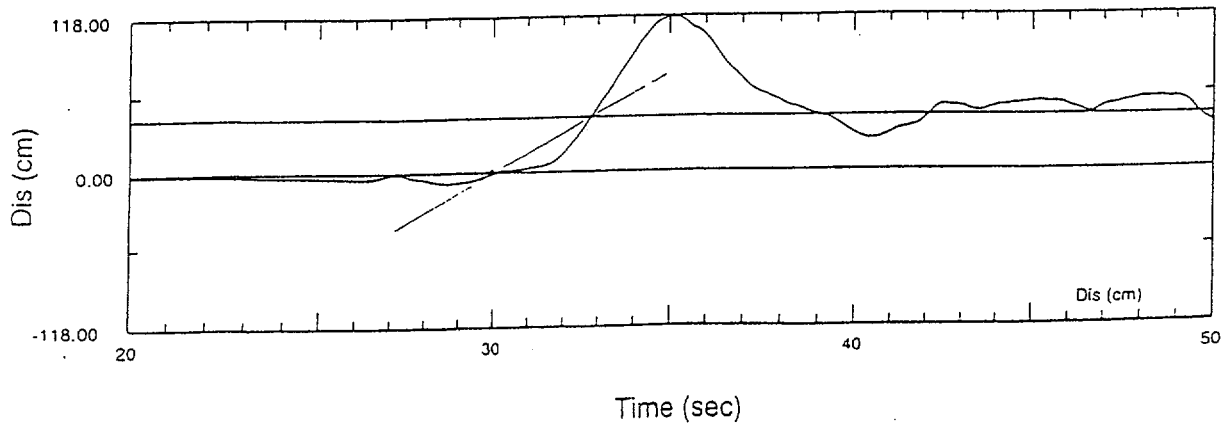

Chi-Chi Earthquake: Station TCU056, East, Fling Model

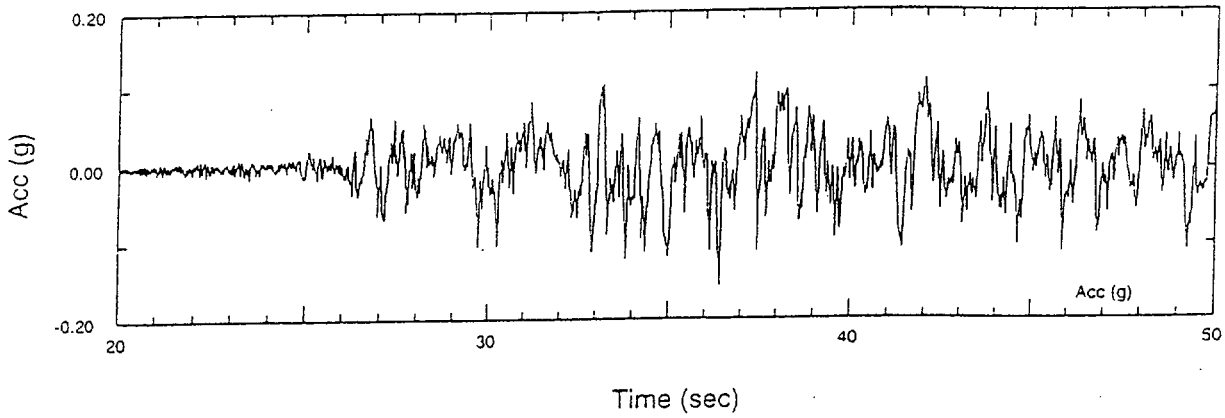

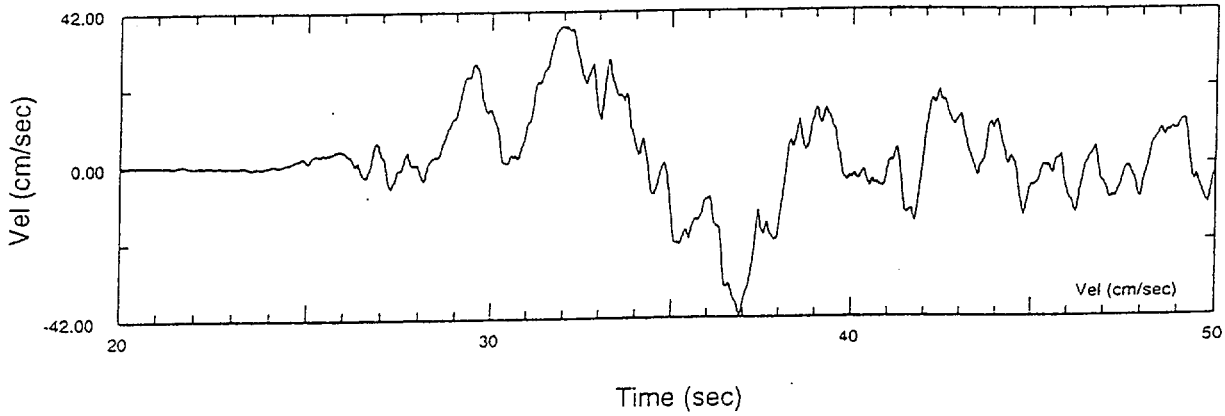

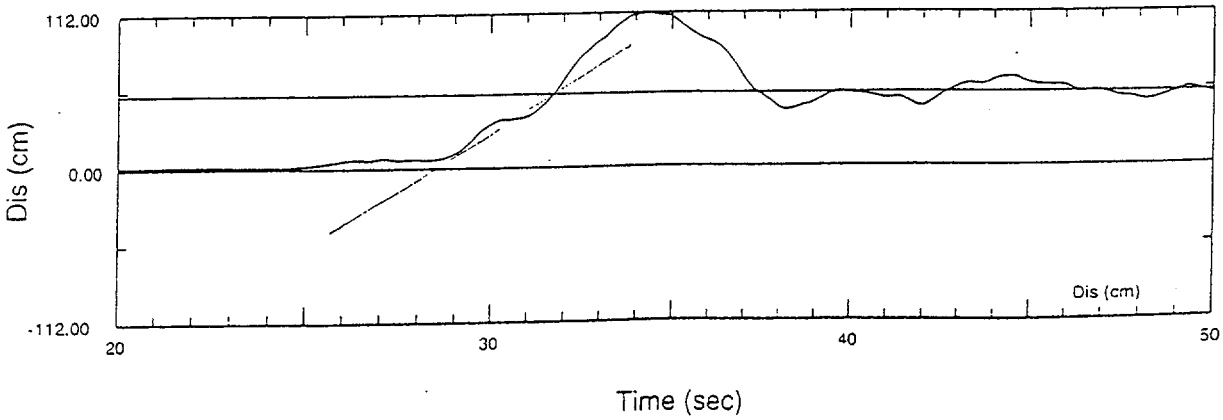

Chi-Chi Earthquake: Station TCU057, East, Fling Model

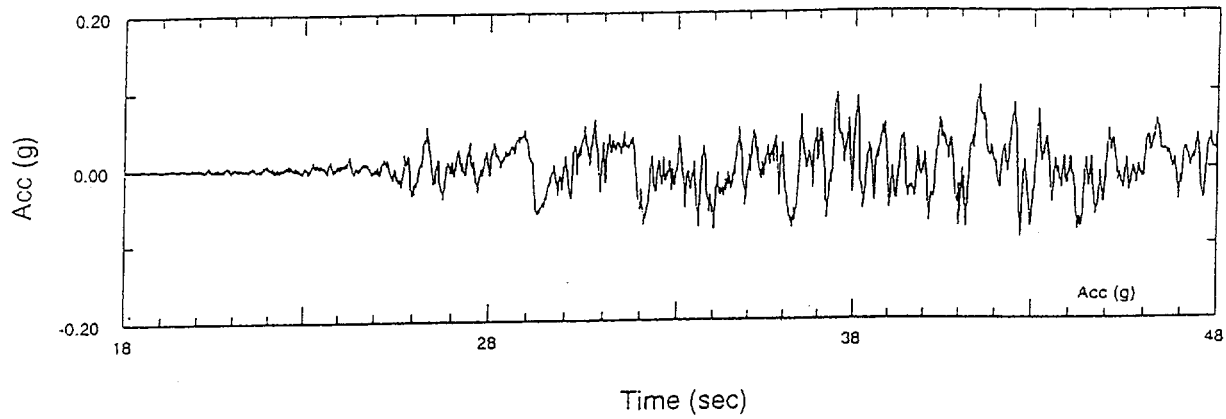

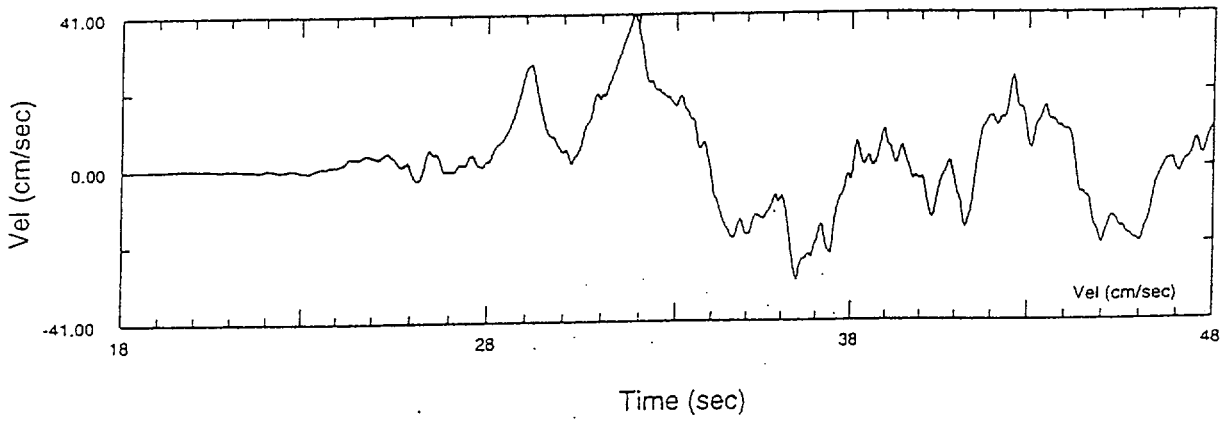

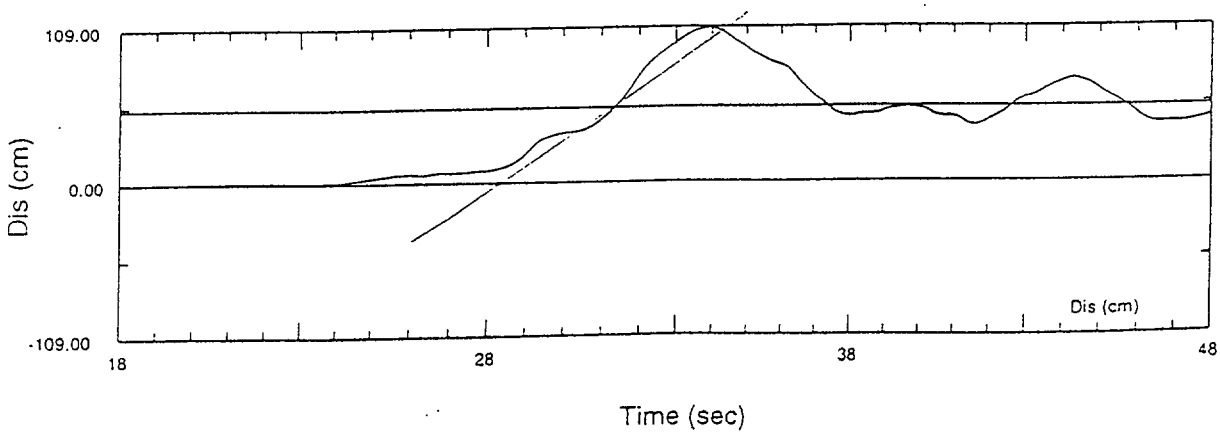

Chi-Chi Earthquake: Station TCU060, East, Fling Model

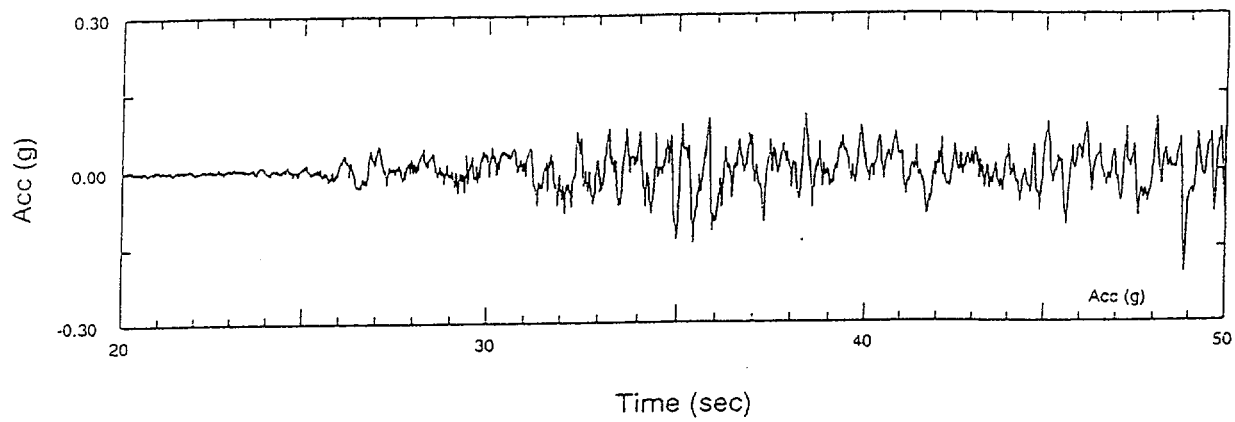

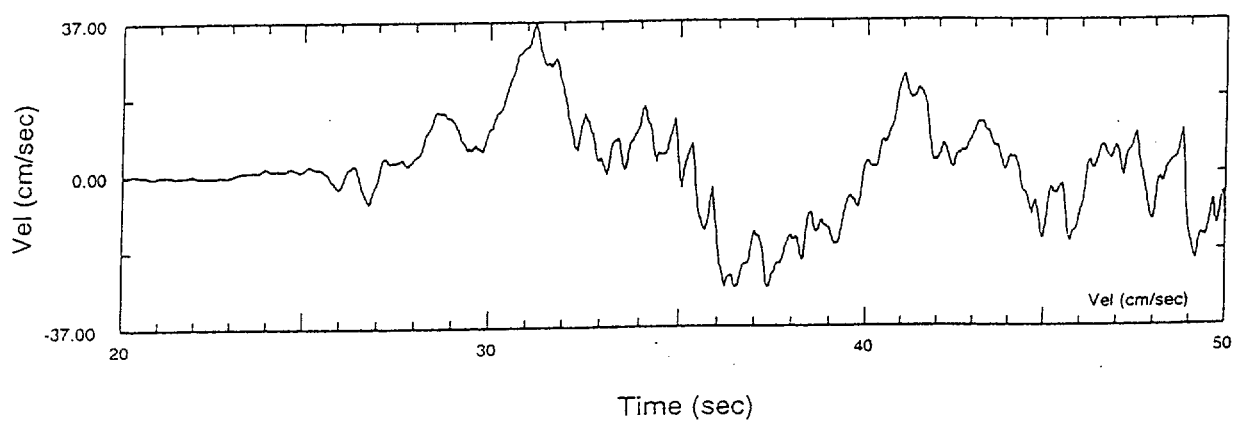

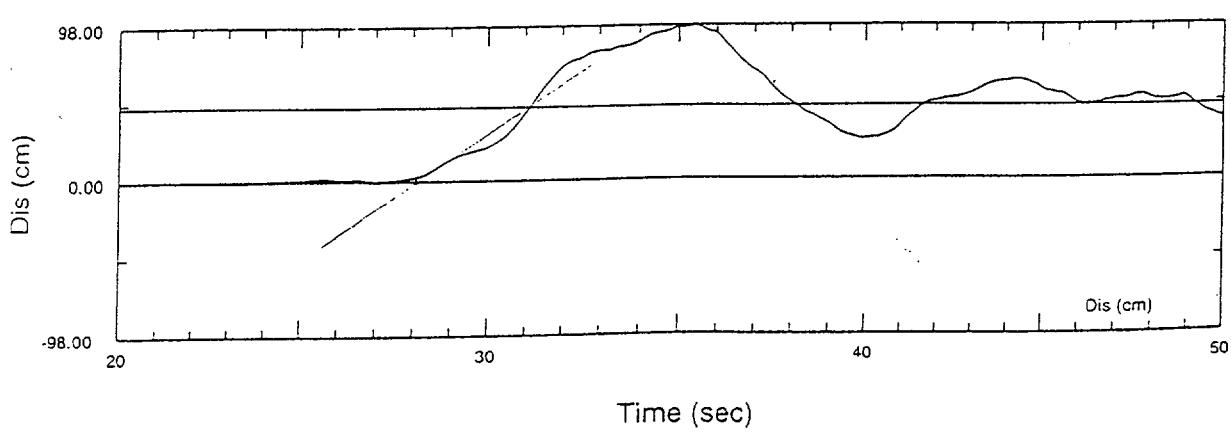

Chi-Chi Earthquake: Station TCU063, East, Fling Model

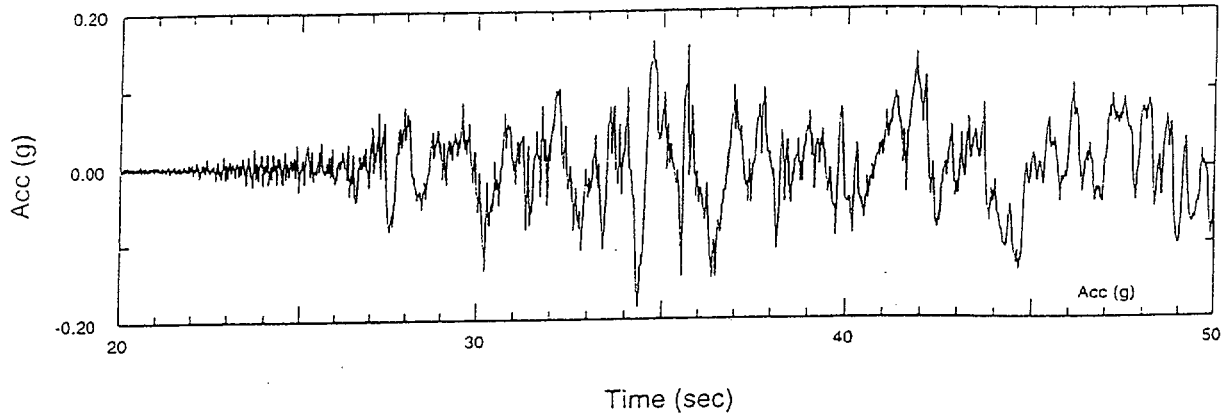

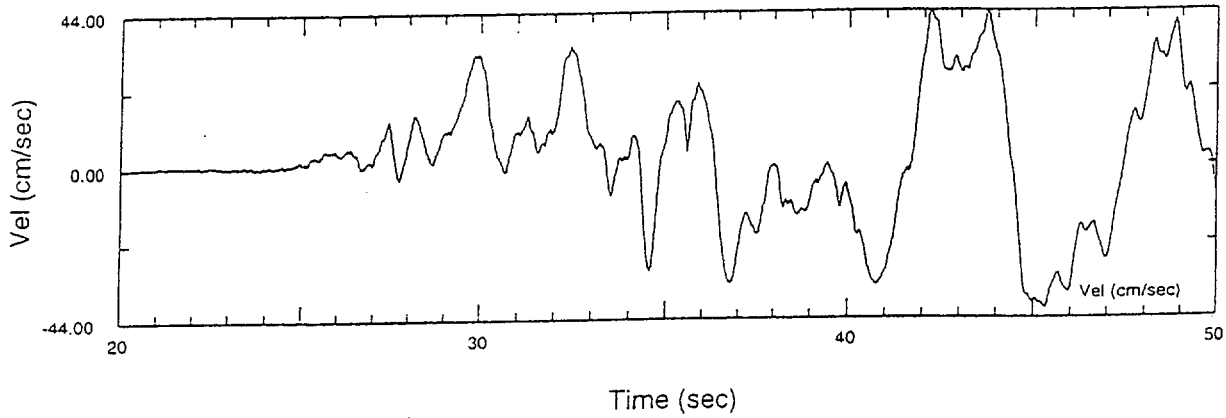

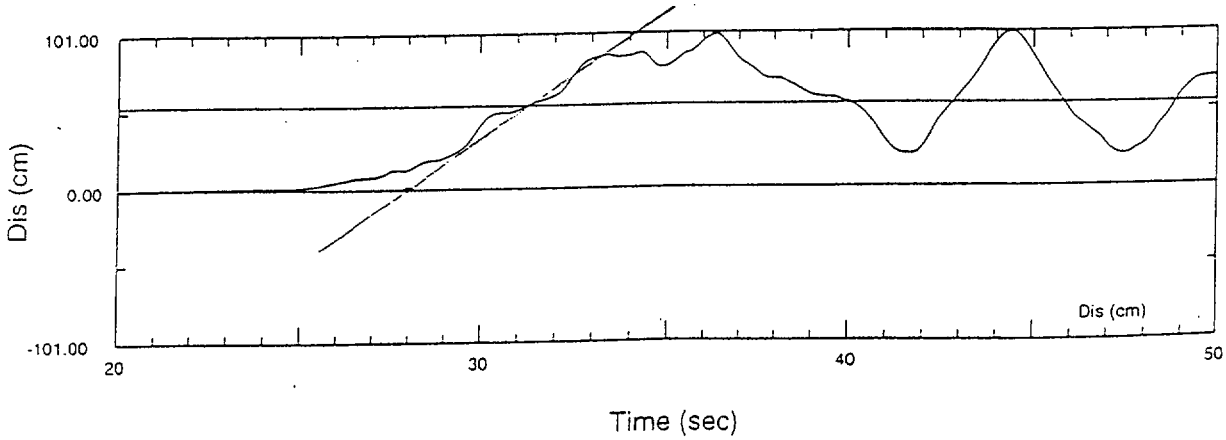

Chi-Chi Earthquake: Station TCU064, East, Fling Model

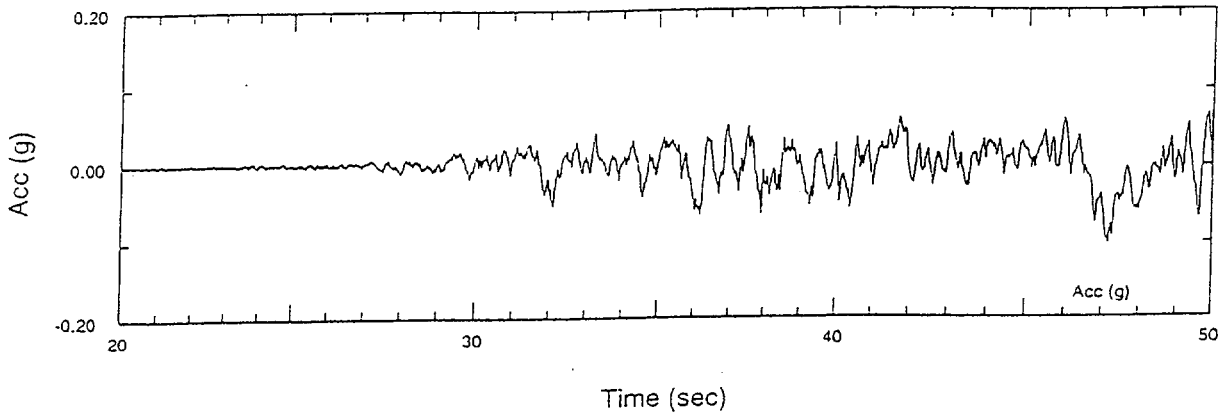

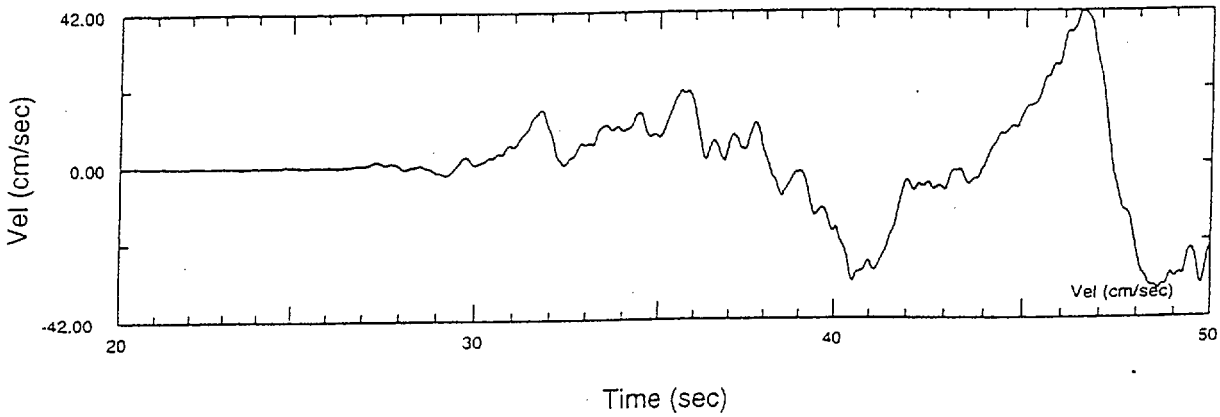

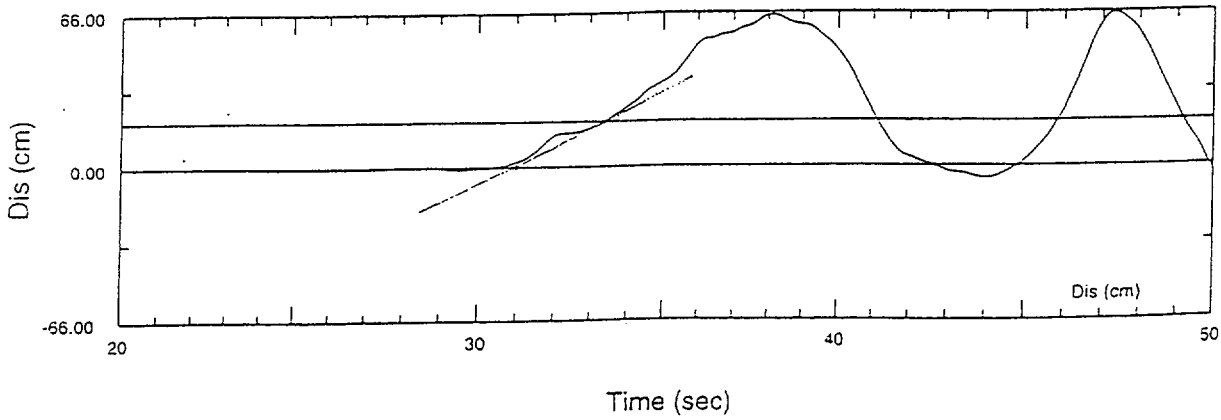

Chi-Chi Earthquake: Station TCU067, East, Fling Model

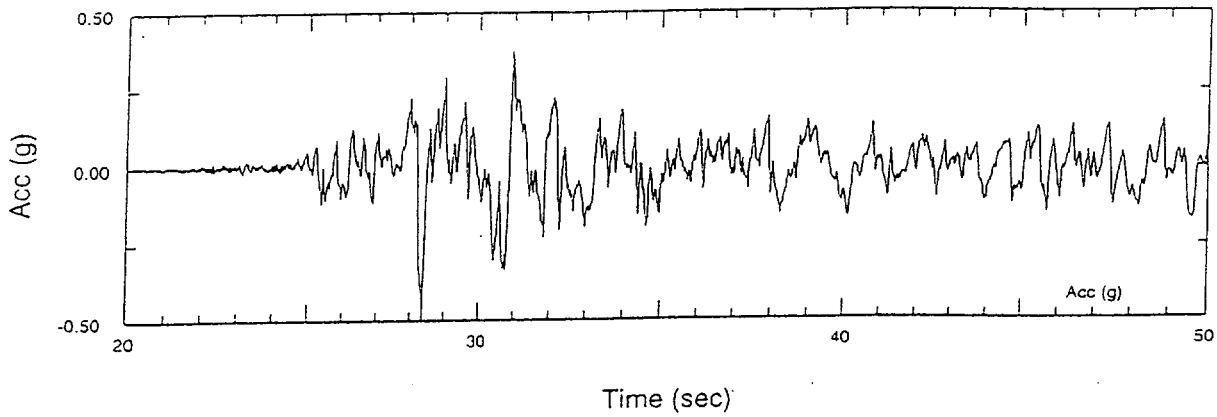

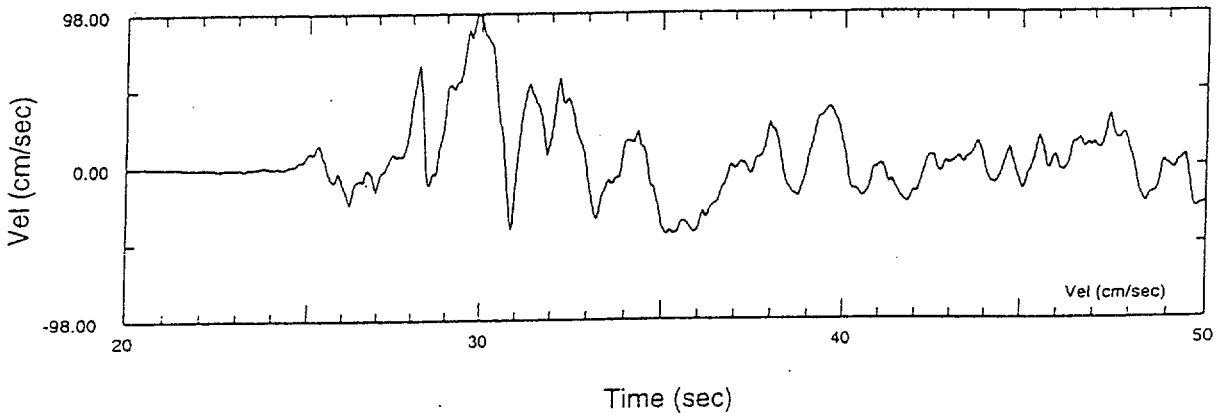

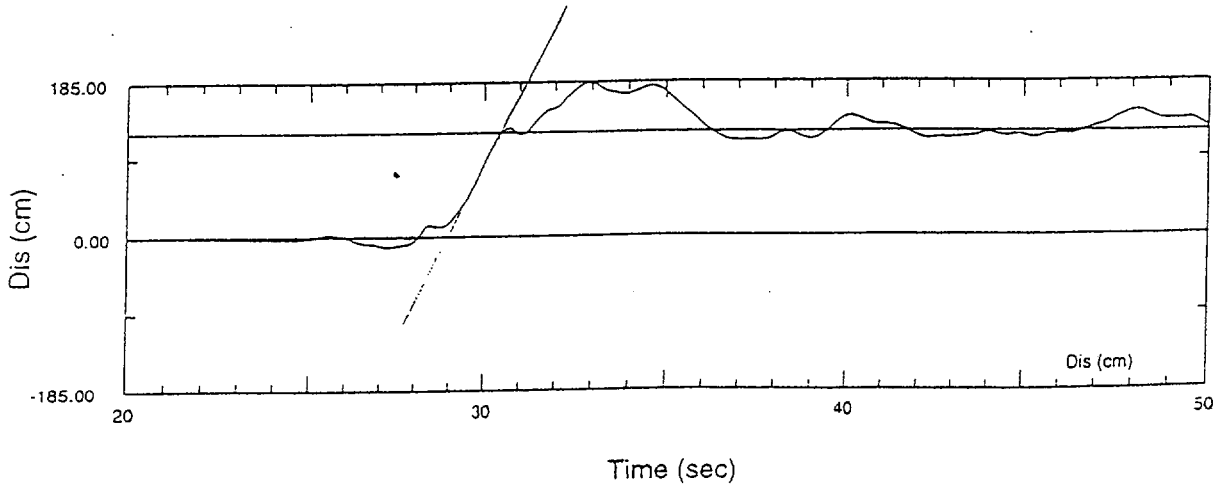

Chi-Chi Earthquake: Station TCU068, North, Fling Model

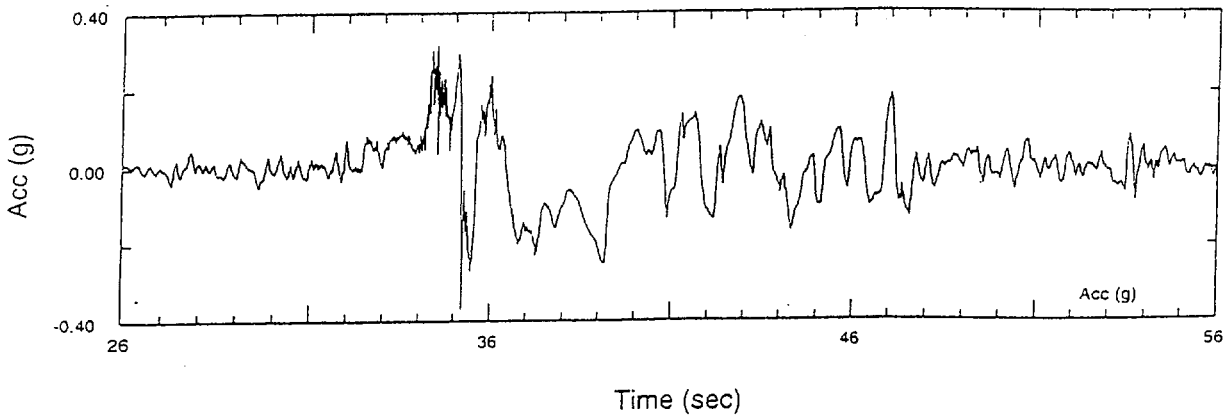

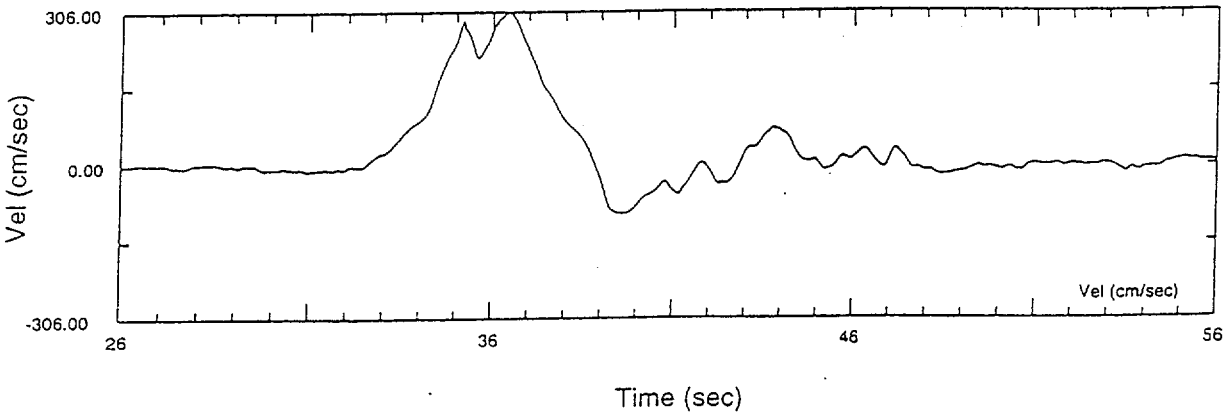

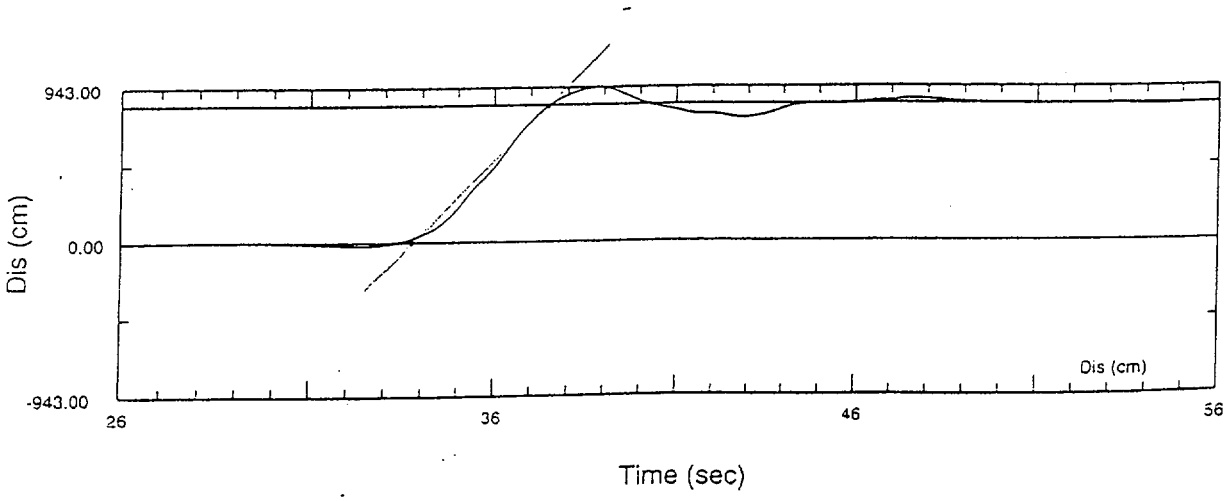

Chi-Chi Earthquake: Station TCU070, East, Fling Model

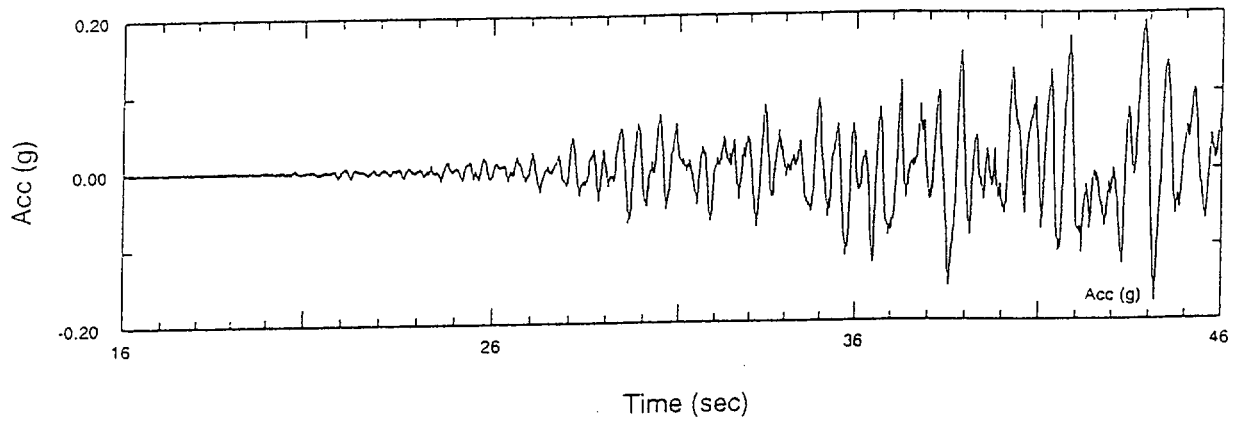

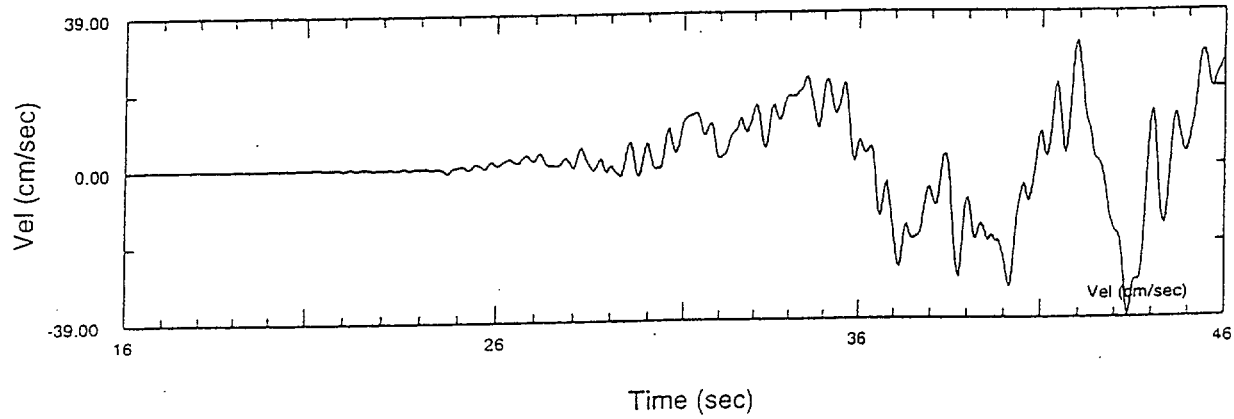

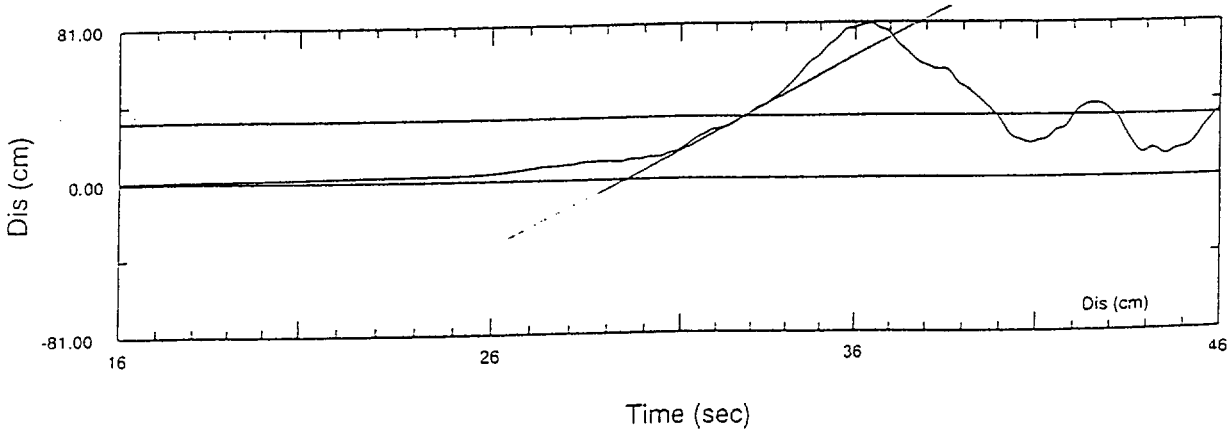

Chi-Chi Earthquake: Station TCU075, East, Fling Model

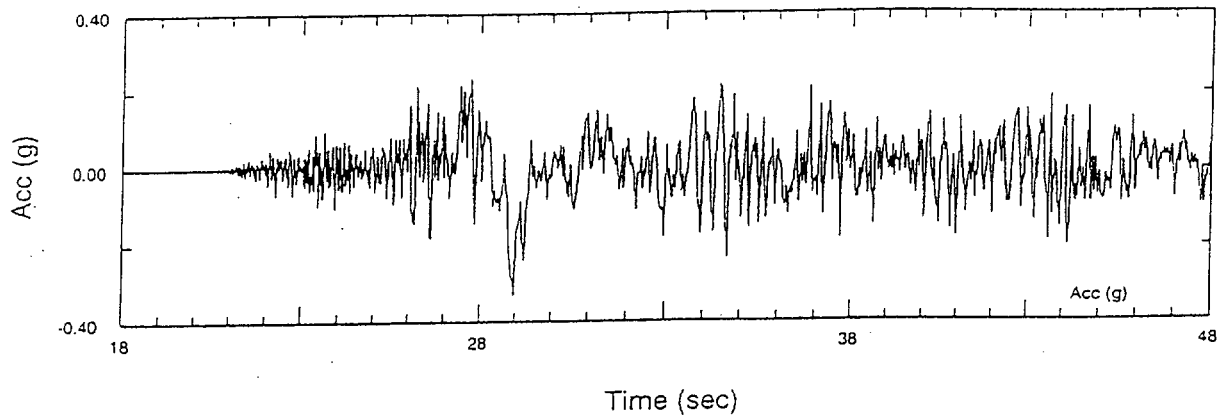

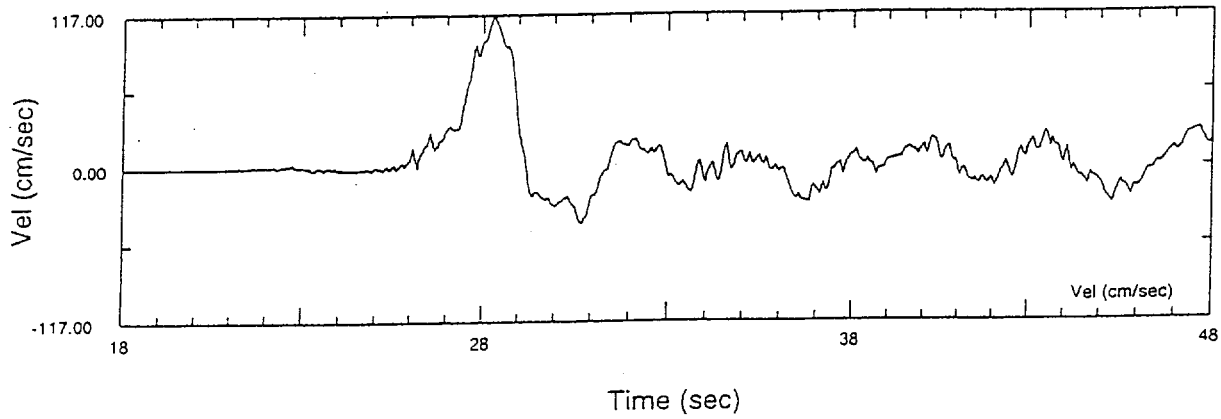

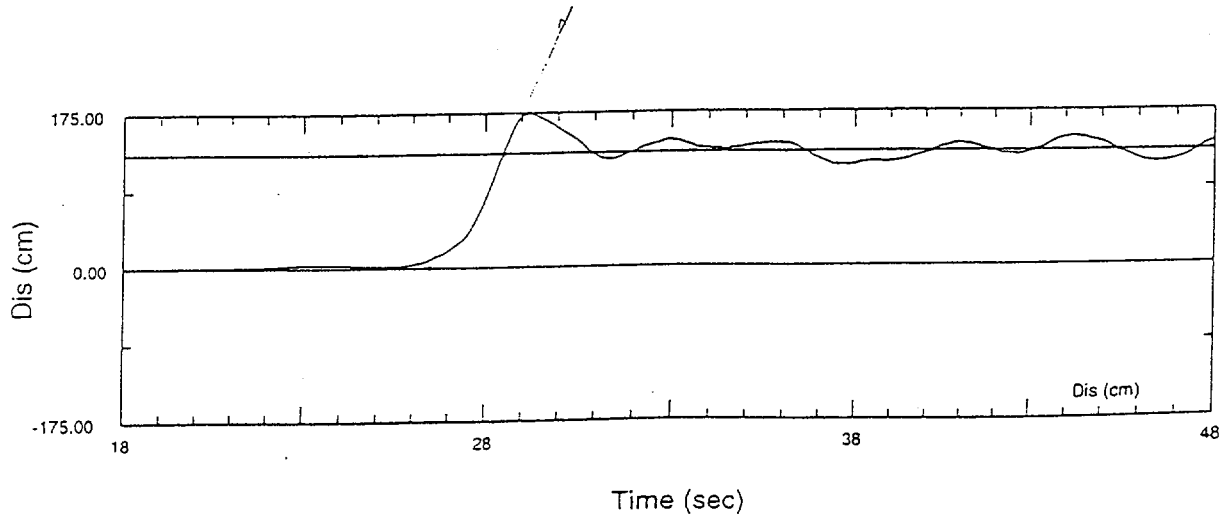

Chi-Chi Earthquake: Station TCU076, East, Fling Model

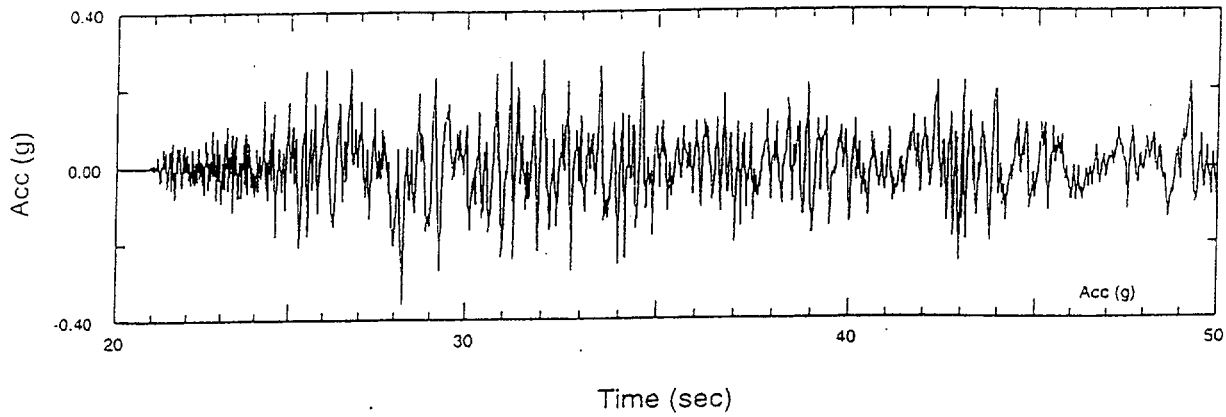

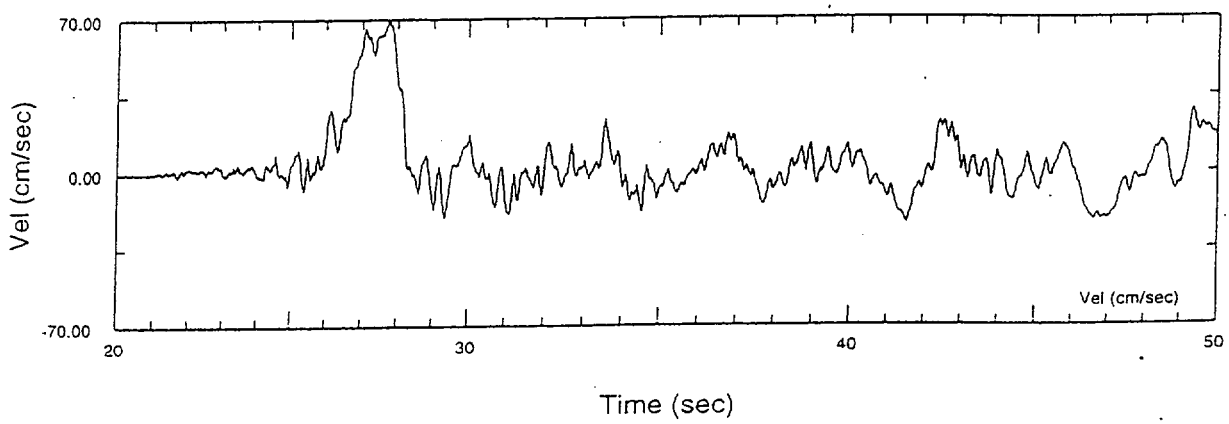

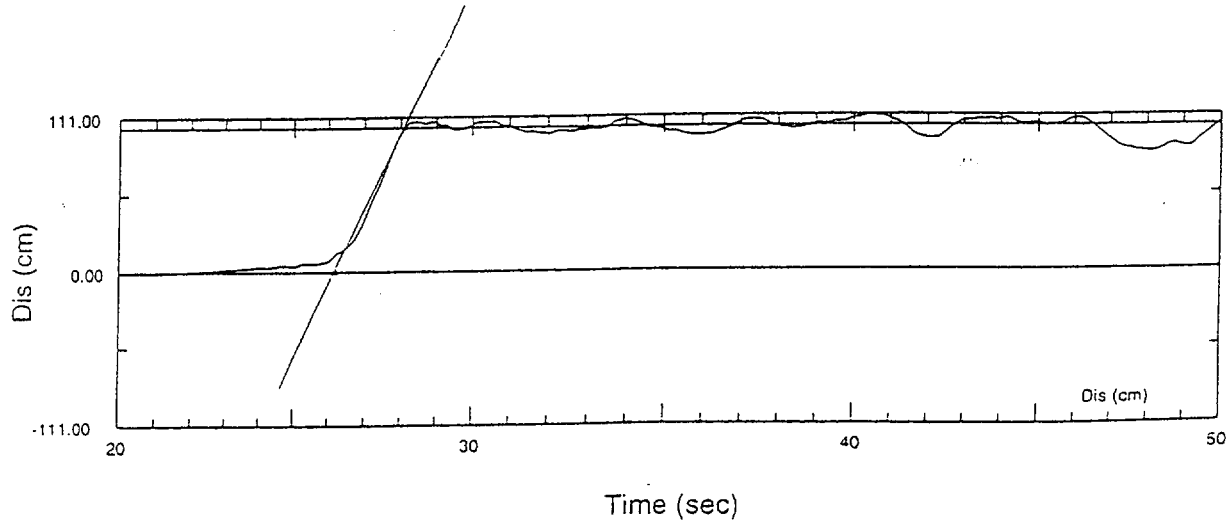

Chi-Chi Earthquake: Station TCU082, East, Fling Model

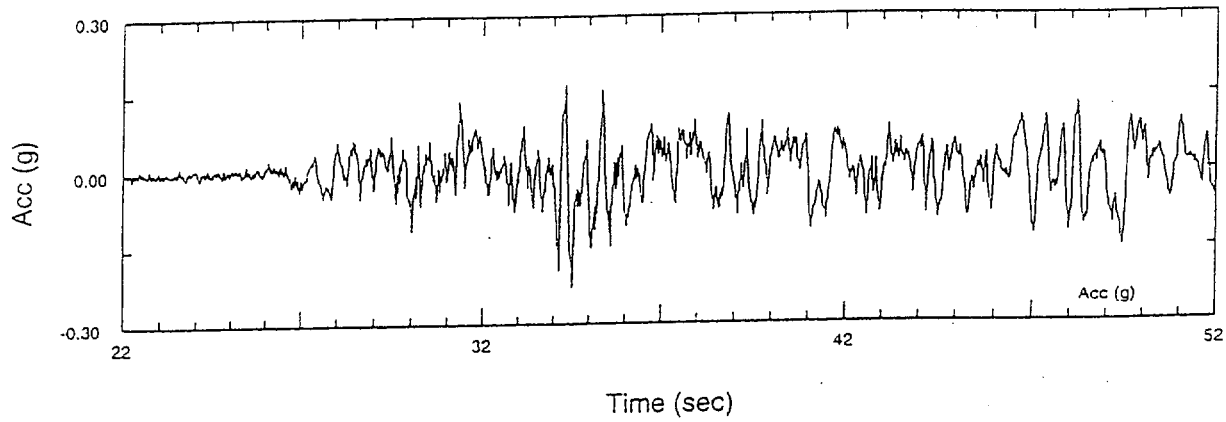

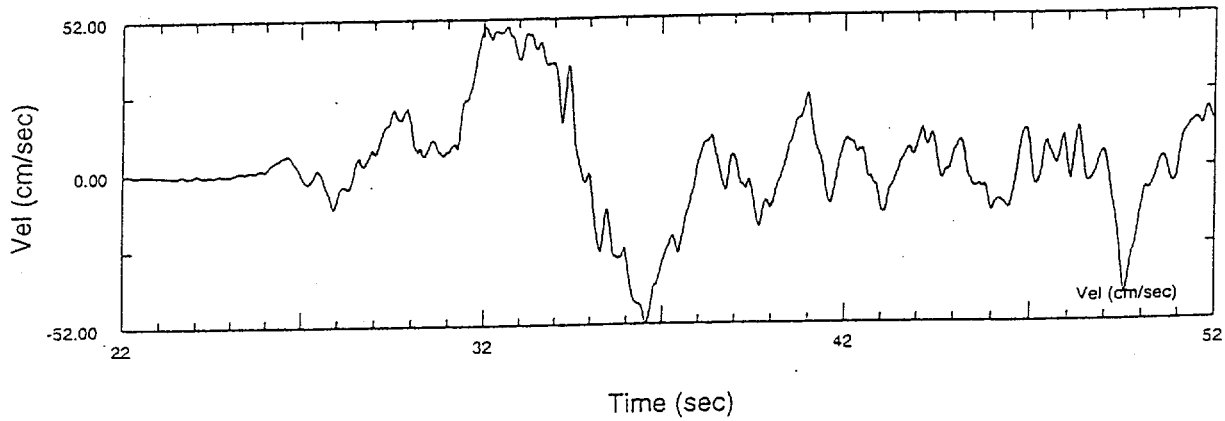

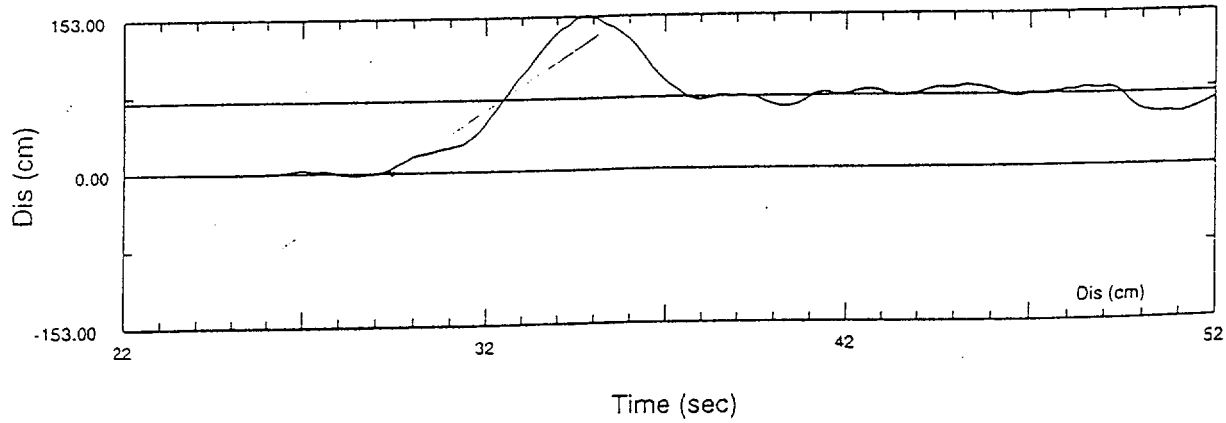

Chi-Chi Earthquake: Station TCU100, East, Fling Model

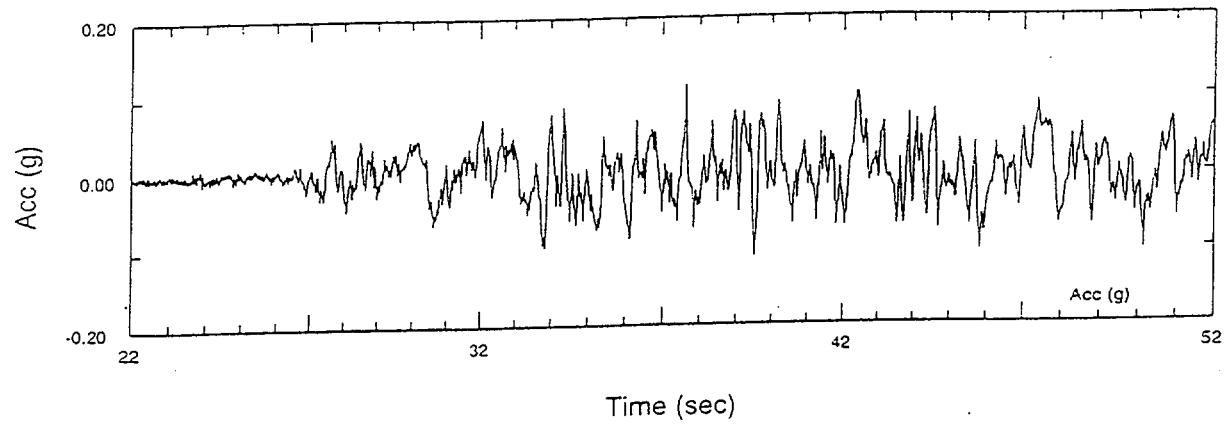

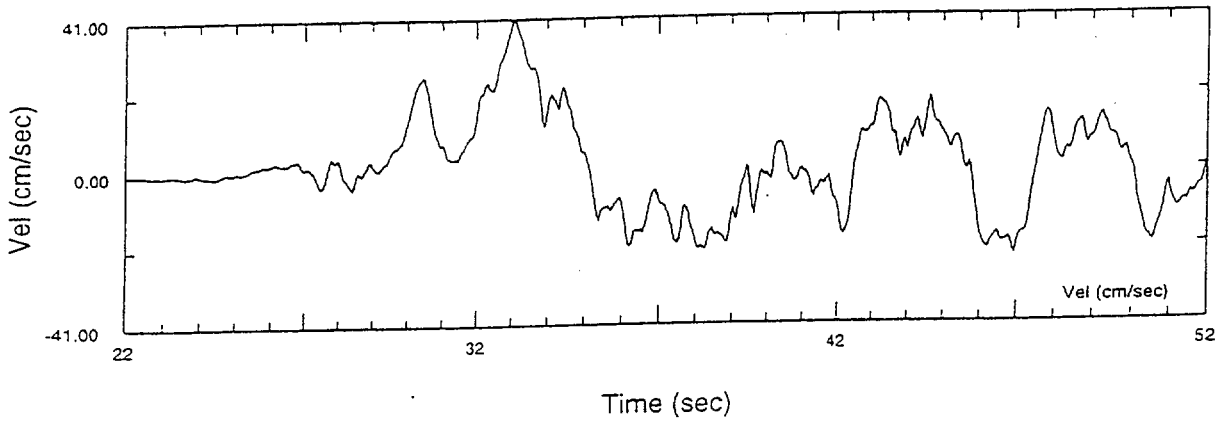

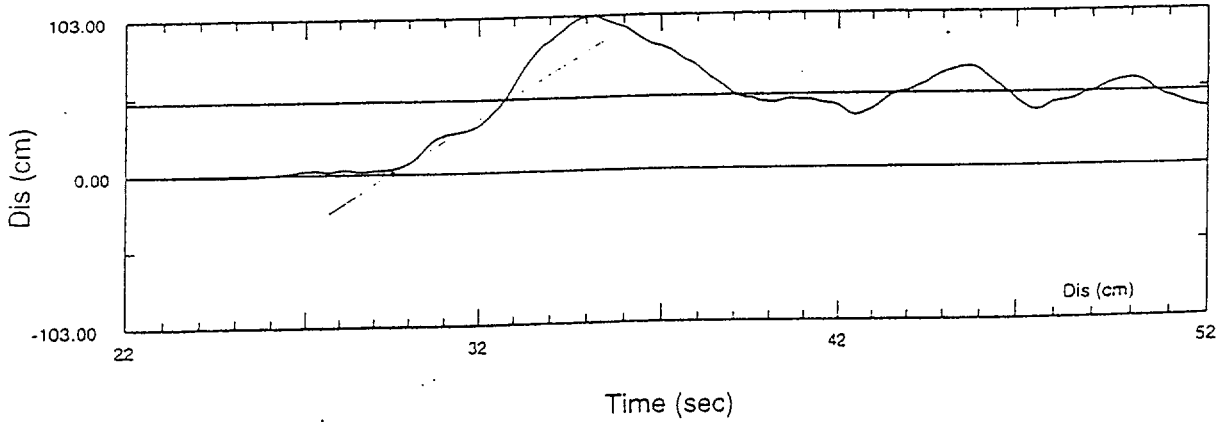

Chi-Chi Earthquake: Station TCU101, East, Fling Model

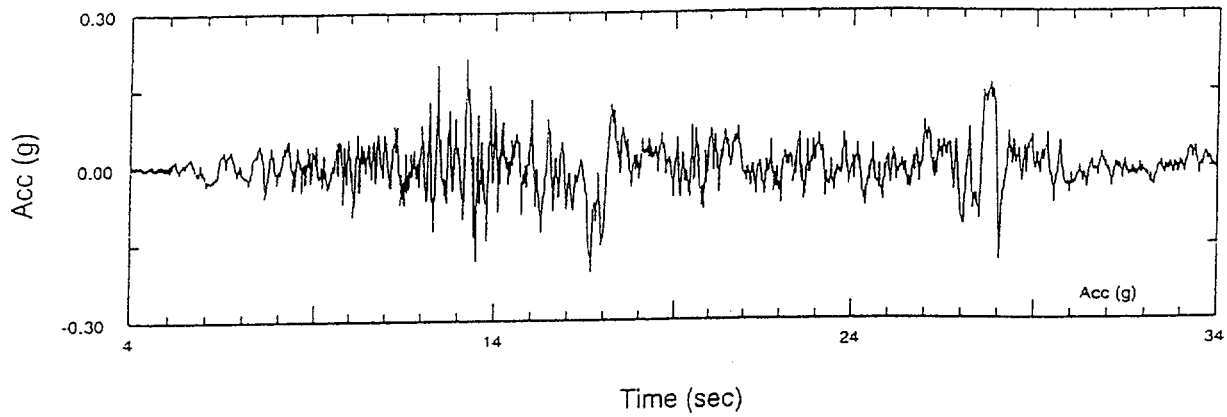

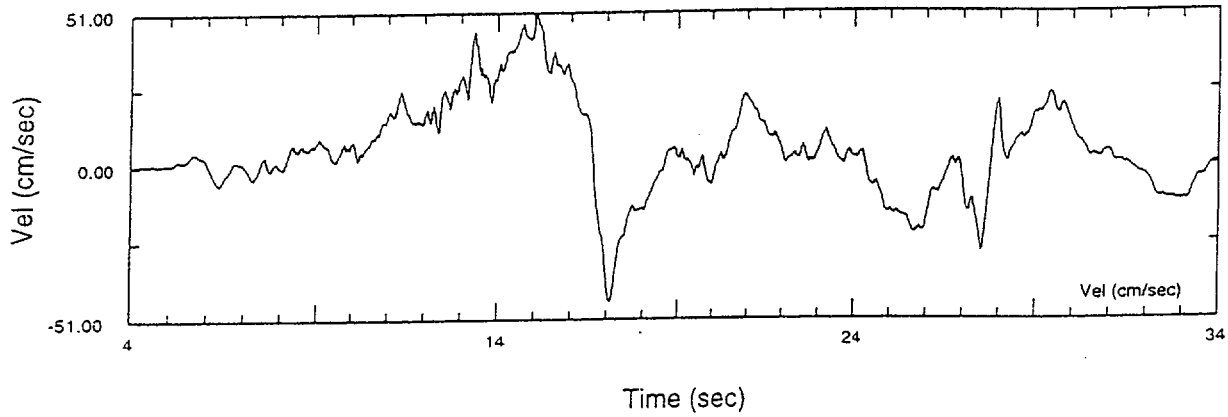

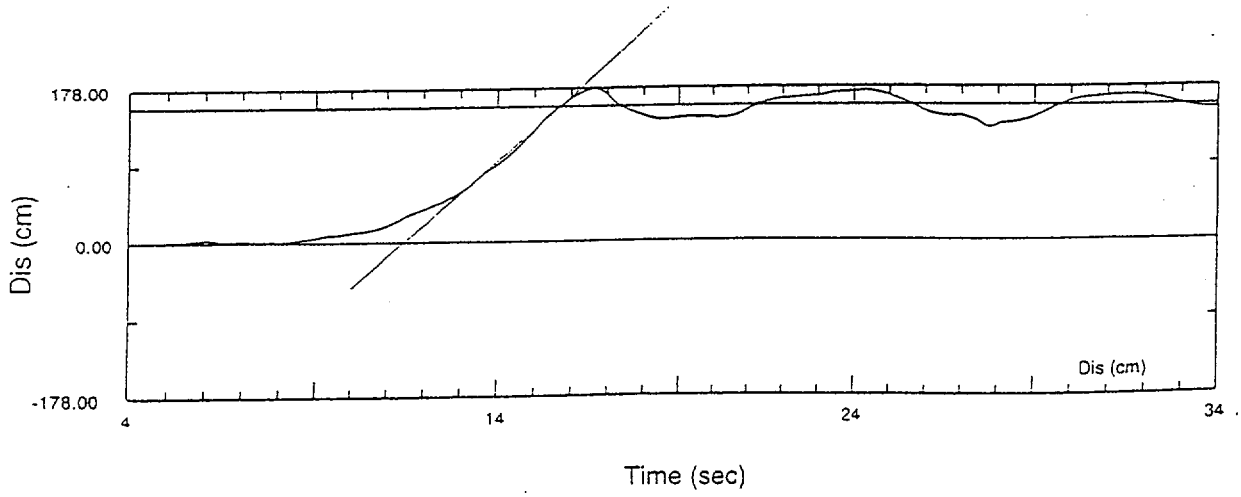

Chi-Chi Earthquake: Station TCU104, East, Fling Model

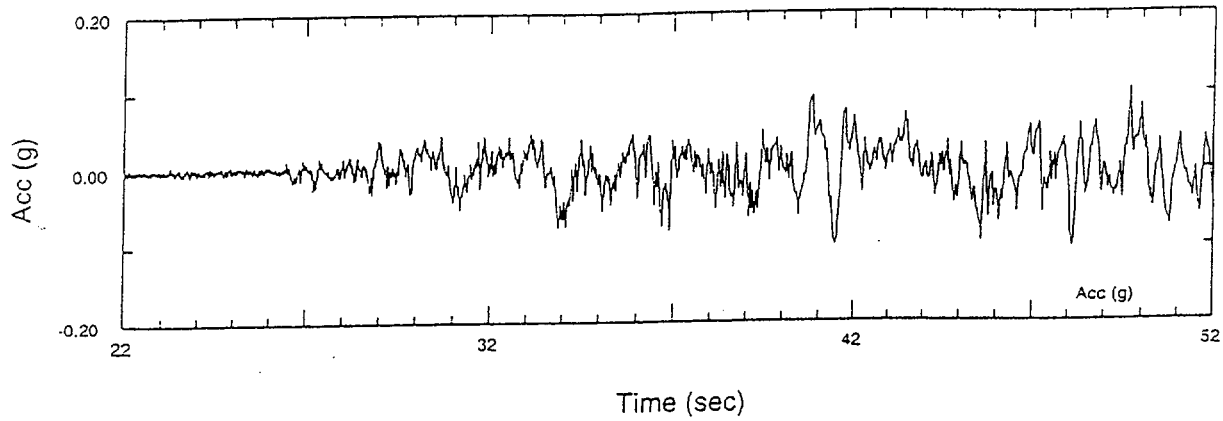

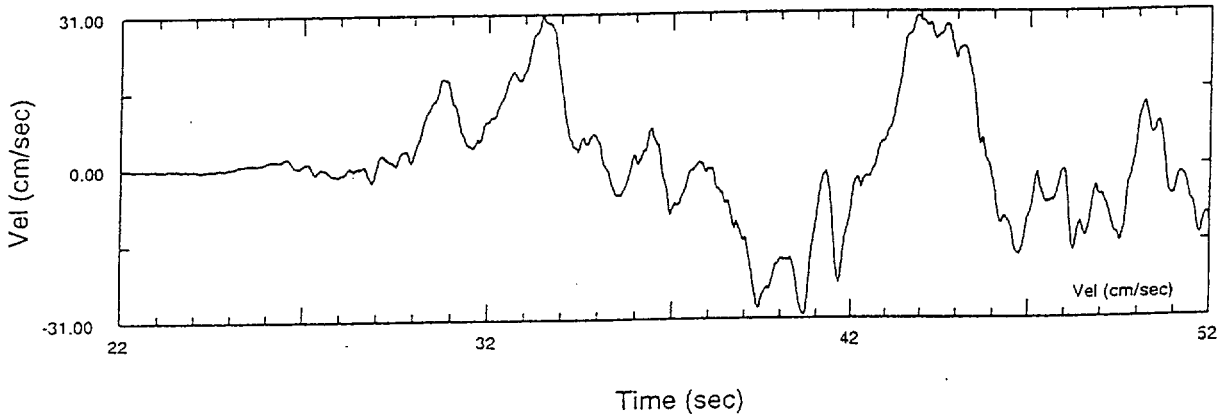

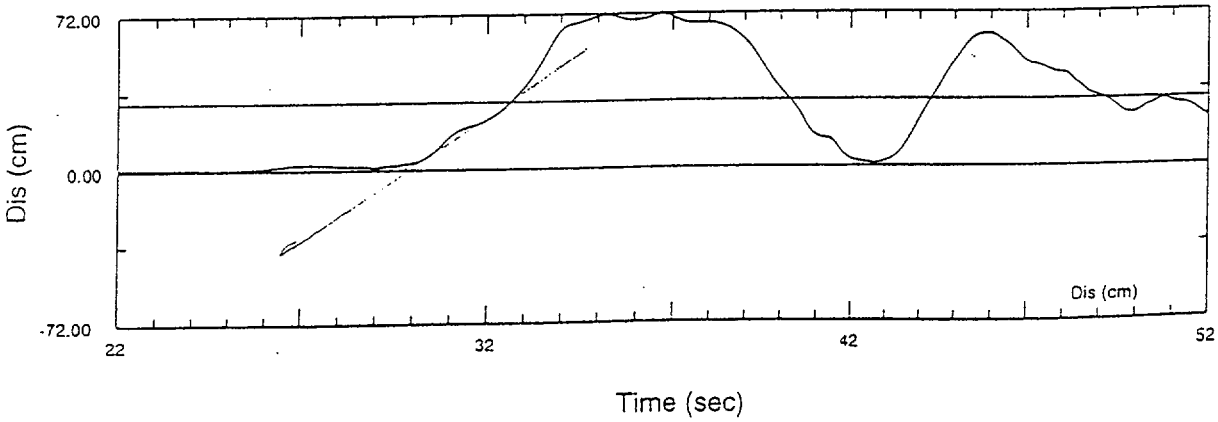

Chi-Chi Earthquake: Station TCU105, East, Fling Model

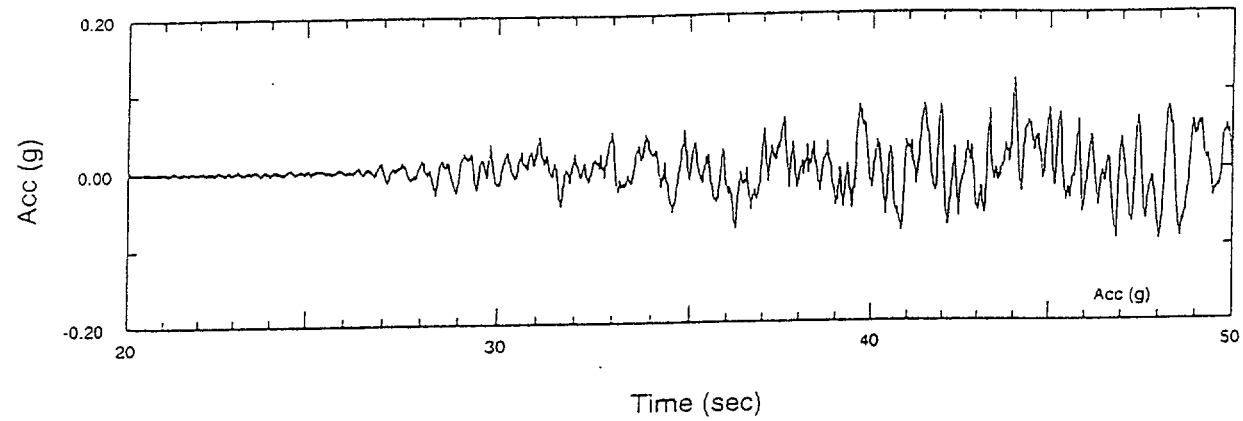

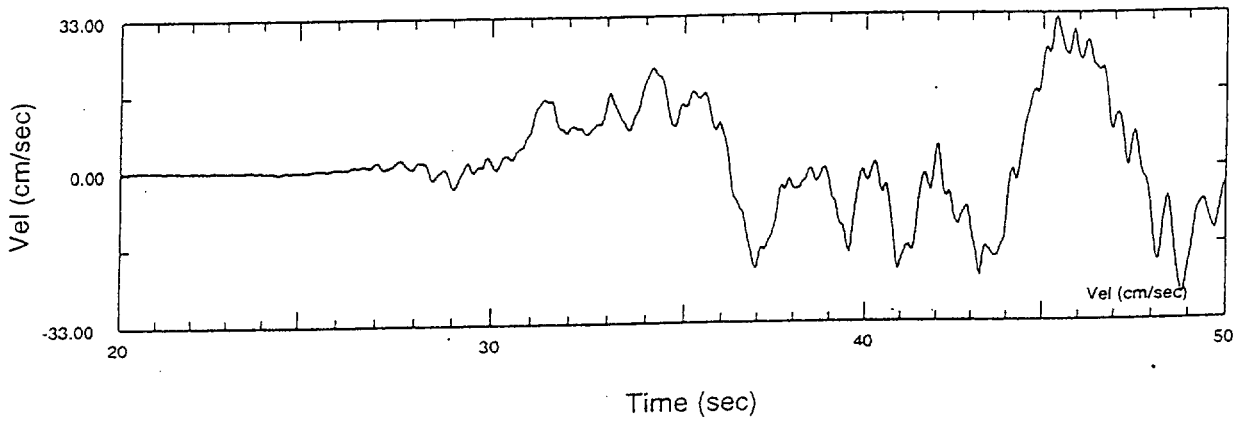

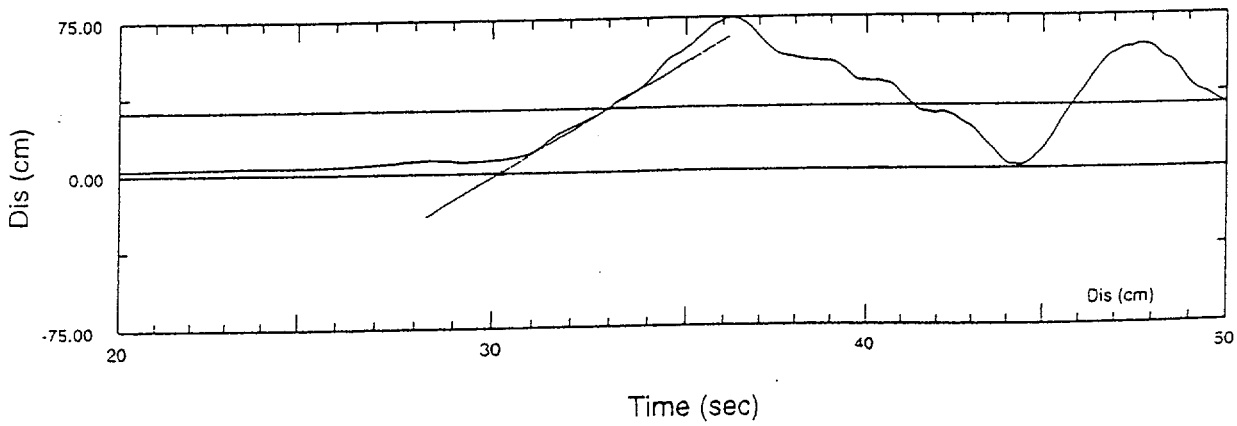

Chi-Chi Earthquake: Station TCU106, East, Fling Model

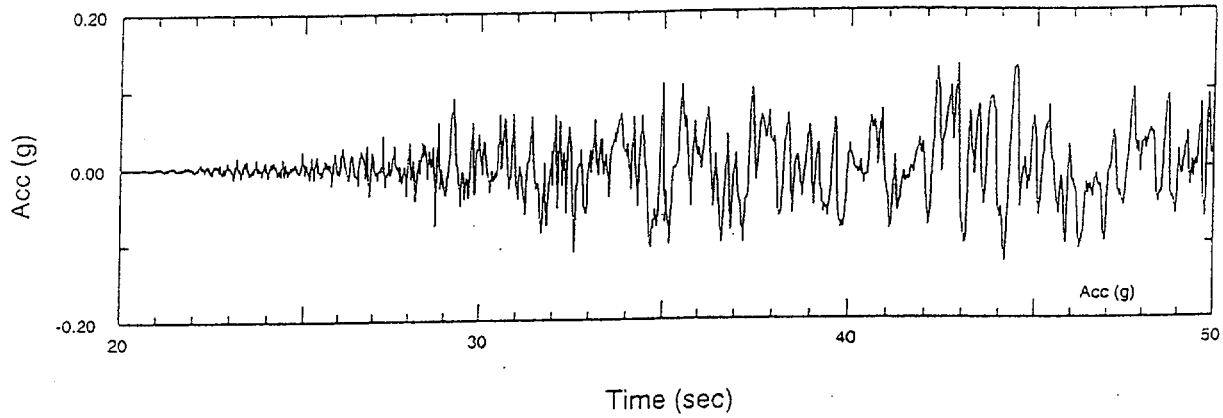

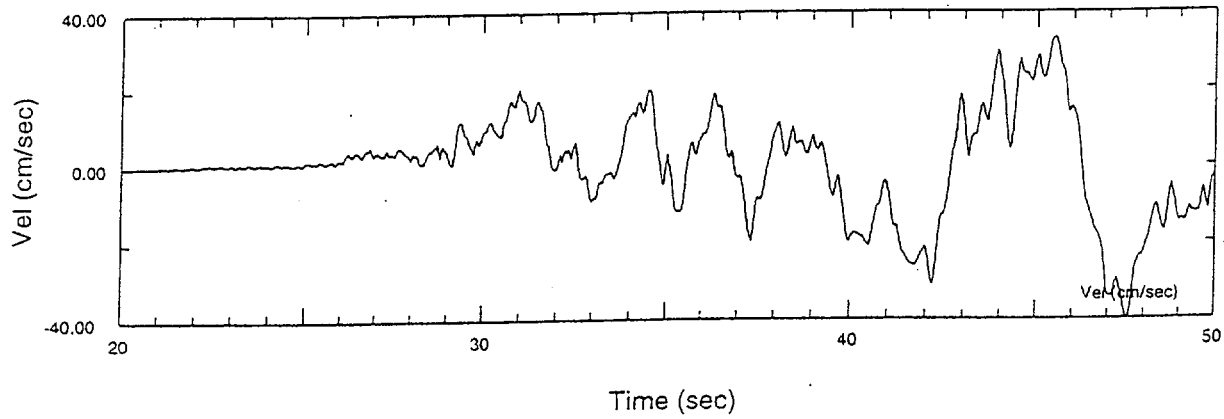

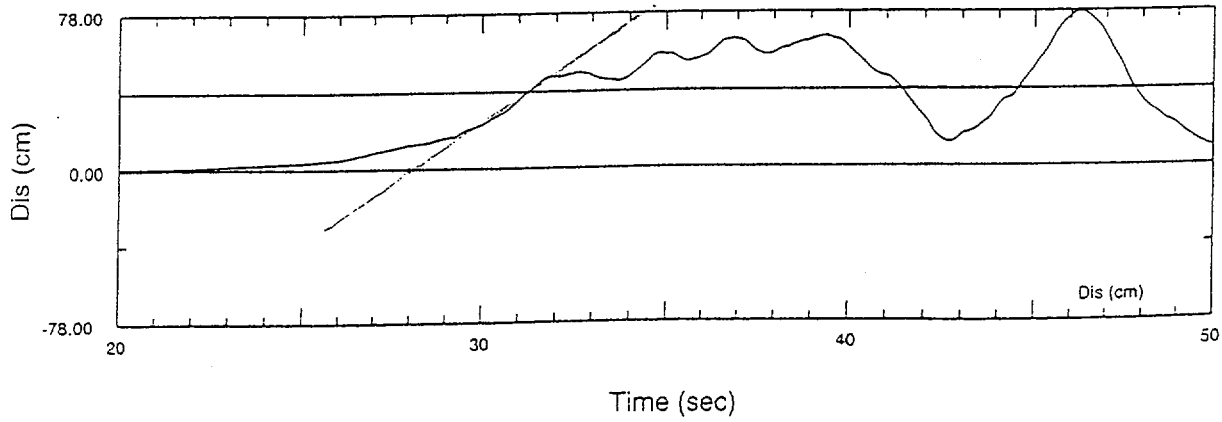

Chi-Chi Earthquake: Station TCU109, East, Fling Model

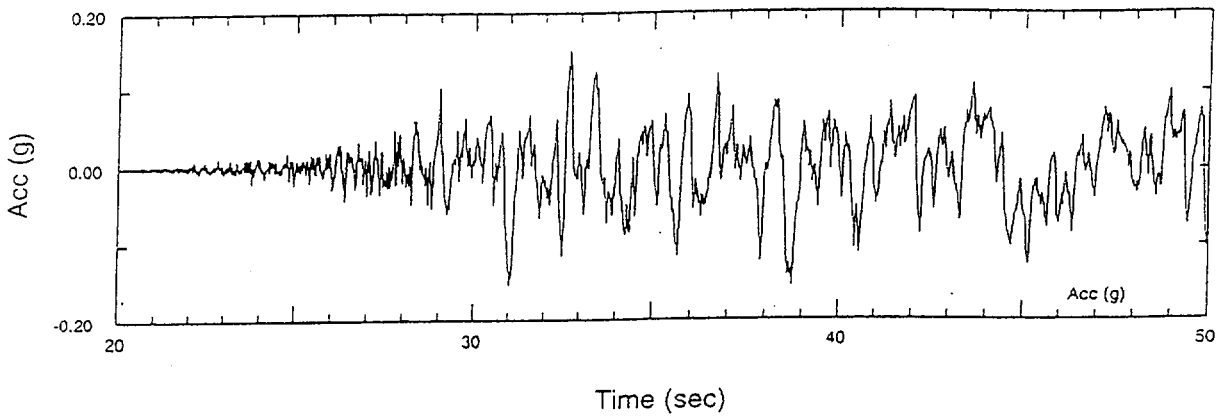

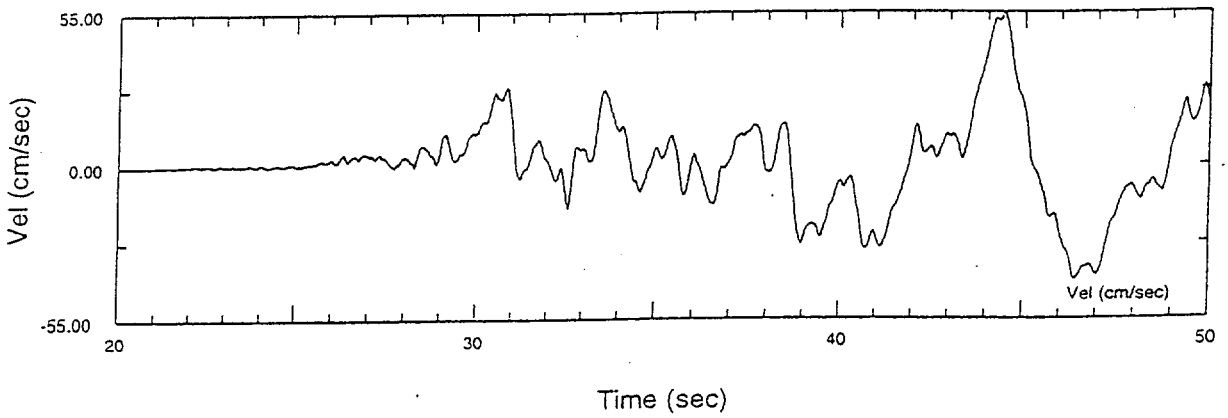

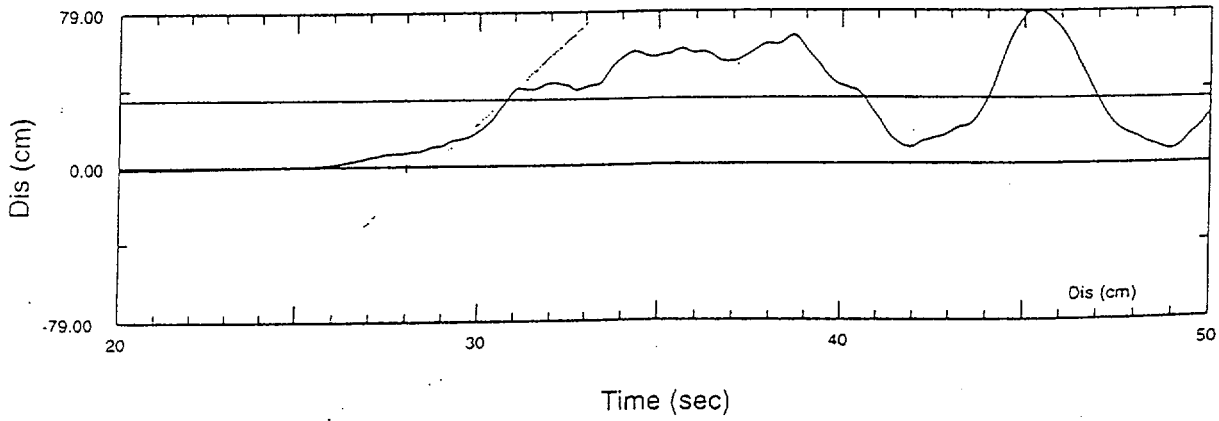

Chi-Chi Earthquake: Station TCU116, East, Fling Model

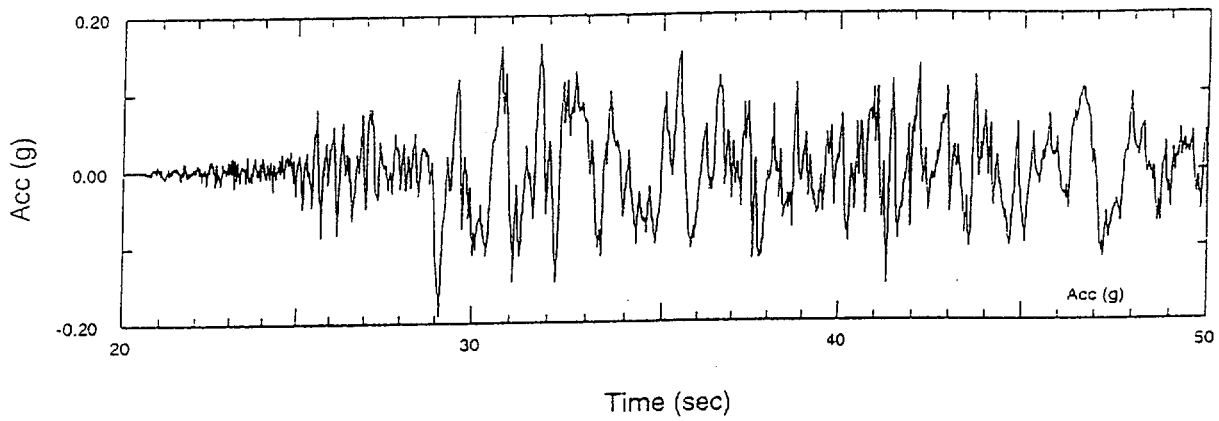

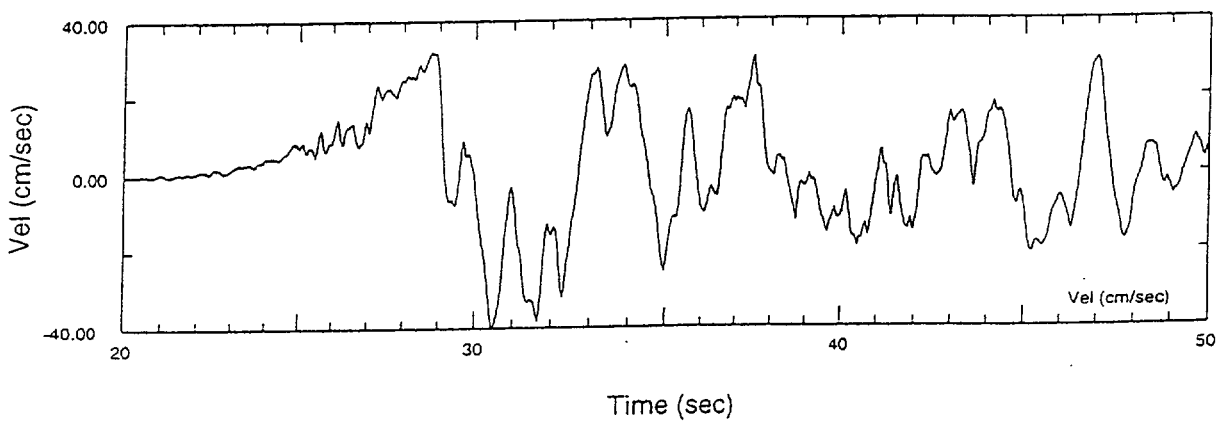

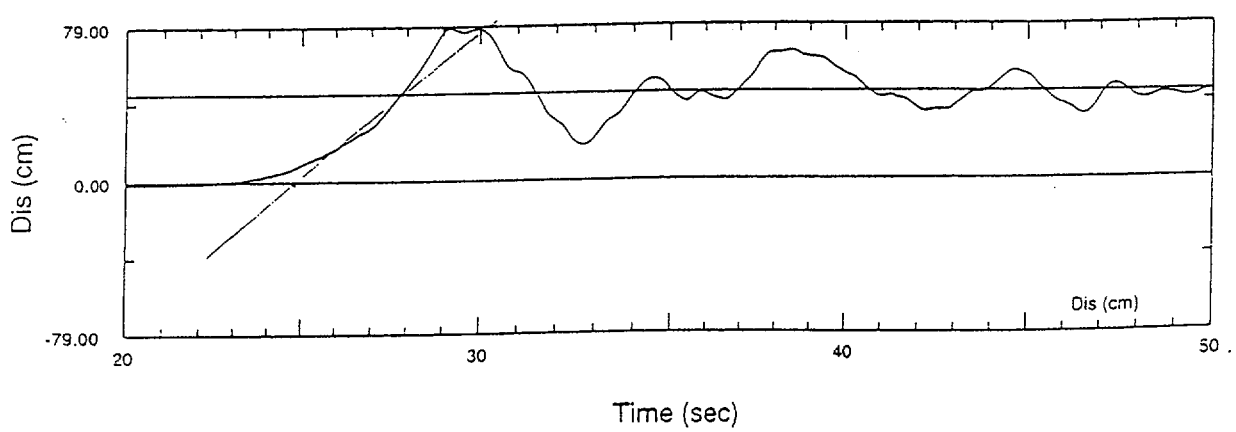

Chi-Chi Earthquake: Station TCU120, East, Fling Model

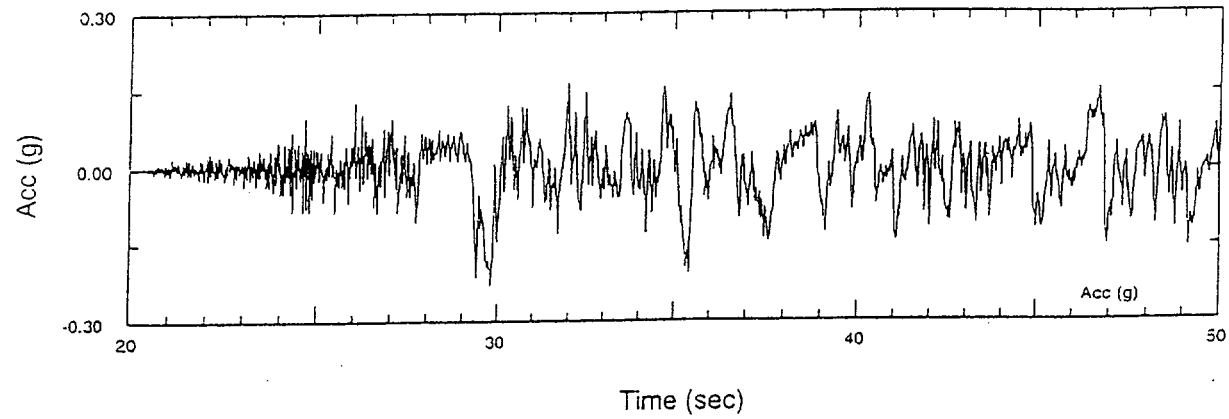

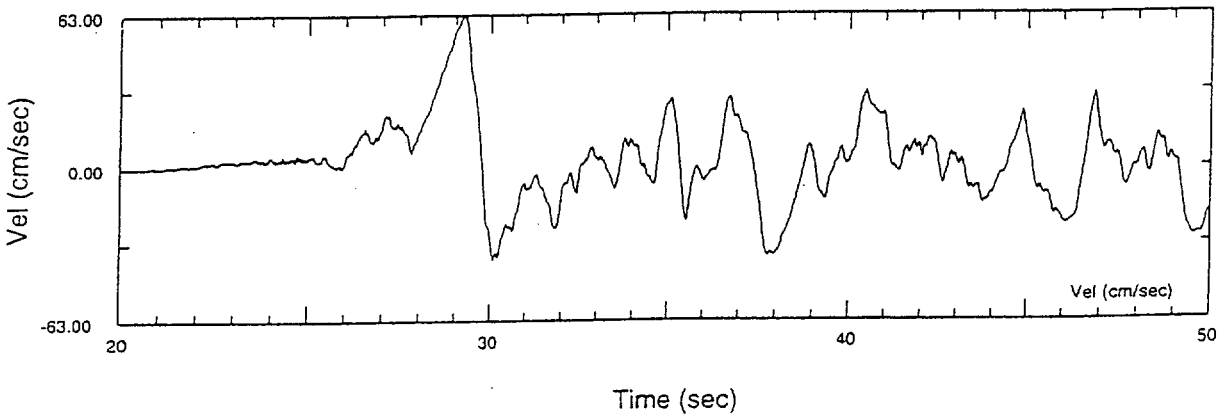

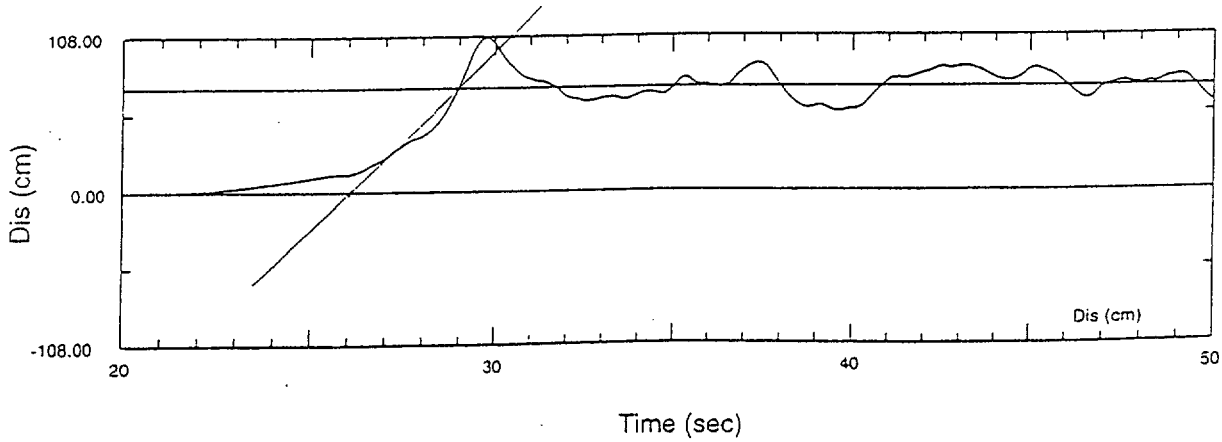

Chi-Chi Earthquake: Station TCU122, East, Fling Model

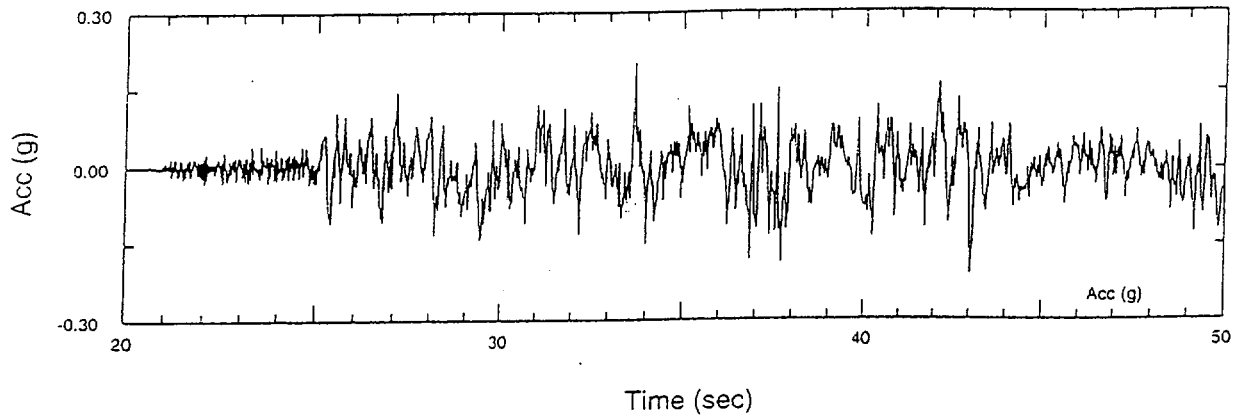

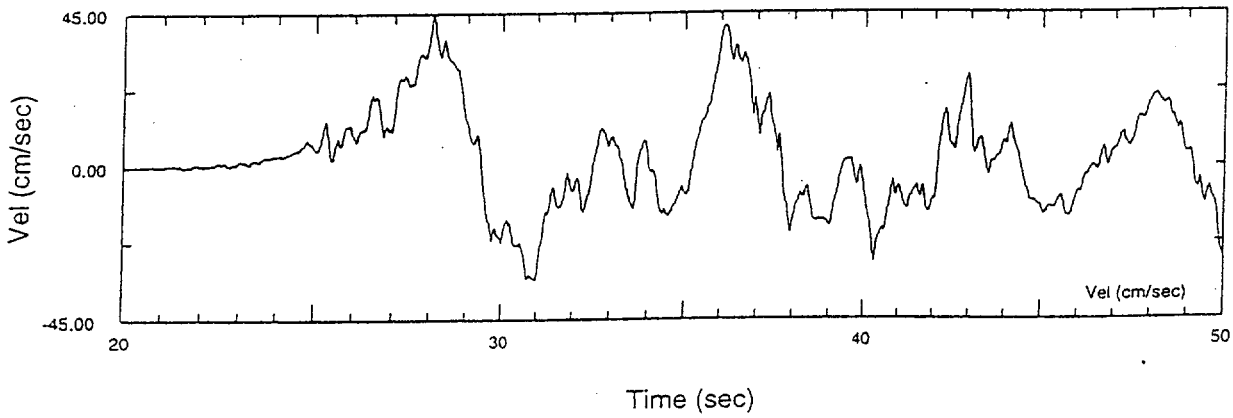

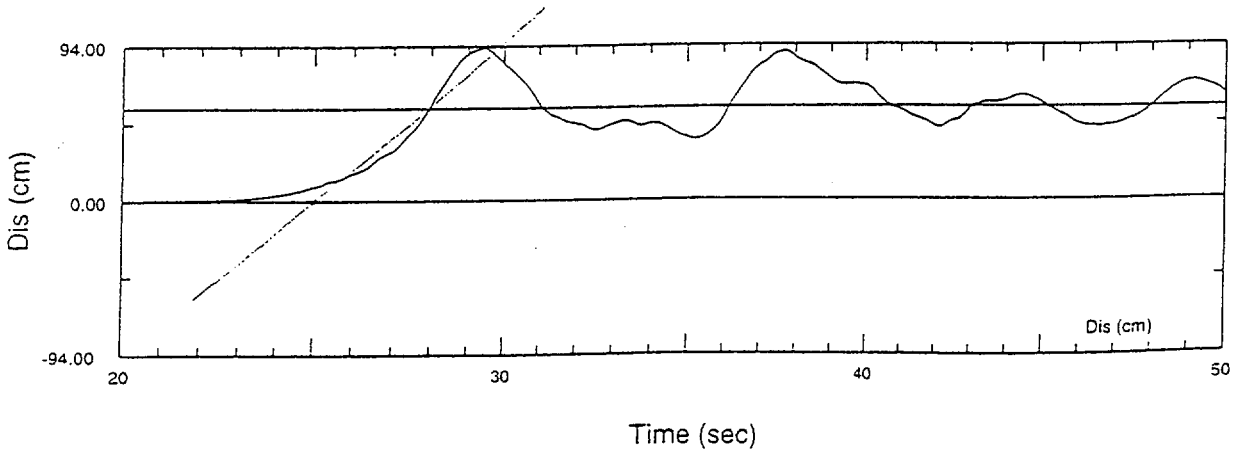
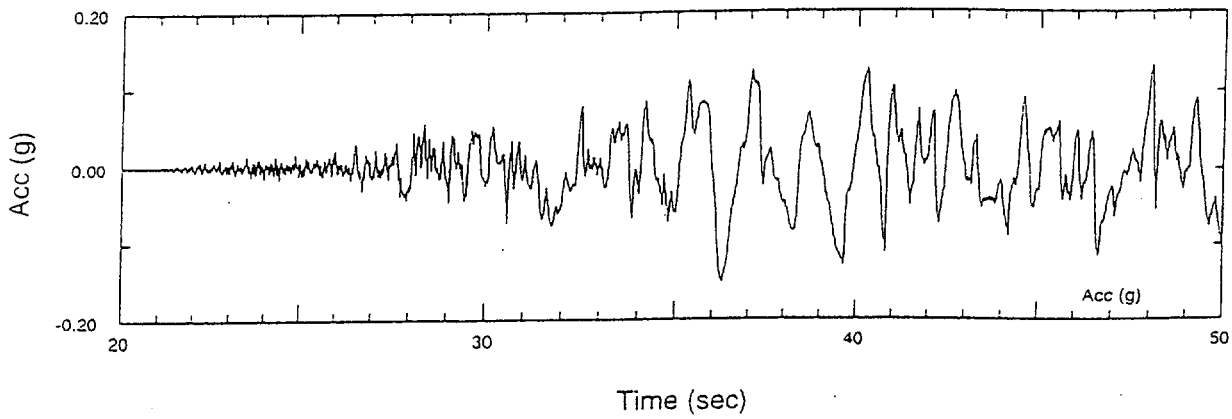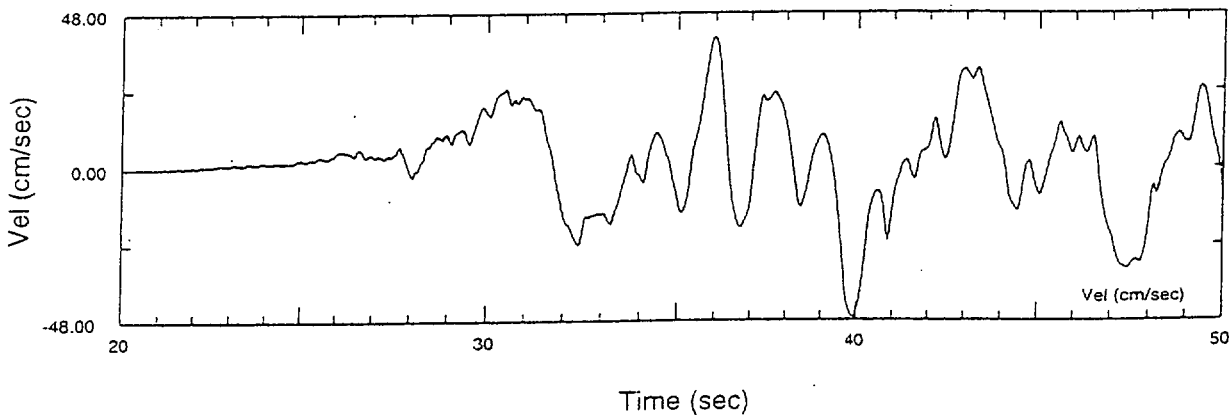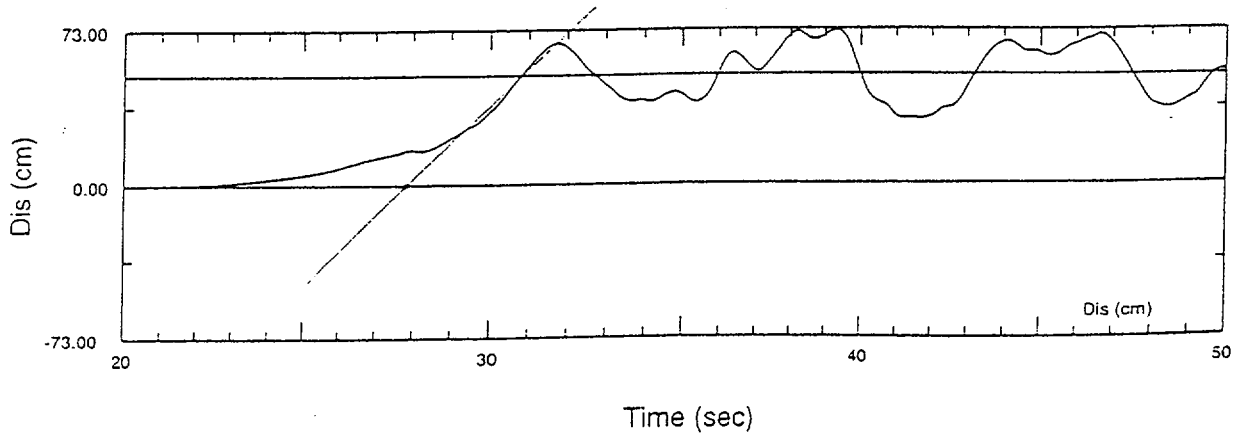
Chi-Chi Earthquake: Station TCU123, East, Fling Model